Elucidation of feeding-related neuronal networks involved in the regulation of the hypophysiotropic thyrotropin-releasing hormone- and corticotropin-releasing hormone-synthesizing neurons in the rat

Ph.D. Thesis

Gábor Wittmann

Department of Endocrine Neurobiology
Institute of Experimental Medicine, Hungarian Academy of Sciences

Semmelweis University
János Szentágothai Ph.D. School of Neuroscience

Tutors: Dr. Csaba Fekete Ph.D. and Dr. Zsolt Liposits Ph.D., D.Sc.

Opponents: Dr. Katalin Köves Ph.D., D.Sc.
Dr. Árpád Párducz Ph.D., D.Sc.

Chairman of committee: Dr. Károly Rácz Ph.D., D.Sc.
Members of committee: Dr. Ida Gerendai Ph.D., D.Sc.
Dr. Magdolna Kovács Ph.D., D.Sc.

Budapest
2007

TABLE OF CONTENTS

List of abbreviations

11β-HSD-1	-	11β-hydroxysteroid-dehydrogenase 1
11β-HSD-2	-	11β-hydroxysteroid-dehydrogenase 2
2DG	-	2-deoxy-glucose
α-MSH	-	alpha-melanocyte stimulating hormone
ACTH	-	adrenocorticotropic hormone
AGRP	-	agouti-related protein
BAT	-	brown adipose tissue
BSA	-	bovine serum albumin
CART	-	cocaine- and amphetamine-regulated transcript
CNS	-	central nervous system
CRE	-	cAMP-response-element
CREB	-	cAMP-response-element binding protein
CRH	-	corticotropin-releasing hormone
DAB	-	3,3'-diaminobenzidine
DBH	-	dopamine-β-hydroxylase
DMN	-	hypothalamic dorsomedial nucleus
GALP	-	galanin-like peptide
HPA axis	-	hypothalamic-pituitary-adrenocortical axis
HPT axis	-	hypothalamic-pituitary-thyroid axis
icv.	-	intracerebroventricular
IL-1	-	interleukin 1
IR	-	immunoreactive
LPS	-	bacterial lipopolysaccharide
MC3-R, MC4-R	-	melanocortin 3 and 4 receptors

MCH	-	melanin-concentrating hormone
Ni-DAB	-	nickel-diaminobenzidine
NPY	-	neuropeptide Y
NTS	-	nucleus of the solitary tract
PB	-	phosphate buffer
PBS	-	phosphate buffered saline
PCREB	-	phosphorylated cAMP-response-element binding protein
PKA	-	protein kinase A
PNMT	-	phenylethanolamine-N-methyltransferase
PVN	-	hypothalamic paraventricular nucleus
SEM	-	standard error of the mean
SSC	-	standard sodium citrate
STAT3	-	signal transducer and activator of transcription 3
T3	-	3,5,3'-triiodothyronine
T4	-	thyroxine
TB	-	Tris buffer
TRH	-	thyrotropin-releasing hormone
TSH	-	thyrotropin
UCP-1	-	uncoupling protein 1
UCP-3	-	uncoupling protein 3
VMN	-	hypothalamic ventromedial nucleus

Introduction

The hypothalamic paraventricular nucleus (PVN) contains hypophysiotropic neuron populations that control the hormone secretion of the anterior pituitary gland. The hypophysiotropic thyrotropin-releasing hormone (TRH)-synthesizing neurons are located in the periventricular and medial parvocellular subdivisions of the PVN (1), and govern the hypothalamic-pituitary-thyroid (HPT) axis **(Fig. 1)**. The hypophysiotropic corticotropin-releasing hormone (CRH)-synthesizing neurons, located laterally from the TRH neurons in the medial parvocellular subdivision (2, 3), are the central regulators of the hypothalamic-pituitary-adrenocortical (HPA) axis **(Fig. 1)**. Hypophysiotropic TRH and CRH neurons integrate a wide variety of humoral and neural signals and serve as final common pathways in the regulation of the HPT and HPA axes, respectively. These signals set the activity of the hypophysiotropic neurons to adapt to the altered external or internal environment. The resulted alterations in the peripheral levels of thyroid hormones and corticosterone play essential role for promoting survival during the periods of challenges, such as fasting or stress (4-6).

The role of HPT and HPA axes in the regulation of energy homeostasis

The long-term maintenance of body weight requires a balance between energy intake and energy expenditure. Energy intake is determined primarily by feeding behaviour, while energy expenditure can be broken down into basal metabolism, voluntary and involuntary activity, and adaptive thermogenesis (7). Energy homeostasis is maintained through behavioural, autonomic and endocrine pathways (7). Both the HPT and HPA axes play critical role in maintaining energy homeostasis and normal metabolic processes. Large amount of data has been accumulated about the role of thyroid hormones and glucocorticoids in the regulation of energy homeostasis (8, 9).

Thyroid hormones are well known to regulate energy expenditure through effects on basal metabolism and adaptive thermogenesis. In most tissues, thyroid hormones raise the metabolic rate by increasing the number and size of mitochondria in the target cells, stimulating the synthesis of enzymes in the respiratory chain, increasing membrane Na^+/K^+ ATP-ase concentration and membrane Na^+ and K^+ permeability (10). Hyperthyroidism increases metabolic rate and metabolic processes, while basal metabolic rate can be reduced by as much as 30% in the absence of thyroid hormones (11).

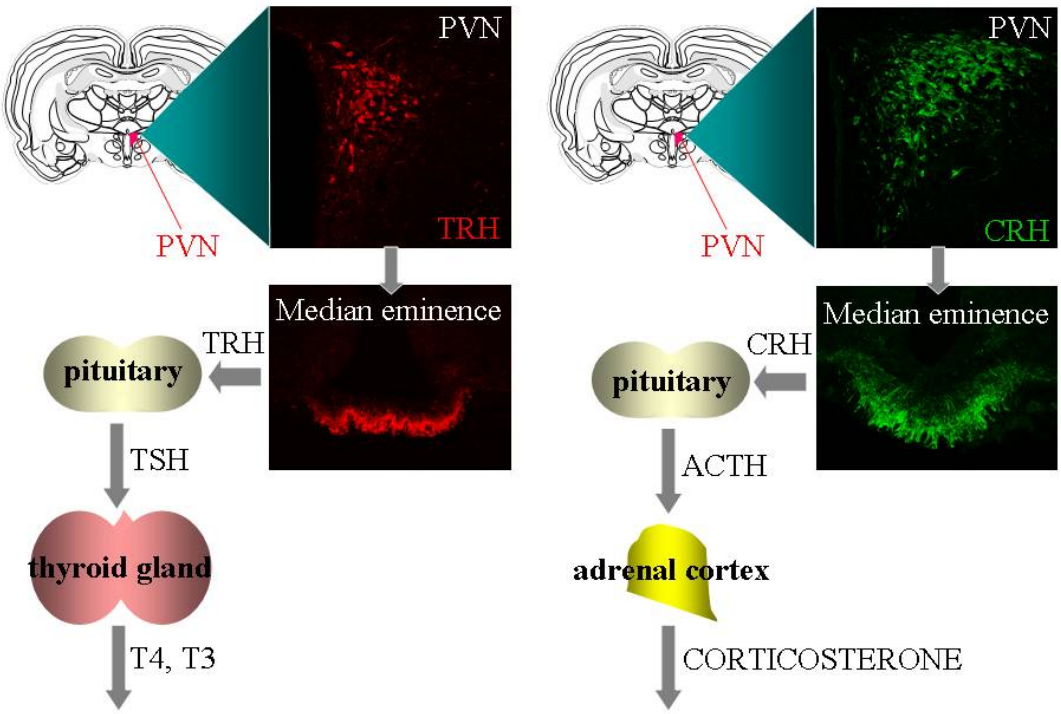

Figure 1. Schematic illustration of the HPT and HPA axes in the rat. Hypophysiotropic TRH- and CRH-synthesizing neurons residing in the PVN secrete TRH and CRH, respectively, into the portal capillary system of the median eminence. The secreted TRH controls the release of thyroid hormones T4 and T3 through the regulation of TSH secretion from the pituitary gland, whereas CRH controls the release of corticosterone through the regulation of ACTH secretion from the pituitary.

Thyroid hormones in brown adipose tissue (BAT) are essential for diet-induced thermogenesis, an important way for wasting excess energy in rodents (12). In response to a calorie-rich diet, increased sympathetic activity causes a large increase in heat production in interscapular BAT (13, 14). This is achieved mainly by increasing the activity of uncoupling protein 1 (UCP-1) which disassociates or 'uncouples' the respiratory chain from ATP production and dissipates the resulting oxidation energy as heat (12). The presence of thyroid hormones and the activation of type 2 iodothyronine deiodinase that converts intracellular T4 to its active form T3 are crucial for the increase in UCP-1 expression in BAT (15, 16). Other thermogenic effects of thyroid hormones are exerted in the muscle. For example, increased UCP-3 and sarcoendoplasmic reticulum Ca^{2+} ATP-ase expressions (17-22) have been hypothesized to participate not only in cold-induced, but also in diet-induced thermogenesis (23).

In addition to effects on heat generation, thyroid hormone also has effects on lipogenesis and appetite regulation. T3 increases expression of genes coding for

lipogenic enzymes such as malic enzyme, glucose 6-phosphate dehydrogenase and acetyl-coenzyme A carboxylase (24-28) that use fatty acids derived from adipose tissue as the primary source of substrate (29), and is well known to increase food intake (29). The latter effect may be mediated centrally by increased ATP utilization in the mediobasal hypothalamus, perhaps as a result of increased Na^+/K^+ ATP-ase activity (30), and/or direct effects on the hypothalamic ventromedial nucleus (VMN) (31). Kong et al. have demonstrated that T3 increases immediate early gene activation in the VMN and induces a four-fold increase in food intake when injected directly into the VMN (31). Presumably, the effects of T3 on lipogenesis and appetite are compensatory, preventing obligatory and/or adaptive thermogenesis from depleting fat stores and to counterbalance increased energy expenditure when T3 levels are elevated (11).

Corticosterone, which is the main glucocorticoid hormone in rodents, is also crucial for the maintenance of energy homeostasis and normal metabolism. Corticosterone acting on glucocorticoid receptors enhance the transcription of several genes that encode proteins involved in the regulation of energy balance, such as metabolic enzymes, plasmamembrane transporters and hormones. Corticosterone increases hepatic gluconeogenesis mainly by the transcriptional activation of phosphoenolpyruvate carboxykinase, the rate-limiting enzyme in the gluconeogenic pathway (32, 33). In addition, corticosterone also increases cellular concentrations of enzymes and the substrates for gluconeogenesis (34). Glucocorticoids decrease glucose uptake into the skeletal muscles and increase protein degradation (35). In concert with these well-established effects of glucocorticoids on blood glucose concentration, corticosterone has also been shown to directly inhibit insulin release from pancreatic β cells (36). During stress this could be an important regulatory mechanism, allowing a transient attenuation of the insulin response to hyperglycemia in order to ensure sufficient glucose for the needs of the brain (36).

In adipose tissue, glucocorticoids regulate several processes including metabolic activity (37), production and secretion of leptin (38, 39), and the differentiation of adipocytes (40). In the recent years, the effects of excess or reduced corticosterone levels in adipose tissue have been extensively studied. A modest increase in the activity of 11β-hydroxysteroid-dehydrogenase 1 (11β-HSD-1), the enzyme that regenerates corticosterone from inactive 11-dehydrocorticosterone, in adipose tissue of mice is sufficient to cause hyperphagia with visceral obesity and its most critical metabolic

complications: hyperglycemia, glucose intolerance, insulin resistance, hyperleptinemia and leptin resistance (37). In contrast, adipocyte-specific glucocorticoid inactivation by the transgenic expression of 11β-HSD-2, which converts corticosterone to the inactive 11-dehydrocorticosterone, causes resistance to diet-induced obesity on high fat diet, reduced fat mass, decreased food intake, increased energy expenditure, improved glucose tolerance and insulin sensitivity, and reduced expression of leptin (41).

In addition to its effects on the liver, adipose tissue, muscle and other peripheral organs, corticosterone has been suggested to regulate energy homeostasis via acting in the central nervous system (CNS). 11β-HSD-1 is expressed in important hypothalamic metabolic centers (e.g. the arcuate nucleus). Furthermore, in 11β-HSD-$1^{-/-}$ mice that have normal corticosterone levels, the expression levels of several feeding-related neuropeptides and receptors are altered either on normal or high-fat diet (42).

Regulation of hypophysiotropic TRH and CRH neurons during fasting: connectivity with AGRP/NPY and α-MSH/CART neurons in the arcuate nucleus

The key elements of the extremely complex regulatory system that maintains energy balance are the central neural circuits that are capable of sensing metabolic signals (hormones, metabolites) from the periphery, and in turn regulate food intake and energy expenditure (43). Recent data, partly from our laboratory, suggest that the adaptation of hypophysiotropic CRH and particularly TRH neurons to fasting, a severe deficit in energy balance, is achieved by key feeding-related neurons in the hypothalamic arcuate nucleus.

Regulation of hypophysiotropic TRH neurons during starvation

Fasting induces central hypothyroidism characterized by fall of circulating thyroid hormone levels, reduction in TRH gene expression in the hypophysiotropic neurons and inappropriately normal or low plasma TSH levels (4, 5, 44). This inhibition of the HPT axis is highly adaptive because the low level of thyroid hormones entails reduced thermogenesis and decreased metabolic rate which help to preserve the energy stores during the period of food restriction. These alterations can be completely reversed by the systemic administration of leptin (4, 45), a white adipose tissue-derived hormone, to fasting animals, suggesting that the falling levels of leptin in the peripheral blood of fasting animals play an important role in the fasting-induced inhibition of the HPT axis.

The pharmacological ablation of the hypothalamic arcuate nucleus, that contains important feeding-related neuronal groups, not only abolishes the response of the HPT axis to fasting, but its response to the exogenous administration of leptin is lost as well (46). Therefore, it has been suggested that the regulatory effects of leptin on the HPT axis are primarily indirect, mediated by neurons of the hypothalamic arcuate nucleus which expresses the greatest amount of leptin receptor in the brain (47).

The input of TRH neurons that originates from the arcuate nucleus includes afferents from two separate groups of neurons with opposing functions that either co-synthesize alpha-melanocyte stimulating hormone (α-MSH) and cocaine- and amphetamine-regulated transcript (CART) (48, 49), or agouti-related protein (AGRP) and neuropeptide Y (NPY) (50, 51). These two cell groups are regarded as the principal neurons of the CNS that mediate the effects of leptin on food intake and energy expenditure (the functions of these neurons are summarized briefly in the **boxed text**). Both types of neurons express leptin receptor (52, 53), but their neuropeptide transmitter synthesis is oppositely regulated by leptin: α-MSH and CART gene expressions are increased (54, 55), whereas AGRP and NPY expressions are inhibited by leptin administration (56, 57). Conversely, during fasting, the syntheses of AGRP and NPY are increased (56, 58, 59), whereas α-MSH and CART syntheses are inhibited (54, 55, 59). A large body of evidence strongly suggests that, by signaling on TRH neurons, these arcuate nucleus-derived neuropeptides are important mediators of the effects of leptin and fasting on hypophysiotropic TRH neurons. It is worth of note that there are indications that hypophysiotropic TRH neurons can also be directly regulated by leptin, however, to a lesser extent (60-62).

Axons of α-MSH/CART neurons establish synapses on TRH neurons, contacting the cell bodies and first order dendrites of about 70% of TRH neurons in the periventricular parvocellular subdivision, and of 34% of TRH neurons in the medial parvocellular subdivision of the PVN (63). Both α-MSH (63, 64) and CART (65, 66) have activating effects on hypophysiotropic TRH neurons. When administered intracerebroventricularly to fasting animals, α-MSH and CART have potent effects in restoring the fasting-induced suppression of proTRH mRNA in hypophysiotropic neurons to levels found in freely feeding animals (63, 65). The molecular mechanisms

Feeding-related neurons of the arcuate nucleus

AGRP/NPY and α-MSH/CART neurons in the arcuate nucleus are two antagonistic cell populations that have primary importance in the regulation of energy homeostasis. Both cell groups possess receptor molecules for peripheral satiety signals, such as leptin and insulin (43, 52, 53). The peripheral hormones oppositely regulate the activity of these two cell types of the arcuate nucleus (43). Leptin, an adipose tissue-derived hormone that circulates in proportion to body adipose stores, appears to be the most important but certainly the most studied hormonal input to these neurons: it stimulates α-MSH/CART cells and inhibits AGRP/NPY neurons. Leptin directly depolarizes α-MSH/CART neurons (67) and increases the synthesis of α-MSH and CART (54, 55). In contrast, leptin suppresses the gene expression of NPY and AGRP (56, 57), and inhibits the electrophysiological activity of AGRP/NPY neurons: the spike frequency of AGRP/NPY neurons is markedly increased in fasting animals when leptin levels are low, which is reversed by exogenous leptin administration (68). In addition to its regulatory function, leptin also has a trophic action on these cells because the development of axonal projections of AGRP/NPY and α-MSH/CART neurons at neonatal age is dependent on leptin (69).

The distributions of the nerve fibers of AGRP/NPY and α-MSH/CART neurons show a high degree of overlap (70); individual target neurons were demonstrated to receive dual innervation from both cell types (63). Therefore, AGRP can act as a competitive antagonist of α-MSH on the MC3 and MC4 receptors, as it was shown *in vitro* (71, 72). By innervating several brain areas including important metabolic centers (70), AGRP/NPY and α-MSH/CART neurons act on second order neurons to regulate food intake and energy expenditure (43). Centrally injected α-MSH effectively reduces food intake (73). A similar anorexigenic effect of CART has also been observed (54). In contrast, both NPY and AGRP markedly stimulate feeding (74-77). AGRP/NPY and α-MSH/CART neurons oppositely regulate energy expenditure as well, by inhibiting and activating, respectively, the HPT axis (63, 65, 78, 79), and possibly also by changing the sympathetic activity to brown adipose tissue to affect thermogenesis (79, 80).

Studies of several genetic animal models indicate that AGRP/NPY and α-MSH/CART neurons have critical roles in maintaining energy balance. MC4-$R^{-/-}$ mice develop severe obesity with hyperphagia and decreased energy expenditure (81). MC3-$R^{-/-}$ mice, although only slightly heavier than wild-type littermates, have higher feed efficiency (the ratio of weight gain to food intake) and markedly increased fat mass with reduced lean body mass (82). In addition, mice lacking both MC3-R and MC4-R become significantly heavier than MC4-$R^{-/-}$ mice (82). In the absence of NPY, the extremely obese leptin-deficient ob/ob mice become less obese because of reduced food intake and increased energy expenditure (83). The role of AGRP/NPY neurons is best demonstrated by the specific ablation of these neurons in adult animals which causes a rapid and dramatic decrease of food intake that leads to starvation (84, 85). Interestingly, neonatal ablation of AGRP/NPY neurons has only minimal effects on feeding (85), suggesting that network-based compensatory mechanisms can evolve during development. These compensatory mechanisms probably also account for the observations that $NPY^{-/-}$, $AGRP^{-/-}$ and $NPY^{-/-}$/$AGRP^{-/-}$ mice have no obvious feeding or body weight deficits and maintain a normal response to starvation (86, 87).

that probably underlie the direct stimulatory effects of α-MSH on TRH neurons have been investigated in detail. A major receptor for α-MSH, type 4 melanocortin receptor (MC4-R) is coupled to Gs protein that activates adenylate cyclase (73), and is expressed at least in half of the TRH neurons in the PVN (61). Since the promoter region of the TRH gene contains a cAMP-response-element (CRE) (88), activation of the cAMP/protein kinase A (PKA) pathway, through inducing the phosphorylation of cAMP-response-element binding protein (CREB), can increase the transcription of the TRH gene. This is supported by the observation that central administration of α-MSH to fasted animals rapidly induces CREB phosphorylation in the majority of hypophysiotropic TRH neurons (89). Moreover, *in vitro,* α-MSH acting on the human MC4-R is able to increase transcription from the human TRH promoter, which is mediated by CREB phosphorylation (61). In contrast, the mechanism by which CART signals to TRH neurons is not known, largely due to the lack of any information regarding the receptor(s) to which CART binds. However, icv. CART administration does not induce CREB phosphorylation in hypophysiotropic TRH neurons (90), suggesting that CART might activate the TRH promoter through a second messenger system other than the cAMP/PKA/CREB pathway. Therefore, it is tempting to speculate that CART and α-MSH may have potentiating effects on hypophysiotropic TRH neurons by utilizing different signaling mechanisms.

The AGRP/NPY neurons also send monosynaptic projections to hypophysiotropic TRH neurons, innervating virtually all TRH neurons on the somata and proximal dendrites (91). However, in contrast to α-MSH and CART, NPY and AGRP have inhibitory actions on hypophysiotropic TRH neurons (78, 79). Chronic (3 days) icv. administration of NPY results in a profound reduction in proTRH mRNA levels in the PVN, with low or inappropriately normal TSH levels and a marked reduction in T4 and T3 levels (78). Central AGRP administration also mimicks the effects of fasting on the HPT axis, very similarly to NPY (79). The effect of NPY on TRH neurons is mediated by Y1 and Y5 receptors (92), and TRH neurons in the PVN have been demonstrated to express Y1 receptor (93, 94). All known NPY receptors are coupled to Gi protein which inhibits the activity of adenylate cyclase (95), therefore NPY would be able to antagonize the effects of signals that activate adenylate cyclase and cause CREB phosporylation to increase TRH gene expression. Indeed, when animals are pretreated intracerebroventricularly with NPY before α-MSH infusion, the percentage of TRH

neurons containing PCREB is significantly reduced compared with α-MSH infused animals (96). AGRP acts on TRH neurons probably also by decreasing intracellular cAMP signaling. AGRP is an endogenous antagonist and may also be an inverse agonist of type 3 and 4 melanocortin receptors (MC3-R and MC4-R) (71, 72, 97, 98). Therefore, AGRP can antagonize the effect of α-MSH on TRH neurons at the receptor level, or as an inverse agonist, may decrease the spontaneous activity of the melanocortin receptors on TRH neurons

All these data suggest a model by which leptin regulates the HPT axis through arcuate nucleus-derived neuropeptides. α-MSH/CART- and AGRP/NPY-containing axons of arcuate nucleus origin converge on the hypophysiotropic TRH neurons and these peptides can exert a potent central effect to stimulate (α-MSH and CART) or inhibit (AGRP and NPY) TRH gene expression in the PVN. Therefore, during fasting, inhibition of α-MSH/CART neurons and activation of AGRP/NPY-producing neurons in the hypothalamic arcuate nucleus by the fall in circulating levels of leptin result in a net inhibitory effect on the hypophysiotropic TRH synthesis and a concomitant decline in circulating thyroid hormone levels (**Fig. 2**).

The ability of leptin to directly activate TRH neurons was also suggested based on the observations that leptin administration induces phosphorylation of signal transducer and activator of transcription 3 (STAT3), an indirect marker of the action of leptin, in a subpopulation of TRH neurons (62). In addition, STAT3 has been shown to increase the transcription of the TRH gene *in vitro* (61) and it binds to the TRH promoter *in vivo* after leptin administration (60). Although this direct effect of leptin may have physiological significance, the critical importance of the indirect stimulation of the hypophysiotropic TRH neurons through α-MSH/CART neurons is emphasized by the experiment showing that the stimulatory effect of centrally administered leptin on TRH synthesis is completely reversed by administration of a melanocortin antagonist (62).

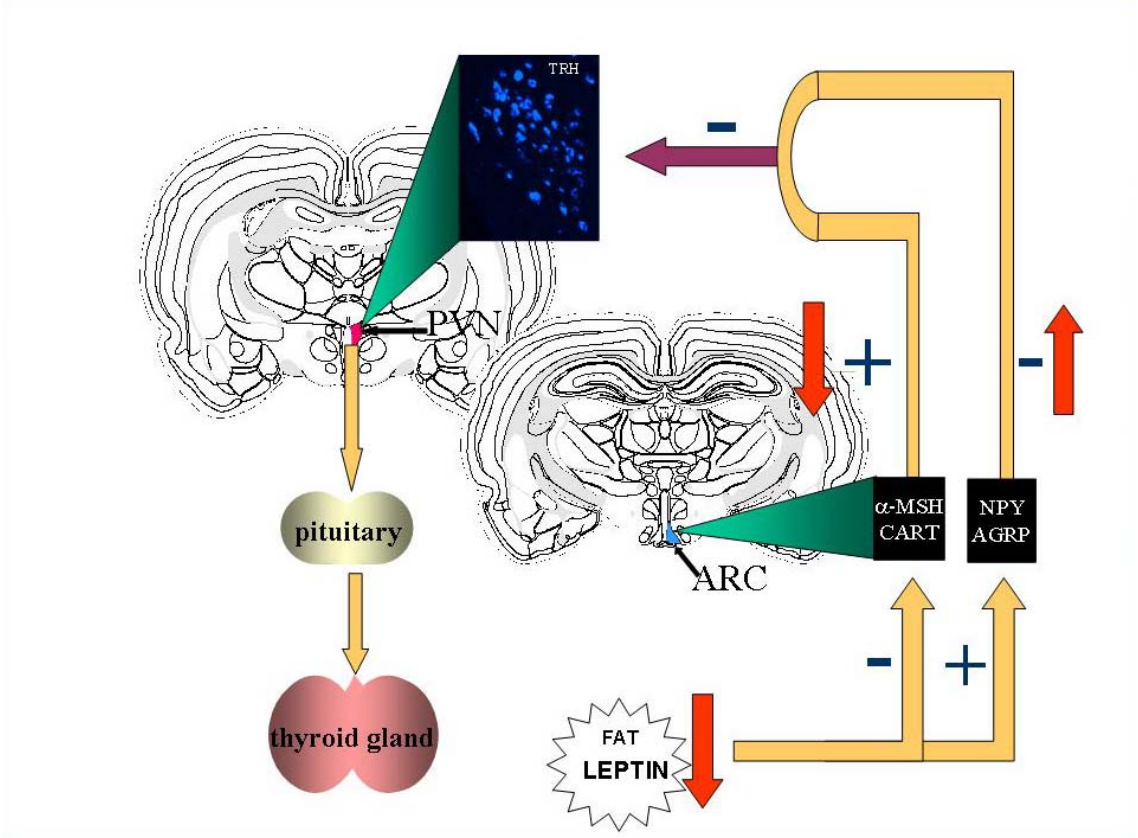

Figure 2. Schematic illustration of the regulation of the HPT axis by leptin. During fasting, the falling level of leptin inhibits α-MSH/CART neurons and stimulates NPY/AGRP-producing neurons in the arcuate nucleus. These changes decrease the stimulatory and increase the inhibitory effects resulting in an inhibition of the TRH synthesis in the hypophysiotropic neurons and decreased TSH and thyroid hormone secretion at the periphery. ARC, arcuate nucleus.

Regulation of hypophysiotropic CRH neurons in starvation

At present, the regulation of the HPA axis during fasting is less well understood. CRH mRNA levels are reduced in the PVN of fasting rats (58, 99, 100), whereas circulating ACTH and corticosterone levels are increased compared to the fed state (45, 101-103). The rise in corticosterone could be an adaptive response to maintain fasting blood glucose levels and might also promote survival in the case of an acute stress during fasting (104, 105). The discrepancy between reduced CRH mRNA levels in the PVN and elevated serum ACTH levels raises the possibility that factor(s) other than CRH stimulate ACTH secretion in fasting, and the high corticosterone levels by negative feedback effect may contribute to the reduced CRH expression.

Since the icv. infusion of leptin prevents the fasting-induced suppression of CRH mRNA (100, 106), it appears that the inhibition of hypophysiotropic CRH neurons during starvation is caused at least partly by reduced fasting leptin levels. Similarly as in

the case of hypophysiotropic TRH neurons, leptin-responsive α-MSH/CART and NPY/AGRP neurons were suggested as mediators of leptin action on CRH neurons: both cell groups have been described to innervate hypophysiotropic CRH neurons (107, 108), although the extent of these innervations has not been analysed quantitatively. Both α-MSH and CART have been shown to activate hypophysiotropic CRH neurons. Intracerebroventricular injection of a melanocortin agonist induces the expression of CRH heteronuclear RNA in the PVN, and increases circulating corticosterone levels in a CRH-dependent way (109, 110). Chronic central infusion of α-MSH to fasting animals restores CRH mRNA levels in the PVN to the fed state (99). The direct effect of α-MSH on CRH neurons is supported by the observation that about 30% of CRH neurons in the PVN were found to express MC4-R (110). The remaining part of CRH neurons might either express MC4-R under the detection level or express MC3-R, a possibility of which has not been investigated yet. Since the promoter region of the CRH gene contains a CRE (111), the activation of MC4 through increasing intracellular cAMP level and CREB phosphorylation possibly underlies the effect of α-MSH on CRH gene expression. The appearance of PCREB in about half of the hypophysiotropic CRH neurons in response to icv. α-MSH infusion also supports this idea (89). The stimulatory effect of CART on CRH neurons is suggested by data that CART increases CRH mRNA levels in hypothalamic explants, and when injected into the PVN, CART causes a rapid increase in plasma ACTH and corticosterone levels, through induction of CRH release (112).

The direct effects of NPY and AGRP on CRH production should be inhibitory, since all NPY receptors are coupled to Gi proteins (95), and AGRP, either as an antagonist or inverse agonist, antagonizes intracellular signaling of MC3 and MC4 receptors that are coupled to Gs proteins (71, 72, 76, 98). However, a single icv. administration of NPY markedly increases CRH mRNA in the PVN and elevates serum ACTH and corticosterone levels (113, 114). In contrast, continous icv. NPY infusion for 3 days to freely-feeding animals causes a dramatic decrease in CRH mRNA level in the PVN (unpublished data from our laboratory). Interestingly, in pregnancy, when NPY expression in the arcuate nucleus is elevated similarly as in starvation (115), a single dose of intracerebroventricularly administered NPY does not elevate CRH mRNA (114). Thus, it raises the possibility that a prolonged stimulation of NPY receptors on CRH neurons, probably occuring in starvation, is necessary to enforce effective

inhibition of CRH synthesis. In contrast, single NPY injections may simulate presynaptic stimulatory actions of NPY which was shown to reduce GABA-ergic inhibition of parvocellular PVN neurons (116). A stimulatory role was also suggested for AGRP because centrally injected AGRP increases ACTH levels (109), but its chronic (3 days) icv. administration did not change CRH mRNA levels in the PVN (unpublished data from our laboratory).

In summary, (i) the innervation of hypophysiotopic CRH neurons by AGRP/NPY and α-MSH/CART neurons, (ii) the inverse changes in neuropeptide mRNA expression of these cell groups in fasting, (iii) the types of G proteins to which the receptors of these peptides are coupled and (iv) at least partly the effects of these peptides on CRH neurons are all in favour of a hypothesis that during fasting, changes in the activity of AGRP/NPY and α-MSH/CART cells contribute to the fasting-induced suppression of CRH expression in the PVN **(Fig. 3)**. However, further studies should be performed to exactly determine the role of arcuate-derived peptides in the regulation of hypophysiotropic CRH neurons.

It is worth of note that CRH neurons were shown to contain leptin receptor-immunoreactivity (117), raising the possibility that direct action of leptin may also contribute to the regulation of CRH neurons by the energy availability.

Whether the inhibition of hypophysiotropic CRH neurons is an adaptive response to fasting is not yet understood. Since CRH has anorectic effects when injected into the PVN (118, 119), the fasting-induced suppression of CRH synthesis would be in concert with the hypothesis that hypophysiotropic CRH neurons might release CRH locally in the PVN and thus inhibit food intake. However, the role of CRH as a physiologically relevant endogenous anorexigenic signal has been questioned, because the daily pattern of CRH released in the PVN correlates inversely with the daily feeding pattern (120, 121). Alternatively, hypophysiotropic CRH neurons could inhibit food intake through axon-collaterals in other brain regions.

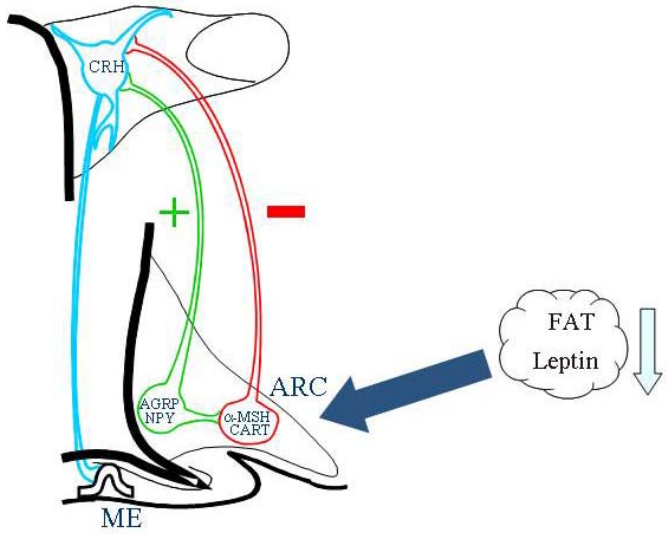

Figure 3. Presumed regulation of hypophysiotropic CRH neurons by leptin in fasting animals. Decreased circulating leptin causes a reduction in the synthesis of α-MSH and CART, while stimulates the expression of NPY and AGRP. This probably decreases the stimulatory and increases the inhibitory effects on CRH neurons, resulting in the inhibition of CRH production. ARC: arcuate nucleus, ME: median eminence.

Possible other feeding-related inputs to hypophysiotropic TRH and CRH neurons

Among the four arcuate nucleus-derived neuropeptides described above, the AGRP and α-MSH innervation of the PVN, and therefore, that of the hypophysiotropic TRH and CRH neurons, originate exclusively from the arcuate nucleus (50, 65, 122). In contrast, AGRP-containing NPY fibers of arcuate nucleus origin comprise only a portion of all NPY-containing axons in the PVN (123-125), and α-MSH-containing CART fibers constitute only a fraction of all CART-containing fibers in the PVN (65). Morphologic studies suggested that these NPY- and CART-containing axons arising outside the arcuate nucleus also contribute to the innervation of hypophysiotropic TRH and CRH neurons (65, 123, 126-128).

The NPY innervation of hypophysiotropic TRH neurons originates primarily from the arcuate nucleus (123). However, after pharmacological ablation of the arcuate nucleus, approximately 18% of close appositions between NPY fibers and TRH perikarya remain intact (123). The other major source of NPY innervation of the PVN originates from brainstem adrenergic and noradrenergic neurons (124). Since adrenergic fibers densely innervate the hypophysiotropic TRH neurons (126), and the majority of

adrenergic neurons in the C1-3 areas that project to the PVN co-express NPY (124), we raised the question whether adrenergic fibers contribute to the NPY-ergic innervation of hypophysiotropic TRH neurons.

Previous observation from our laboratory indicated that α-MSH/CART-containing axon varicosities constitute only a minor part of all CART-containing varicosities that are juxtaposed to the hypophysiotropic TRH neurons in the PVN (65). CART is widely expressed throughout the brain, also in many of the areas that are known to project to the PVN (129-131). Therefore, as a first step to identify possible CART-expressing cell groups outside the arcuate nucleus that innervate TRH and CRH neurons, we mapped the origin of CART innervation of the PVN by retrograde neuronal tract-tracing. The couple of CART cell populations found to project to the PVN included adrenergic neurons in the medulla, thus we also determined the ratio of adrenergic CART fibers in the total CART innervation of hypophysiotropic TRH neurons. In the course of examining the CART innervation of hypophysiotropic CRH neurons, we demonstrated the presence of synaptic associations between CART-containing nerve terminals and CRH neurons, and also performed a detailed quantitative analysis to reveal the contribution of α-MSH/CART fibers from the arcuate nucleus and adrenergic CART fibers from the medulla to the innervation of CRH neurons.

Our results demonstrated that medullary adrenergic neurons substantially contribute to the NPY and CART innervation of the hypophysiotropic TRH and CRH neurons. Several experiments suggest that adrenergic neurons mediate the effects of different types of physical stress, such as inflammatory processes and cold exposure (132-135). During the recent years, several pieces of evidence have emerged that adrenergic neurons are critical in the feeding and corticosterone responses to a metabolic stress, glucoprivation (136-138) (i.e. reduced cellular availability of glucose, generally induced either by insulin or 2-deoxy-glucose, a glycolytic inhibitor), most probably through increased NPY and catecholamine release from their nerve terminals (139-142). The activation of adrenergic neurons to hypoglycemia raised the possibility that fasting may also exert a potent effect on adrenergic neurons and their neuropeptide synthesis, that may contribute to the fasting-induced suppression of hypophysiotropic TRH and CRH neurons. Therefore, by quantitative *in situ* hybridization, we examined whether NPY and/or CART gene expression is altered in adrenergic neurons of the C1-3 areas in fasting animals.

We were also interested in finding out whether other peptidergic systems are also involved in the adaptation of the HPT axis to fasting. Galanin, a neuropeptide broadly distributed in the CNS (143, 144), has long been known as an orexigenic peptide (144-146), and its mRNA in the hypothalamus is regulated by leptin (147). A second member of the galanin peptide family, the recently discovered galanin-like peptide (GALP) (148) is synthesized exclusively in a cell population of the arcuate nucleus that is separate from the α-MSH/CART and AGRP/NPY neurons (149), has a profound orexigenic effect (150), and its expression is inhibited by leptin (151). Furthermore, both peptides have recently been shown to reduce the peripheral TSH levels after central administration and decrease TRH release from hypothalamic explants (152). Since both galanin- and GALP-containing axons innervate the PVN (149, 153), we determined whether galanin- and GALP-containing axon terminals are in anatomical position to directly regulate hypophysiotropic TRH neurons.

Specific Aims

1. Determine whether adrenergic NPY-containing axon terminals innervate hypophysiotropic TRH neurons
2. Delineate the precise location of CART-containing cell populations that innervate the PVN
3. Reveal the contribution of adrenergic CART-containing fibers to the CART innervation of TRH neurons
4. Demonstrate the presence of synaptic associations between CART-containing axon terminals and CRH neurons
5. Estimate the proportion of CART-containing afferents to CRH neurons that originate from the arcuate nucleus and adrenergic neurons of the medulla
6. Elucidate whether NPY and CART mRNA levels are changed during fasting in the C1-3 regions
7. Examine whether galanin- and GALP-containing axons innervate TRH neurons in the PVN

Materials and Methods

Animals

The experiments were carried out on adult male Wistar (TOXI-COOP KKT, Budapest, Hungary) and Sprague-Dawley (Taconic Farms, Germantown, NY) rats weighing 200-500g. The animals were kept under standard environmental conditions (light between 06:00-18:00 h, temperature 22±1°C, rat chow and water *ad libitum*). All experimental protocols were reviewed and approved by the Animal Research Committees at the Institute of Experimental Medicine of the Hungarian Academy of Sciences and Tufts-New England Medical Center.

Table 1 summarizes the main methods used in the experiments of the thesis.

Table 1. Summary of main methods used in different experiments of the thesis

Study	Method
PNMT/NPY-immunoreactive (IR) innervation of proTRH-IR neurons in the PVN	Triple-labeling immunofluorescence
CART-IR innervation of the PVN	Retrograde neuronal tract-tracing, double- and triple-labeling immunofluorescence
CART/PNMT-IR innervation of proTRH mRNA-containing perikarya in the PVN	Combined *in situ* hybridization and double-labeling immunofluorescence
Ultrastructural examination of CART-IR innervation of CRH-containing neurons in the PVN	Double-labeling immunocytochemistry at electron microscopic level
CART/PNMT-IR and CART/α-MSH-IR innervation of CRH neurons in the PVN	Quadruple-labeling immunofluorescence, confocal microscopic analysis
Expression of NPY and CART mRNA in medullary C1-3 areas in fasting rats	Quantitative isotopic *in situ* hybridization
Galanin- and GALP-IR innervation of proTRH neurons in the PVN	Double-labeling immunocytochemistry at light- and electron microscopic level

1. Triple-labeling immunofluorescence for detection of NPY- and PNMT-IR axons and proTRH-IR perikarya in the PVN

Animals (n=3) were deeply anesthetized with sodium pentobarbital (35 mg/kg body weight, ip.), and 100 μg colchicine in 5 μl 0.9% saline was stereotaxically injected into the lateral ventricle to increase the number of detected proTRH-IR neurons. After 20 hours of survival, the animals were perfused transcardially with 20 ml 0.01 M

phosphate-buffered saline (PBS), pH 7.4, followed sequentially by 100 ml of 3% paraformaldehyde/1% acrolein in 0.1M phosphate buffer (PB), pH 7.4, and 30 ml of 3% paraformaldehyde in the same buffer. Brains were removed and cryoprotected in 30% sucrose in PBS overnight and quickly frozen on dry ice. Serial 25 μm thick coronal sections were cut from the hypothalamus with a freezing microtome and stored in anti-freeze solution (30% ethylene glycol; 25% glycerol; 0.05M PB) at -20°C until use. The sections were treated for 30 min with 1% sodium borohydride, followed by 0.5% H_2O_2 and 0.5% Triton X-100 in PBS for 15 min. To reduce the nonspecific antibody binding, the sections were treated with 2% normal horse serum in PBS for 20 min.

Then, the tissue sections containing the PVN were incubated in a mixture of sheep anti-NPY (1:16.000; gift from Dr István Merchenthaler, University of Maryland, Baltimore, MD) and rabbit anti-phenylethanolamine-N-methyltransferase (PNMT) (1:1000; gift of Dr. Martha C. Bohn, Northwestern University Medical School, Chicago, IL) for 2 days at 4°C. All antisera were diluted in PBS containing 2% normal horse serum and 0.2% sodium-azide. The sections were rinsed in PBS and then incubated in a mixture of CY3-conjugated donkey anti-sheep IgG (1:200; Jackson ImmunoResearch, West Grove, PA) and fluorescein isothiocyanate (FITC)-conjugated donkey anti-rabbit IgG (1:50; Jackson) for 2 h. The tissues were then incubated in rabbit anti-proTRH 178-199 (1:2500, gift of Dr. Éva Rédei) for 2 days at 4°C, followed by incubation in 7-amino-4-methylcoumarin-3-acetic acid (AMCA)-conjugated donkey anti-rabbit IgG (1:50; Jackson) for 2 h.

The sections were mounted, coverslipped with Vectashield mounting medium (Vector Laboratories, Burlingame, CA), and analyzed under a Zeiss Axiophot epifluorescent microscope using the following filter sets: for CY3, excitation of 540–590 nm, bandpass of 595 nm, and emission of 600–660 nm; for FITC, excitation of 460–500 nm, bandpass of 505 nm, and emission of 510–560 nm; and for AMCA, excitation of 320–400 nm, bandpass of 400 nm, and emission of 430–490 nm. Thus, NPY-containing fibers (labeled by CY3) were labeled in red, PNMT-containing fibers (labeled by FITC) were labeled in green, and proTRH-containing perikarya (labeled by AMCA) were labeled in blue under their respective filter sets. Images were captured with an RT Spot digital camera (Diagnostic Instrument, Sterling Heights, MI). The same field was triple-exposed while switching the filter sets for each fluorochrome and superimposed using Adobe Photoshop (Adobe Systems Incorporated, San Jose, CA)

and an IBM compatible personal computer to create composite images for analysis. Fibers co-containing both NPY and PNMT appeared yellow in the composite images. Axon varicosities that were juxtaposed to proTRH-IR neurons and contained NPY, PNMT or NPY plus PNMT were counted on superimposed images of periventricular and medial parvocellular subdivisions of the PVN. Four sections of each brain were analyzed. The ratios of all NPY vs. the NPY/PNMT varicosities and all PNMT vs. NPY/PNMT varicosities were calculated in each brain. Data are presented as means ± standard error of the mean (SEM).

2. Mapping the origin of CART-IR innervation of the PVN

2. a) Retrograde neuronal tract-tracing

To elucidate the origin of CART-IR fibers innervating the PVN, the retrogradely transported cholera toxin subunit β (CTB) (List Biological Labs, Campbell, CA) was injected into 10 animals by iontophoresis (Stoelting, Wood Dale, IL; 7.0 μamps, pulsed at 7-second intervals, for 15 min) through a stereotaxically positioned glass micropipette (tip diameter 20 μm) into the parvocellular division of the PVN, based on the coordinates of the atlas of Paxinos and Watson (154). Following 6–7 day of transport time, the animals received 100 μg of colchicine by stereotaxic injection into the lateral ventricle and 24 hours later they were deeply anesthetized and perfused as described above. Through the forebrain and brainstem 25 μm thick sections were cut with freezing microtome (Leica Microsystems, Wetzlar, Germany), and collected in anti-freeze solution in four identical sets of sections from each of the brains and stored at -20°C until used.

For evaluation of injection sites, after pretreatments of the sections described above, every fourth section through the hypothalamus was incubated in goat anti-CTB serum (List Biological Labs) at 1:10.000 dilution for 2 days at 4°C. After rinses in PBS the sections were immersed in biotinylated donkey anti-sheep IgG (1:500; Jackson) for 2 hours and then in streptavidin-peroxidase (1:1000; Jackson) for 1 hour at room temperature. The immunoreaction was developed with 0.025% 3,3'-diaminobenzidine (DAB) and 0.0036% H_2O_2 in PBS. After mounting the sections were counterstained using Nissl's method. Brain sections from three animals with injection sites in the parvocellular PVN were used for further studies.

2. b) Mapping of the CART-IR neurons projecting to the PVN by double- and triple-labeling immunofluorescence

Three different immunostainings were performed. First, every fourth section through the forebrain and brainstem of each animal was reacted with anti-CART antibody and anti-CTB antiserum. Then a triple immunolabeling was performed to detect CART, CTB and melanin-concentrating hormone (MCH) in every fourth section of the hypothalamus. Finally, every fourth section through the medulla was immunostained for CART, CTB and PNMT. At each immunostaining, sections were incubated in the mixture of primary antibodies, followed by the mixture of secondary antibodies, listed in **Table 2**. Then sections were incubated in the avidin-biotin-peroxidase complex (ABC Elite, at 1:100, Vector) in PBS for 2 hours at room temperature. After intensification of the peroxidase signal in 0.1% biotinylated tyramide and 0.01% H_2O_2 in PBS (biotinylated tyramide amplification, (155)) for 10 minutes, the sections were incubated in FITC Avidin DCS (1:250; Vector).

Table 2. Antibodies used for mapping the CART-IR innervation of the PVN

Primary antibodies	**Secondary antibodies**
goat anti-CTB serum (List Biological Labs), 1:30.000	biotinylated donkey anti-sheep IgG (Jackson), 1:500
murine monoclonal antibody against CART, at 3.34 μg/ml (gift from Dr. Jes Thorn Clausen, Novo Nordisk, Bagsvaerd, Denmark)	CY3-conjugated donkey anti-mouse IgG (Jackson), 1:200
rabbit anti-PNMT serum (gift from Dr. Martha C. Bohn), 1:1000	AMCA-conjugated donkey anti-rabbit IgG (Jackson), 1:50
rabbit anti-MCH serum (gift from Dr. Eleftheria Maratos-Flier, Joslin Diabetes Center, Boston, MA)	AMCA-conjugated donkey anti-rabbit IgG (Jackson), 1:50

The sections were mounted and then analyzed under a Zeiss Axiophot epifluorescent microscope as described above. According to the emission spectra of used fluorochromes, FITC-labeled CTB-IR cells appeared in green, CY3-labeled CART-IR cells appeared in red, and AMCA-labeled MCH-IR and PNMT-IR cells

appeared in blue. Neurons co-containing both CTB and CART appeared yellow and neurons co-containing CART and MCH or PNMT appeared purple in the composite images. The distribution of double- or triple-labeled neurons were digitally mapped under 10× objective lens by superimposing each layer in Photoshop and assembling into camera lucida-like drawings of representative sections by using Corel Draw (Corel Corporation, Ottawa, Canada).

3. Combined in situ hybridization and double-labeling immunofluorescence detection of proTRH mRNA-containing perikarya and CART- and PNMT-IR axons in the PVN

Three animals were perfused with 20 ml diethylpyrocarbonate (DEPC)-treated PBS, followed by 150 ml 4% paraformaldehyde in PBS. The brains were removed and postfixed by immersion in the same fixative for 2 h at room temperature. Tissue blocks containing the hypothalamus were cryoprotected in 20% sucrose in PBS at 4°C overnight, then frozen on dry ice. Serial 20 μm thick coronal sections through the rostrocaudal extent of the PVN were cut with a freezing microtome and collected in anti-freeze solution and stored at -20°C until used.

Serial sections through the PVN were washed in 2-fold concentration of standard sodium citrate (2×SSC), acetylated with 0.25% acetic anhydride in 0.1M triethanolamine for 10 min and then treated in 50, 70 and 50% acetone, for 5, 10 and 5 min, respectively. After further washes in 2×SSC for 2×5 min, the sections were hybridized with digoxigenin-11-UTP (Roche, Basel, Switzerland)-labeled cRNA probe for proTRH. Digoxigenin-labeled antisense proTRH cRNA was synthesized using a 1241 base pair cDNA template corresponding to the coding sequence of proTRH mRNA and portions of its 5' and 3' untranslated sequences (156). The hybridization was performed in PCR tubes in hybridization buffer (50% formamide, 2×SSC, 10% dextran sulfate, 0.5% sodium dodecyl sulfate, 250 μg/ml denatured salmon sperm DNA) containing the digoxigenin-labeled probe diluted at 1:50, for 16 h at 56°C. The sections were washed in 1×SSC for 15 min and then treated with RNase A (100 μg/ml) for 1 h at 37°C. After additional washes in 1×SSC (15 min), 0.5×SSC (15 min) and 0.1×SSC (2×30 min) at 65°C, sections were washed in PBS, treated with the mixture of 0.5% Triton X-100 and 0.5% H_2O_2 for 15 min and then with 1% bovine serum albumin BSA; Sigma-Aldrich Co., St. Louis, MO) in PBS for 20 min to reduce the nonspecific antibody binding. The sections were incubated in Fab fragments of sheep anti-

digoxigenin antibody, conjugated with peroxidase (1:100, Roche) in 1% BSA in PBS overnight at 4°C. The sections were rinsed in PBS and then the biotinylated tyramide amplification was applied for 10 min. After further washes, the sections were incubated in AMCA-conjugated Avidin D (1:250, Vector) for 1 h. Then sections were transferred to the mixture of murine monoclonal anti-CART antibody (2.23 μg/ml, gift of Dr. Jes Thorn Clausen) and rabbit anti-PNMT serum (1:1000, gift of Dr. Martha C. Bohn) for 2 days at 4°C, and then incubated in a mixture of CY3-conjugated donkey anti-mouse IgG (1:100; Jackson) and FITC-conjugated donkey anti-rabbit IgG (1:50; Jackson) for 2 h. The sections were mounted onto glass slides, coverslipped with Vectashield mounting medium (Vector), and analyzed under a Zeiss Axiophot epifluorescent microscope as describe above. Varicosities co-containing both CART and PNMT appeared yellow in the composite images. The number of axon varicosities containing only CART, only PNMT or both CART and PNMT in juxtaposition to proTRH neurons were counted on superimposed images of three animals. The ratio of all CART vs. the CART/PNMT varicosities and all PNMT vs. CART/PNMT varicosities were calculated in each brain. Data are presented as mean ± SEM. Presented images were captured by a Radiance 2100 confocal microscope (Bio-Rad Laboratories, Hemel Hempstead, UK) using the following laser excitation lines: 405 nm for AMCA, 488 nm for FITC, 543 nm for CY3; and dichroic/emission filters: 500 nm/420–480 nm for AMCA, 560 nm/500–530 nm for FITC and 570–625 for CY3.

4. Ultrastructural examination of CART-IR innervation of CRH-containing neurons in the PVN

Three animals received 60 μg colchicine in 3 μl 0.9% saline intracerebroventricularly, and after 20 h survival they were perfused with 2% paraformaldehyde/4% acrolein in 0.1M PB, and 30 ml of 2% paraformaldehyde. The brains were rapidly removed and stored in PBS for 24 h at 4°C. Serial 25 μm thick coronal sections were cut on a vibratome through the rostro-caudal extent of the PVN. Then the sections were treated with 1% sodium borohydride in 0.1M PB for 30 min, followed by 0.5% H_2O_2 in PBS for 15 min. The sections were cryoprotected in 15% sucrose in PBS for 15 min at room temperature and in 30% sucrose in PBS overnight at 4°C and quickly frozen on liquid nitrogen to improve antibody penetration into the tissue. To reduce the nonspecific antibody binding, the sections were treated with 2%

normal horse serum in PBS for 20 min. Sections were incubated in the murine monoclonal CART antibody (gift from Dr. Jes Thorn Clausen) at 0.56 μg/ml concentration for 4 days at 4°C, followed by biotinylated donkey anti-mouse IgG (1:500; Jackson) for 3 h, and ABC (1:1000; Vector) for 2 h at room temperature. Immunoreactivity was detected in 0.025% DAB/ 0.0036% H_2O_2 in 0.05 M Tris buffer (TB), pH 7.6. The sections were then placed into rabbit anti-CRH serum (code C70, gift of Dr. Paul E. Sawchenko, Salk Institute, La Jolla, CA) at 1:3000 dilution for 2 days at 4°C and, after rinsing in PBS and 0.1% cold water fish gelatin-1% BSA in PBS, were incubated in goat anti-rabbit IgG conjugated with 0.8 nm colloidal gold (Electron Microscopy Sciences, Fort Washington, PA) diluted at 1:100 in PBS containing 0.1% cold water fish gelatin and 1% BSA, for 2 h. The sections were washed in the same diluent and PBS, followed by a 10 min treatment in 1.25% glutaraldehyde in PBS. After rinsing in 0.2M sodium citrate, pH 7.5, the gold particles were silver intensified with IntenSE Kit (Amersham-Pharmacia Biotech UK, Buckinghamshire, UK). Sections were treated with 1% osmium tetroxide in 0.1M PB for 30 min, dehydrated in an ascending series of ethanol followed by propylene oxide, flat embedded in Durcupan ACM epoxy resin (Fluka, Ronkonkoma, NY) on liquid release agent (Electron Microscopy Sciences)-coated slides, placed at 56 °C for 2 days to allow polymerization of the resin. Ultrathin 50–60 nm thin sections were cut with a Leica ultracut UCT ultramicrotome (Leica Microsystems), collected onto Formvar-coated single-slot grids, contrasted with 2% uranyl acetate and examined with a Hitachi electron microscope.

5. Quadruple-labeling immunofluorescence and confocal microscopic analysis for CART-, PNMT- and α-MSH-IR innervation of CRH neurons in the PVN

Three animals received 40 μg icv. colchicine in 2 μl 0.9% saline, and after 20 h survival were perfused with 2% paraformaldehyde/4% acrolein in 0.1M PB, and 30 ml of 2% paraformaldehyde in the same buffer. The brains were rapidly removed and cryoprotected in 30% sucrose in PBS overnight at 4°C. Serial 40 μm sections were cut through the PVN with freezing microtome. Every third section was processed for immunocytochemistry as described above. Then, sections were immersed in the mixture of primary antibodies for 3 days at 4°C, followed by the mixture of secondary antibodies for 1 day at 4°C, and AMCA Avidin D for 1 day at 4°C (**Table 3.**). The

sections were mounted onto glass slides and coverslipped with Vectashield mounting medium (Vector).

Table 3. Reagents used in quadruple-labeling immunofluorescence for CART, PNMT, α-MSH and CRH in the PVN

Primary antibodies	**Secondary antibodies**	**Avidin**
murine monoclonal antibody to CART at 3.34 μg/ml (gift of Dr. Jes Thorn Clausen)	CY3-conjugated donkey anti-mouse IgG (Jackson), 1:200	
guinea pig anti-CRH serum, 1:3500, (Peninsula Laboratories, San Carlos, CA)	biotinylated donkey anti-guinea pig IgG (Jackson), 1:250	AMCA-conjugated avidin D, 1:200 (Vector)
sheep anti-α-MSH serum, 1:2000 (gift of Dr. Jeffrey B. Tatro, Tufts University, Boston, MA)	CY5-conjugated donkey anti-sheep IgG (Jackson), 1:100	
rabbit anti-PNMT serum, 1:500 (gift of Dr. Martha C. Bohn)	FITC-conjugated donkey anti-rabbit IgG (Jackson), 1:50	

The quadruple-labeled sections were examined using a Radiance 2100 confocal microscope (Bio-Rad). From each brain, at least three sections were analyzed from different rostrocaudal levels of the medial parvocellular subdivision of the PVN in which hypophysiotropic CRH neurons are located. With 60× oil lens, 180×180 μm areas of the entire medial parvocellular subdivision of the PVN in each section were recorded. Two consecutive scans were recorded from each area. The first scan was for FITC, CY3, and CY5 (laser excitation lines 488 nm for FITC, 543 nm for CY3, and 637 nm for CY5; dichroic/emission filters, 560/500–530 nm for FITC, 650/570–625 nm for CY3, and a 660 nm long pass filter for CY5). The second scan was for AMCA (laser excitation line 405 nm and emission filter 420–480 nm). Pinhole sizes were set to obtain optical slices less than 0.7 μm thick, and the series of optical slices were recorded with a 0.6 μm Z step. The series of optical sections were merged and displayed with LaserVox (Bio-Rad) and Image Pro Plus software (Media Cybernetics, Bethesda, MD) and an IBM compatible personal computer. Tracing individual CRH-IR neurons and their dendrites through the series of optical sections, the number of axon varicosities containing only CART, only PNMT, both CART and PNMT, and both CART and α-MSH in juxtaposition to CRH neurons were counted. A varicosity was considered in

contact with or juxtaposed to CRH neurons if a gap could not be recognized between the two profiles by confocal microscopy. CRH neurons were included in the analyses only if the entire cell body of the neuron was contained within the stack of the optical sections. Data are presented as mean ± SEM.

To illustrate quadruple-labeling, we used the three basic colors (red, green, and blue) and show pairs of triple-colored images of the same field and magnification in adjacent figures. Thus, CART, CRH, and PNMT immunoreactivities were displayed in one image, whereas CART, CRH, and α-MSH immunoreactivities were shown in the second image. Accordingly, CART and CRH immunoreactivities were displayed in *red* and *blue*, respectively, in both images, whereas the *green* color labeled either PNMT or α-MSH immunoreactivity. Therefore, CART/PNMT-IR and CART/α-MSH-IR double-labeled axons appeared *yellow*. All presented images represent single optical slices. Images captured through 20× objective are less than 2.1 μm thick, whereas images captured through 60× oil lens are less than 0.7 μm thick.

To exclude the possibility that CY3-conjugated anti-mouse IgG binds to the PNMT antibody or that the FITC signal denoting PNMT immunofluorescence is seen in the red channel causing false PNMT and CART double labeling, we performed several control experiments. After the incubation in rabbit anti-PNMT serum, the sections were transferred into the mixture of FITC-conjugated anti-rabbit IgG and CY3-conjugated anti-mouse IgG without incubation in mouse CART antibody. Scanning the sections with confocal laser microscope using the same scanning method described above and the same settings, we found a dense PNMT-IR fiber network, but no signal was detected between 570 and 625 nm wavelengths, corresponding to the emission of CY3. We also performed sequential double immunostainings for CART and PNMT, staining first with anti-CART serum, followed by anti-PNMT serum and *vice versa*. Both resulted in the same degree of colocalizaton, excluding the possibility that the high level of colocalization was the result of any cross-reactivity.

6. Isotopic in situ hybridization for NPY and CART in the medulla of fed and fasted animals

Adult male rats were either fasted (n=8) for 64 hours or fed *ad libitum* (n=8). Animals were perfused transcardially with 20 ml of 0.01M PBS, pH 7.4, followed by 150 ml of 4% paraformaldehyde in 0.1M PB. The brains were removed and post-fixed

by immersion in the same fixative for 2 h at room temperature. Tissue blocks containing the medulla were cryoprotected in 20% sucrose in PBS at 4°C overnight and then frozen on dry ice. Serial 18 μm thick coronal sections through the medulla were cut on a cryostat (Leica Microsystems) and adhered to Superfrost Plus glass slides (Fisher Scientific, Pittsburgh, PA) to obtain four sets of slides, each containing every fourth section through the medulla. The tissue sections were desiccated overnight at 42°C and stored at -80°C until prepared for *in situ* hybridization histochemistry.

Plasmids containing a 431 bp fragment of rat NPY (donated by Dr. Erik Hrabovszky), corresponding to bases 65-495 of rat NPY mRNA (GenBank accession no. NM 012614) and rat CART cDNA of 866 bp (gift of Dr. Michael J. Kuhar) corresponding to the long splice variant of rat CART mRNA were linearized using Apa I or Not I, respectively, purified with phenol/chloroform extraction and then ethanol-precipitated. Linearized plasmids were transcribed for antisense riboprobes with SP6 (for NPY) and T7 (for CART) polymerases in the presence of ^{35}S-UTP (PerkinElmer, Waltham, USA). Incorporation of radioisotope into the RNA probes was quantified in a scintillation counter.

The sections of the medulla were removed from the freezer, washed in 0.1M PBS (0.1M phosphate buffer, pH=7.5, and 0.5% NaCl) for 5 min, and then placed into 10 μg/ml proteinase K in 0.1M Tris, pH 8.0, containing 0.05M EDTA at 37 °C for 30 min. Then sections were put into 4% paraformaldehyde in 0.1M PBS for 5 min to stop proteinase reaction. After washing in PBS two times for 5 min, sections were placed in 0.1M triethanolamine with 0.25% acetic anhydride for 10 min. After rinsing in 0.1M PBS, sections were dehydrated in graded ethanol solutions (80, 96, 100%; 1 min each) and placed into chloroform for 10 min. After immersion in 100% and 96% ethanol for 1 min, sections were allowed to air-dry before the hybridization procedure. The hybridization was performed under plastic coverslips in a buffer containing 50% formamide, 2×SSC, 0.25M Tris (pH 8.0), Denhardt's solution, 10% dextran sulfate, 0.5% sodium dodecyl sulfate, 265 μg/ml denatured salmon sperm DNA, 40 mM dithiothreitol and 3×10^4 cpm/μl of radiolabeled probe for NPY or CART. Hybridized sections were placed in humidity chambers in ovens at 52°C for 16 hr. Following hybridization, slides were washed in 1×SSC for 15 min and then incubated for 1h at 37 °C in RNase buffer (10mM Tris, 0.5M NaCl, 1mM EDTA, pH 8.0) containing 50 μg/ml RNase A. After washing in 1×SSC and 0.5×SSC for 15 min, slides were incubated

twice in 0.1×SSC at 65 °C for 30 min. Sections were then dehydrated in graded ethanol solutions (80, 96, 100%; 1 min each) and allowed to air-dry.

Slides were dipped into Kodak NTB autoradiography emulsion (Eastman Kodak, Rochester, NY), placed in light-tight boxes containing desiccant and stored at 4°C. After 8d (NPY) or 10d (CART) of exposure, the autoradiograms were developed using Kodak D19 developer, and slides were coverslipped with DPX mounting medium (Sigma-Aldrich). Autoradiograms were studied at 10× objective lens under darkfield illumination of a Zeiss Axiophot microscope. The images were captured with RT Spot digital camera (Diagnostic Instrument) and analyzed by using ImageJ image analysis software (public domain at http://rsb.info.nih.gov/ij/download/src/). Background density points were removed by thresholding the images, and areas, mean gray values and integrated density values (area × mean gray value) of hybridized neurons were measured bilaterally in 3 sections for C1, and 4 sections for C2 and C3 areas for each animal. For each regions in the fed and fasted group, numbers of hybridized cells, area/cell, mean gray value/cell and integrated density value/cell were expressed as means ± SEM. Differences in these parameters between fed and fasted animals were tested for statistical significance by paired Student's t-test using Statistica 7.0 software (StatSoft Inc., Tulsa, OK), after testing homogeneity of variance (Levene's test).

7. a) Double-labeling immunocytochemistry at light microscopic level for galanin- and GALP-IR innervation of proTRH neurons in the PVN

Three animals were injected intracerebroventricularly with 60 μg colchicine in 3 μl 0.9% saline. After 20 hours of survival the animals were perfused, brains were removed, coronal hypothalamic sections were cut and were processed for immunocytochemistry similarly as described in *method 1*. The sections were incubated in rabbit anti-galanin serum (1:750.000, gift of Dr. István Merchenthaler) for 2 days at 4°C, rinsed in PBS, and then incubated in biotinylated donkey anti-sheep IgG at 1:500 dilution (Jackson) for 2 h. The sections were then immersed in streptavidin–peroxidase (Jackson) at 1:1000 dilution for 2 h, and the immunoreaction was developed in 0.05% DAB containing 0.15% Ni-ammonium-sulfate and 0.005% H_2O_2 in 0.05 M TB, pH 7.6. The reaction was stopped by immersion of the tissue sections in 0.05M TB, pH 7.6, and the reaction product was further intensified by Gallyas-silver intensification technique (157) without thioglycolic acid for less then 5 min (63, 158) to yield a black precipitate. After

additional washes, the sections were incubated in rabbit anti-proTRH 178–199 serum (gift from Dr. Éva Rédei) at 1:20.000 dilution for 2 days at 4°C. The sections were then washed in PBS and incubated in biotinylated mouse anti-rabbit IgG (Jackson) at 1:500 dilution for 2 h, and after further washes in PBS, incubated in streptavidin-peroxidase at 1:1000 dilution for 2 h. After three washes in PBS, the reaction was developed in 0.025% DAB containing 0.0036% H_2O_2 in 0.05 M TB, pH 7.6, to yield a contrasting brown reaction product. No immunoreaction product or endogenous argyrophilia was observed under these conditions if the primary antibody was omitted.

The method of immunocytochemical labeling for GALP-IR innervation of TRH neurons was essentially the same as for galanin/proTRH double-labeling, except that the biotinylated tyramide amplification was used to enhance GALP-immunoreactivity, and the Ni-DAB precipitate was not silver-intensified. The detailed procedure of immunostaining is included in paper 4. For detection of GALP, a murine monoclonal antibody was used (gift of Dr. Yoshihiro Takatsu, Takeda Chemical Industries Co., Japan) at a dilution of 1:8000.

The frequency of close appositions between galanin- or GALP-IR axon varicosities and proTRH neurons was counted by direct light microscopic examination of the PVN sections under 100× objective lens. Data are presented as mean ± SEM.

7. b) Double-labeling immunocytochemistry at electron microscopic level for galanin-IR innervation of proTRH neurons in the PVN

For electron microscopic examination of galanin-IR axons and proTRH-IR profiles, the colchicine treatment and the perfusion of the animals were the same as for the light microscopic experiment. Brain sectioning and the method of immunolabeling for electron microscopy was the same as previously described in *method 5*. The dilutions of the used antisera were the followings: sheep anti-galanin serum at 1:60.000, biotinylated donkey anti-sheep IgG at 1:500, rabbit anti-proTRH 178-199 serum at 1:8000, and goat anti-rabbit IgG conjugated with 0.8 nm colloidal gold (Electron Microscopy Sciences) at 1:100.

Specificity of the used primary antisera and hybridization signals

In most cases, specificity controls of used antisera were described previously, that are referred. Immunsera are listed in alphabetical order.

sheep anti-α-MSH serum (gift of Dr. Jeffrey B. Tatro): Described in detail in ref. (159). Briefly, prior to immunocytochemical studies, antiserum specificity was determined with radioimmunoassay by using iodine 125 (125I)-α-MSH as tracer. The antiserum is highly specific for α-MSH (with no apparent cross reactivity with MCH) and is dependent on the amidated C-terminal region for recognition. For immunocytochemical control, all specific staining was abolished when rat hypothalamic sections were incubated in α-MSH antiserum that had been preadsorbed with α-MSH (50 μg/ml of diluted antisera).

murine monoclonal antibody against CART (gift of Dr. Jes Thorn Clausen): As shown by HPLC, the monoclonal antibody reacts with CART 42–89 and CART 49–89 peptides, isolated from extracts of rat hypothalamus (160).

guinea pig anti-CRH serum (Peninsula Lab): The specificity of this serum was determined by double immunostaining with rabbit anti-CRH serum (Peninsula Lab), the specificity of which has been demonstrated by the total loss of immunolabeling after preadsorption the antiserum with the excess of synthetic CRH (10^{-5} M) (161). Double-labeling immunocytochemistry showed that guinea pig anti-CRH serum labeled exactly the same neurons in the medial parvocellular subdivision of the PVN as did the rabbit anti-CRH serum.

rabbit anti-CRH serum, C70 (gift of Dr. Paul. E. Sawchenko): Specific staining was eliminated by prior adsorption with the immunogen rat CRH (162).

goat anti-CTB serum (List Biological Labs): Staining with this serum gave only a faint labeling of the ependyma layer when, in missed cases, CTB was injected into the third ventricle.

sheep anti-galanin serum (gift of Dr. István Merchenthaler): Specific staining was abolished by preincubation of the serum with the immunogen rat galanin (163).

murine monoclonal antibody against GALP (gift of Dr. Yoshihiro Takatsu): This monoclonal antibody is directed toward the rat GALP 1–9 sequence, which is specific to GALP and is not shared with galanin. The specificity of immunostaining was confirmed by preadsorption studies in which the immunostaining was blocked with GALP but not with galanin (149).

rabbit anti-MCH serum (gift of Dr. Eleftheria Maratos-Flier): All specific staining was abolished when rat hypothalamic sections were incubated in antiserum that had been preadsorbed with MCH (50 μg/ml of diluted antisera) (159).

sheep anti-NPY serum (gift of Dr. István Merchenthaler): The specificity of immunostaining with NPY antiserum was demonstrated by the loss of immunoreactivity after preadsorption of the diluted antiserum with an excess of synthetic NPY peptide (1 μg/ml) (data not shown).

rabbit anti-PNMT serum (gift of Dr. Martha C. Bohn): This antiserum was determined to be specific for several criteria: (I) it recognized a single band corresponding to the single 35 kDa band obtained with the purified antigen on an immunoblot of adrenal proteins; (II) it did not recognize any band in liver, lung, spleen or cerebral cortex; and (III) it specifically stained soma in adrenal medulla and the C1-C3 cell groups of brainstem at a dilution of 1:2000, but did not stain soma in the locus coeruleus, adrenal cortex or superior cervical ganglia of adult rat when used at a dilution of 1:100 (164). In the hypothalamus, stained fibers had a very characteristic appearance, because PNMT-staining filled the whole length of axons including long intervaricose segments, due to the cytosolic localisation of PNMT.

rabbit anti-proTRH 178-199 serum (gift of Dr. Éva Rédei): This serum was shown by electrophoretic separation of immunoprecipitated radiolabeled peptides from rat hypothalamic neurons in culture to recognize a 2.6 kDa peptide characteristic of prepro-TRH 178–199 (99).

The distributions of all stained peptides and PNMT are well characterized in the rat brain. Therefore, in addition to the previously described controls, the high specificity of antisera are strongly suggested because for all peptides and PNMT we observed the same pattern of labeling in examined regions that is described in the literature. Furthermore, perikaryal labeling of all these antibodies corresponded to *in situ* hybridization patterns of the respective transcripts.

The patterns of *in situ* hybridization histochemistry for proTRH mRNA in the hypothalamus, and NPY and CART mRNA in the medulla were identical to those described earlier (129, 165, 166).

Results

1. Adrenergic NPY neurons contribute to the innervation of TRH neurons in the PVN

NPY-IR axon varicosities were found in close juxtaposition to all proTRH-containing neurons in the periventricular and medial parvocellular subdivisions of the PVN. In most instances, the NPY-IR innervation was so intense that varicosities completely outlined the cell surface of proTRH-IR neurons (**Fig. 4 A**). Axon varicosities immunoreactive for phenylethanolamine-N-methyltransferase (PNMT), the adrenaline-synthesizing enzyme, were similarly closely apposed to the majority of proTRH-synthesizing neurons but less densely than NPY-IR fibers (**Fig. 4 B**). Superimposed images of the three fluorochromes revealed that the majority (74.8 ± 1.1%) of PNMT-IR fibers in contact with proTRH-IR neurons also contained NPY-immunoreactivity (**Fig. 4 C**, **D**). By semiquantitative analysis, PNMT-immunoreactivity was found in 26.6 ± 2.2% of NPY-IR axon varicosities in close apposition to proTRH neurons. Both NPY- and NPY/PNMT-IR fibers distributed uniformly around the perikarya and the dendrites of the proTRH-IR neurons (**Fig. 4 C**, **D**).

2. Origin of CART-IR innervation of the PVN

a) Localization of CTB injection sites

CTB injection sites were centered in the parvocellular parts of the PVN in three animals (**Figs. 5**, **6**). These injection sites were confined primarily to the PVN as shown both by counterstaining (**Fig. 5**) and by double immunofluorescence showing the overlap of CTB injection sites with the cluster of CART neurons that resides within the PVN (**Fig. 6**). The brains of these three animals were used for further studies. Of note, whereas the PVN contained a dense CART innervation, the region lying immediately outside the perimeter of the PVN contained only a low density of CART-IR axons (**Fig. 7**), making any tracer spread into this region unlikely to significantly contribute to the retrograde accumulation of CTB in CART-containing neurons.

b) Distribution of double-labeled CART/CTB neurons

The distribution of double-labeled CART/CTB neurons was similar in all three brains. Numerous double-labeled CART/CTB-IR neurons were found in the retrochiasmatic area, arcuate nucleus, zona incerta, lateral hypothalamus / perifornical

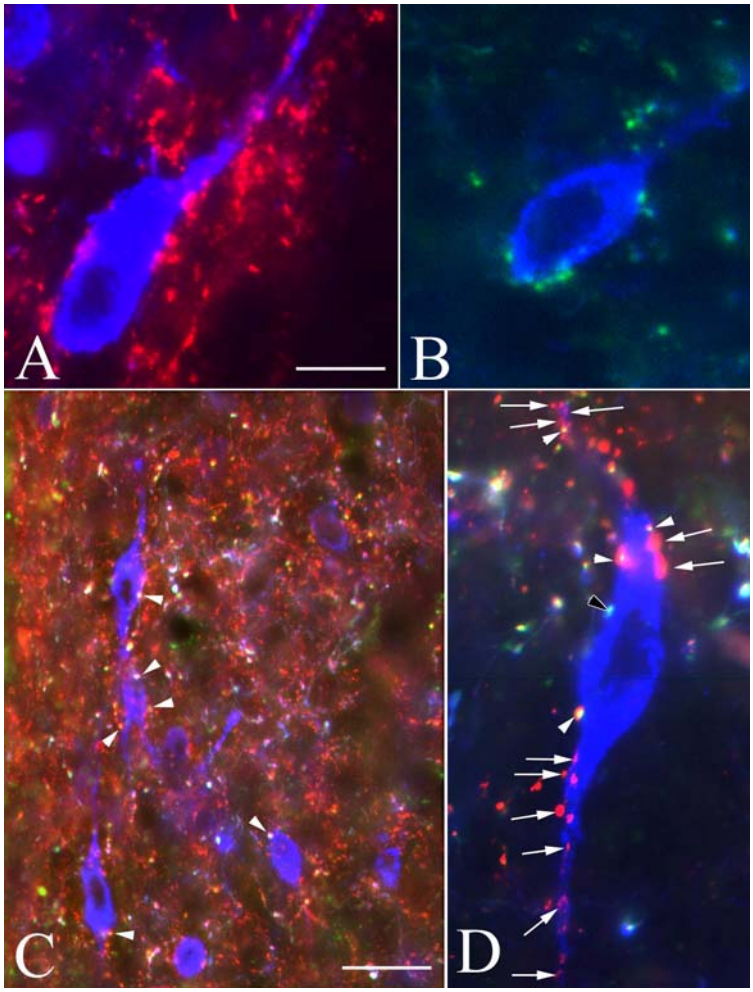

Fig. 4. Colocalization of NPY- and PNMT-immunoreactivity in axon terminals juxtaposed to proTRH-IR neurons. (**A**) NPY-containing axon varicosities (red) outline the surface of the proTRH-IR neuron (blue) in the PVN. (**B**) PNMT-IR axons (green) establish contacts with a proTRH neuron in the PVN. (**C**) A medium power composite image demonstrates that the proTRH-IR neurons in the PVN are embedded in a network of NPY-IR (red), PNMT/NPY-IR (yellow) and PNMT-IR (green) axons. Note that NPY- and NPY/PNMT-IR fibers (arrowheads) densely innervate the proTRH neurons in the PVN. (**D**) A high power image illustrates PNMT- (black arrowhead), NPY- (arrows) and NPY/PNMT-IR axon varicosities (white arrowheads) in contact with a proTRH-IR neuron. Scale bars: 10 µm in **A** corresponds to **A**, **B**, **D**; 25 µm in **C**.

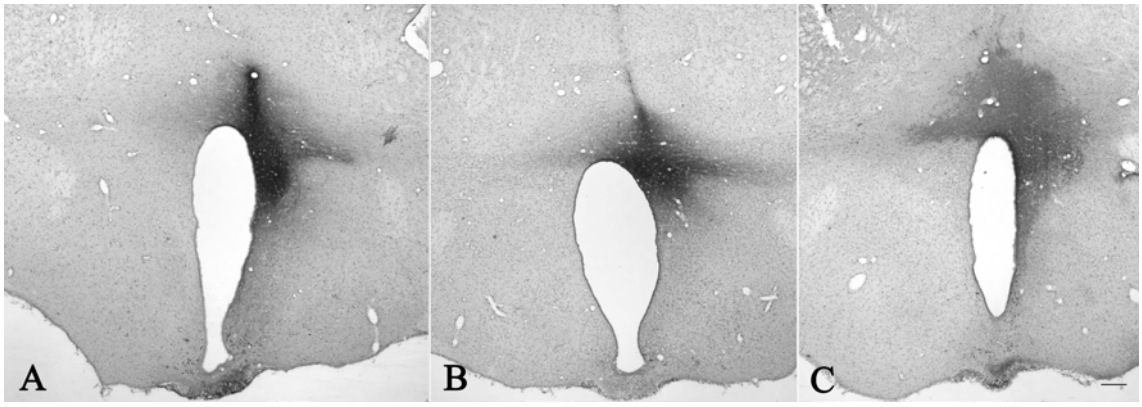

Fig. 5. Location of the CTB injection sites in the PVN (Nissl-stained sections). Scale bar: 400 µm.

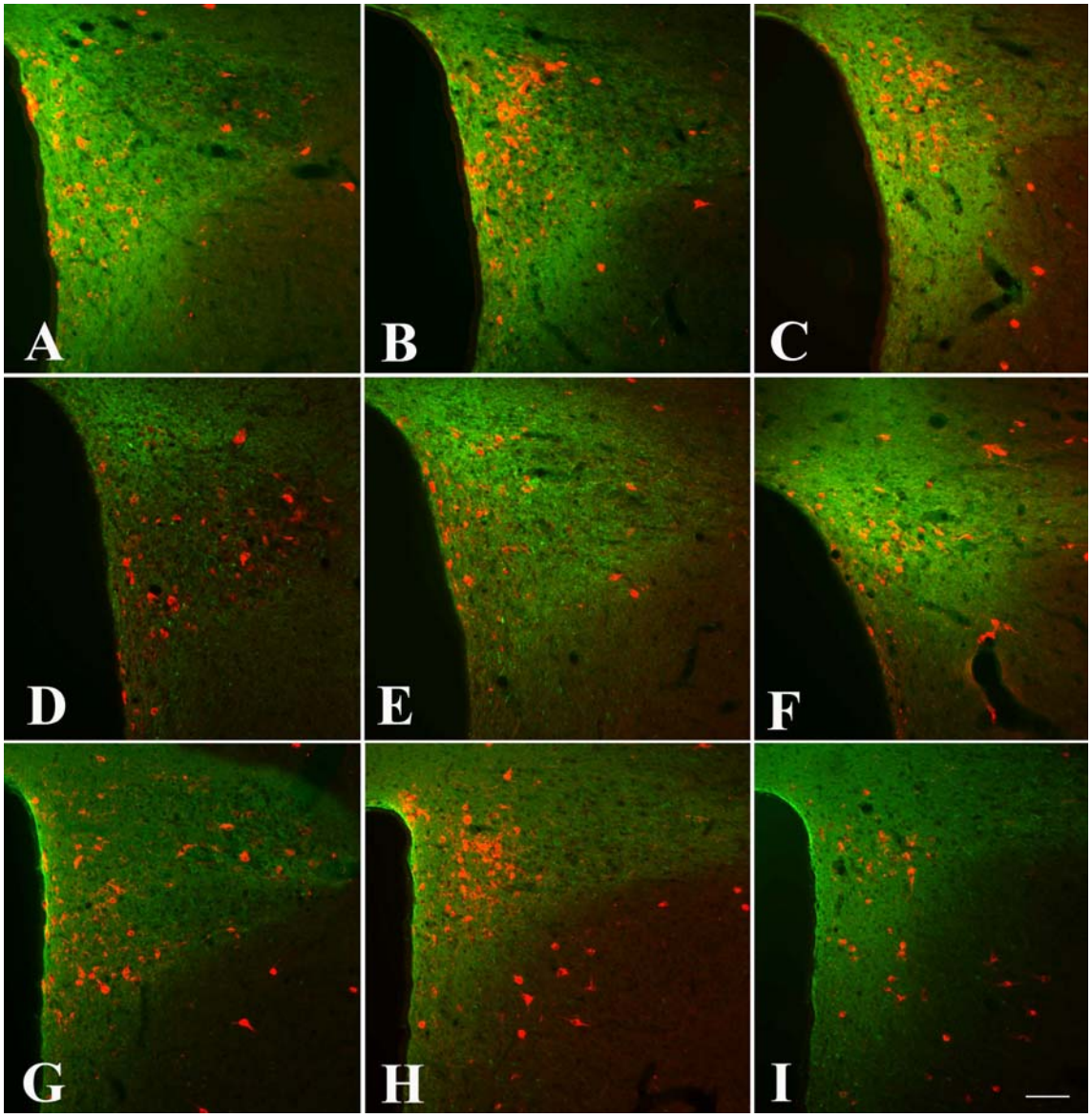

Fig. 6. Double-labeled fluorescent images showing the localization of CTB injection sites (green) using CART-IR neurons (red) as a marker of PVN. The figure demonstrates the location and extent of the injection sites in three brains (**A-C**, **D-F** and **G-I**) in three different anterior-posterior levels of the PVN (anterior (**A**, **D**, **G**), mid (**B**, **E**, **H**) and posterior (**C**, **F**, **I**)). Scale bar: 200 µm.

area, C1-3 areas of the brainstem, and medial subnucleus of the nucleus tractus solitarius (NTS) (**Figs. 8-10**). While the double-labeled neurons in forebrain regions were observed mainly on the side of the injection, neurons both ipsilateral and contralateral to the injection site were observed in the NTS and C1-3 (**Figs. 8-10**). Scattered double-labeled neurons were also found bilaterally in the medial and lateral parts of the parabrachial nucleus.

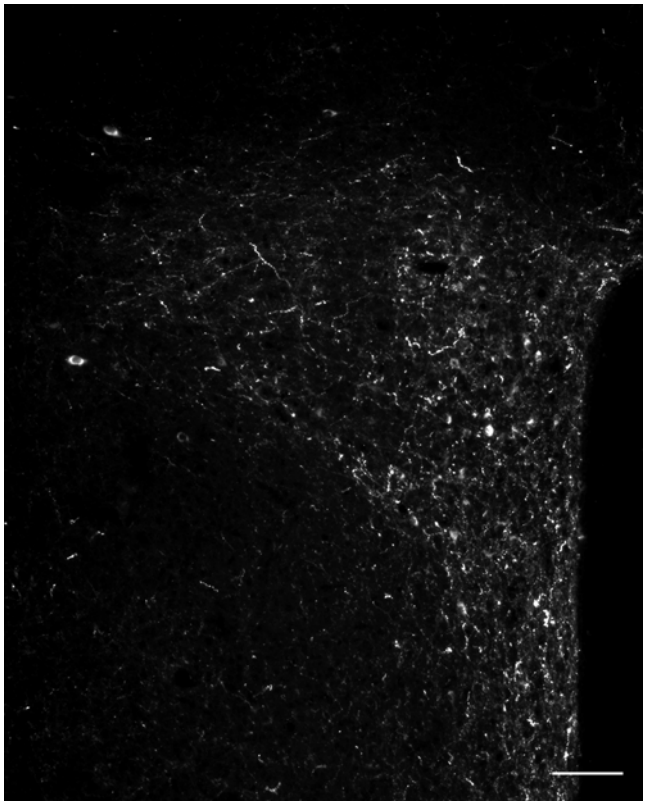

Fig. 7. Distribution of CART-IR axons in intact rats in and around the PVN. Scale bar: 200 μm.

c) Colocalization of CART with other neurotransmitters in neurons projecting to the PVN

Since a subpopulation of CART-IR neurons in the hypothalamus has been reported to also contain melanin-concentrating hormone (MCH) (49, 167), we performed triple-labeling immunofluorescence to determine whether neurons that co-contain CART and MCH project to the PVN. In the zona incerta, lateral hypothalamus, and perifornical area, all neurons co-containing CTB and CART also expressed MCH (**Figs. 8**, **10**). In contrast, only rare MCH-positive but CART-negative neurons contained CTB.

As neurons in the C1-3 areas produce adrenaline (168), we also determined whether CART-containing neurons projecting to the PVN from this region contain PNMT, an enzyme commonly used as a marker of adrenergic neurons. As shown in **Figures 9** and **10**, the majority of CART neurons throughout the C2 and C3 areas contained PNMT, whereas in the C1 area the colocalization of CART and PNMT was found only in its rostral and middle portions; no CART-IR neurons were observed in the caudal part of the C1 region. Of the neurons in the C1-3 regions that co-contained CART and PNMT, the majority also contained CTB (**Figs. 9**, **10**). In contrast, none of the CART/CTB-containing neurons in the medial NTS contained PNMT (**Fig. 10 D**).

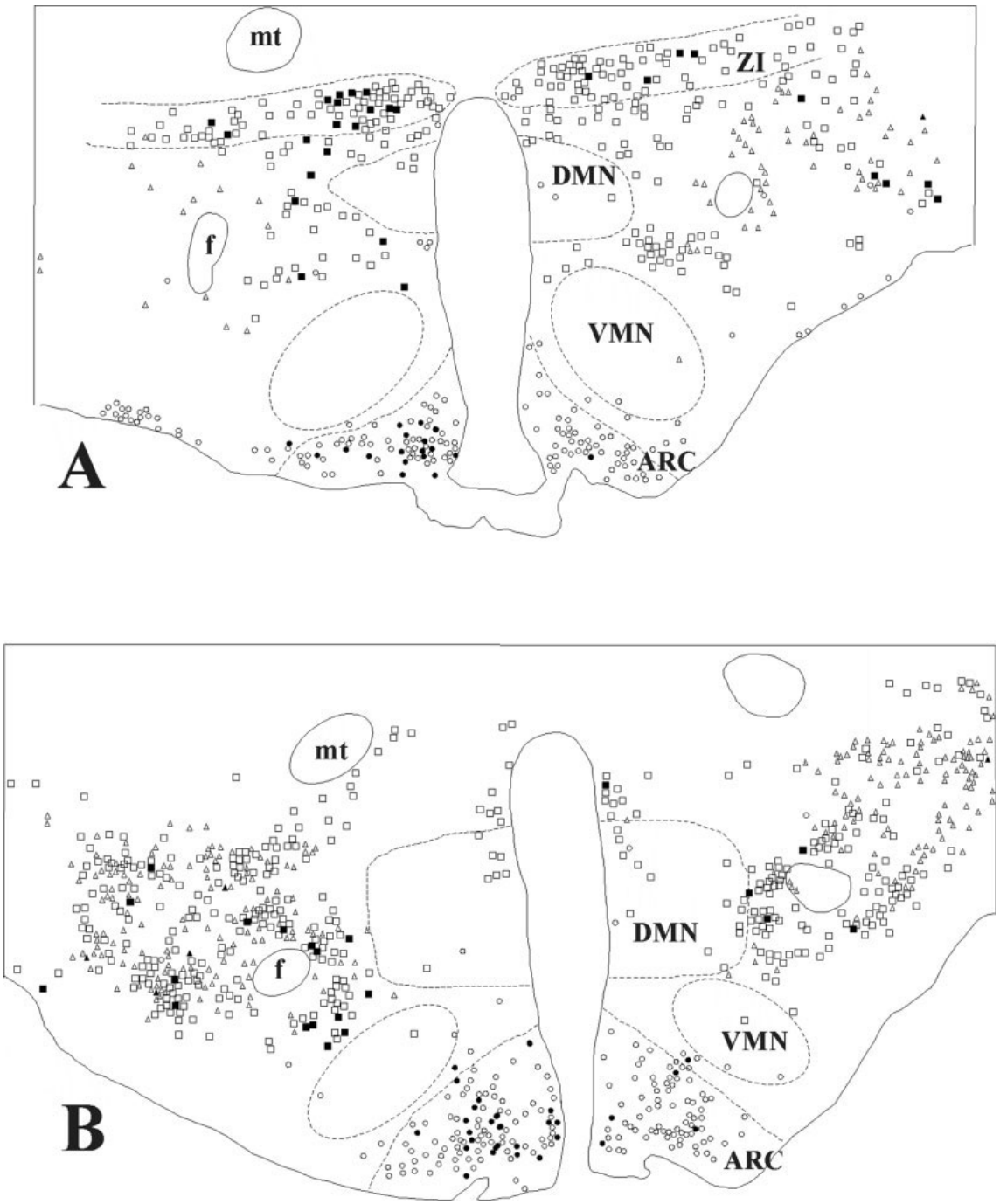

Fig. 8. (continued on the next page) Schematic maps showing the distribution of the CART-, MCH-, CART/MCH-, CART/CTB-, MCH/CTB-, and CART/MCH/CTB containing neurons in four anteroposterior levels of the hypothalamus **(A:** Bregma –2.80; **B:** Bregma –3.30; **C:** Bregma –3.60; **D:** Bregma –3.80). Note that the majority of CART/CTB neurons are ipsilateral to the injection site. The majority of CART neurons projecting to the PVN co-contain MCH in the lateral hypothalamus, perifornical area, and zona incerta. Symbols: open circle: CART; filled circle: CART/CTB; open square: CART/MCH; filled square: CART/CTB/MCH; open triangle: MCH; filled triangle: MCH/CTB. ARC, arcuate nucleus; DMN, dorsomedial nucleus; VMN, ventromedial nucleus; ZI, zona incerta; f, fornix; mt, mammilothalamic tract.

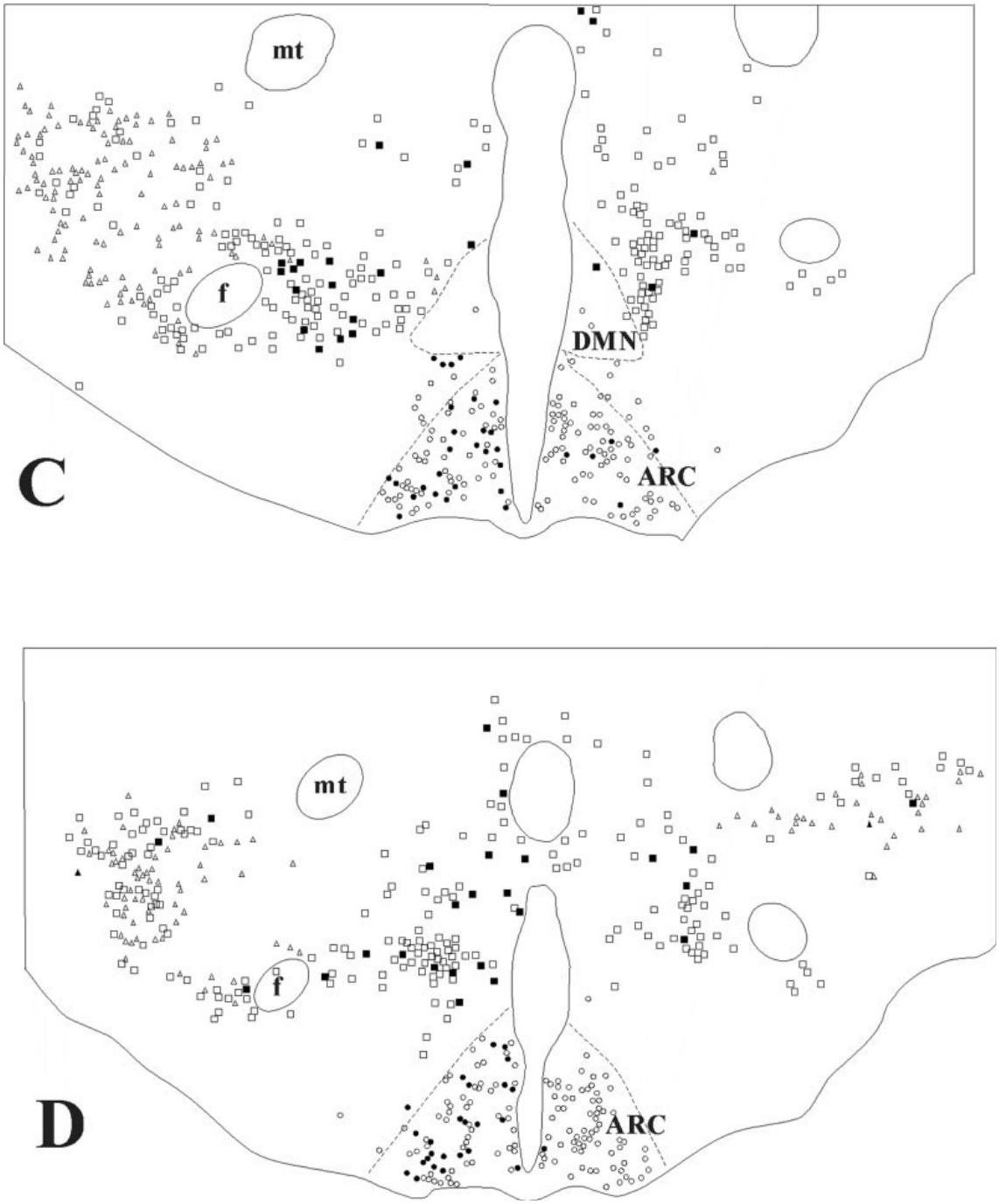

Fig. 9. (shown on the next page) Schematic maps demonstrating the distribution of CART-, PNMT-, CART/PNMT-, CART/CTB-, PNMT/CTB-, and CART/PNMT/CTB-containing neurons in three anteroposterior levels of medulla (**A:** Bregma –11.60; **B:** Bregma –13.20; **C:** Bregma –13.50). Note that the CART/CTB neurons in the C1–3 regions contain PNMT, whereas the CART/CTB neurons in the medial subnucleus of the NTS are not adrenergic. Symbols: open circle: CART; filled circle: CART/CTB; open square: CART/PNMT; filled square: CART/CTB/PNMT; open triangle: PNMT; filled triangle: PNMT/CTB. C1, C1 area; C3, C3 area; NTS, nucleus tractus solitarius; py, pyramidal tract; sp5, spinal trigeminal tract; TS, tractus solitarius.

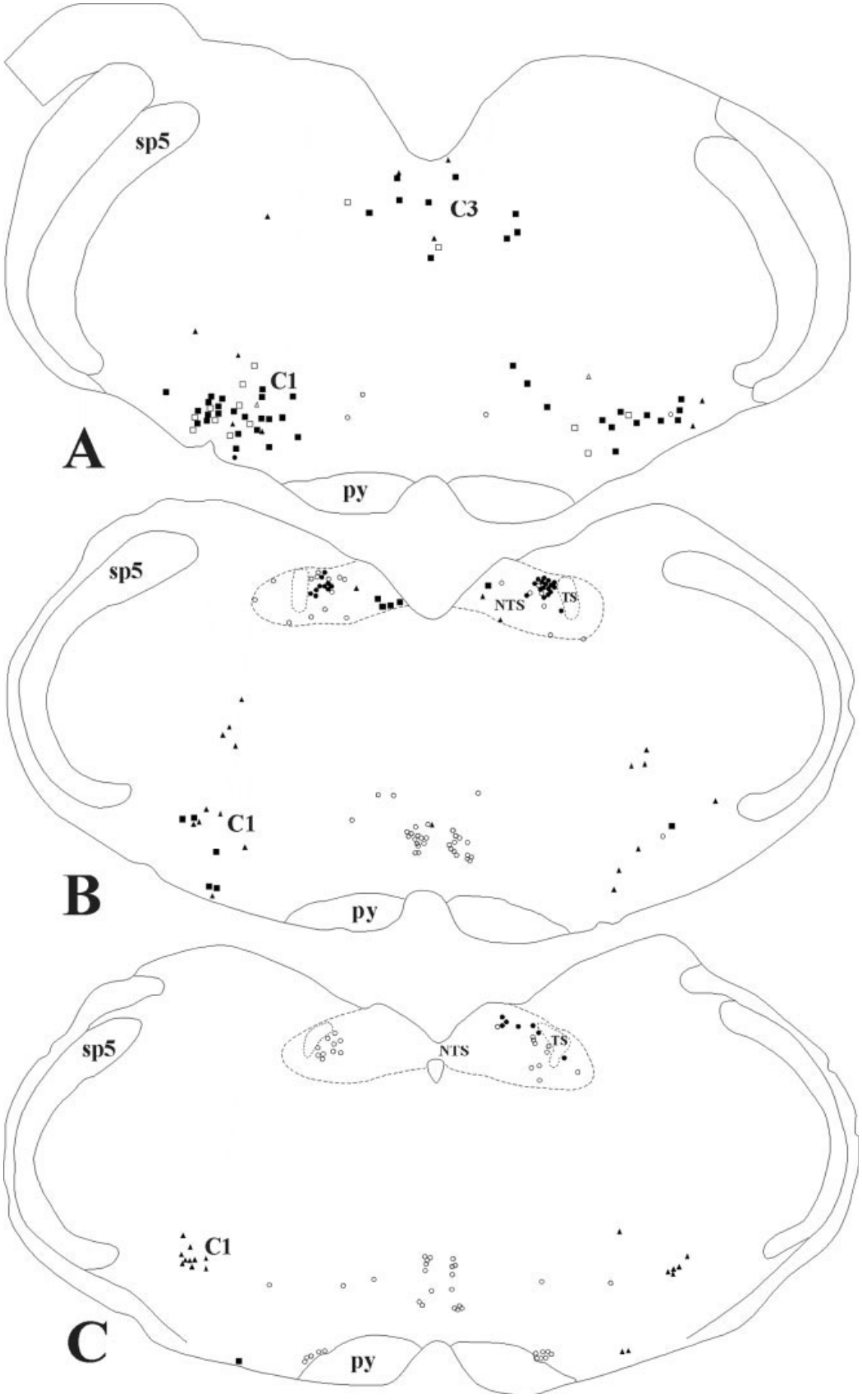
sp5
C3
C1
A
py
sp5
NTS
TS
C1
B
py
sp5
NTS
TS
C1
C
py

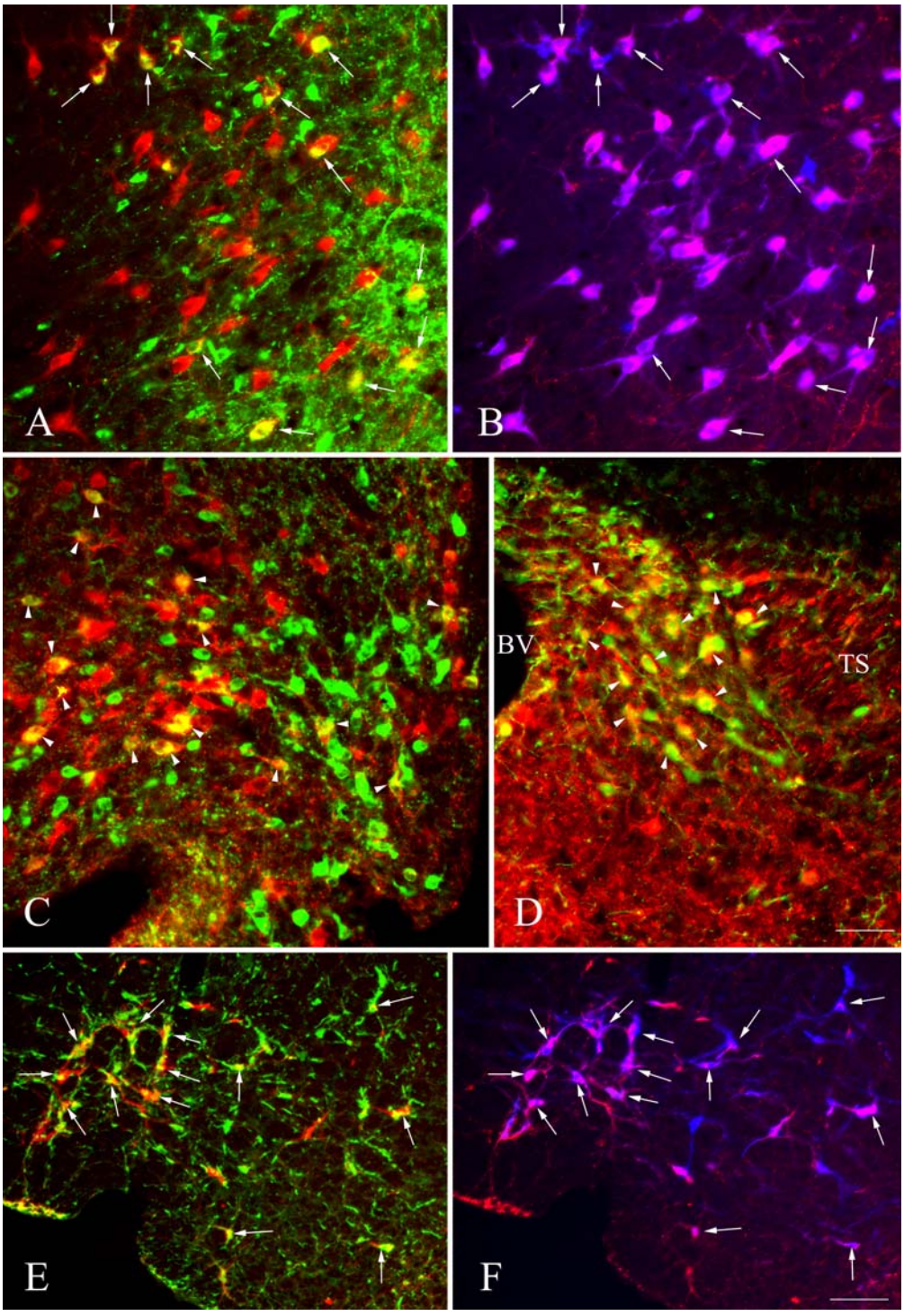

Fig. 10. (**A**, **B)** Images of identical fields of the perifornical region demonstrating immunofluorescence for (**A**) CART (red) and CTB (green) and (**B**) CART (red) and MCH (blue). CART-IR neurons that express MCH and project to the PVN are labeled with arrows on both images. (**C**) Colocalization of CART (red) and CTB (green) in neurons (arrowheads) of the arcuate nucleus and (**D**) medial subnucleus of the nucleus tractus solitarius (NTS). (**E**, **F**) Photomicrographs of the same field of the C1 area demonstrating (**E**) colocalization of CTB (green) with CART (red) and (**F**) colocalization of PNMT (blue) with CART (red). Triple-labeled neurons are denoted by arrows in both images. BV, blood vessel; TS, tractus solitarius. Scale bar: 50 µm in **D** applies to **A–D**; 100 µm in **F** applies to **E**, **F**.

3. Adrenergic CART-IR axons innervate proTRH mRNA-containing perikarya in the PVN

ProTRH mRNA-containing neurons were symmetrically distributed in the parvocellular division of the PVN and readily visualized by blue fluorescence of the AMCA fluorochrome (**Figs. 11** and **12**). The hybridization signal filled the perikarya and in some neurons, its proximal dendrites (**Fig. 12**). As previously reported (65, 167, 169), the majority of the proTRH mRNA-expressing neurons in the periventricular and medial parvocellular subdivisions co-contained CART-immunoreactivity (**Figs. 11** and **12 B**, **C**, **E–G**). In the confocal images, CART-immunoreactivity was organized primarily in a perinuclear distribution reminiscent of the location of the Golgi apparatus, and appeared to be separately compartmentalized from the proTRH hybridization signal (**Fig. 12 E–F**). In other neurons, however, CART-immunoreactivity was more generally dispersed in the perikarya, intermingling with the proTRH hybridization signal (**Fig. 12 B**, **C**).

CART-IR and PNMT-IR nerve fibers showed a similar distribution in all parvocellular subdivisions of the PVN, although the density of CART-IR fibers was higher. In the periventricular and medial parvocellular subdivisions, where hypophysiotropic TRH neurons are located, both CART- and PNMT-IR axon varicosities were found in close juxtaposition to nearly all proTRH-containing neurons (**Fig. 12**). By semiquantitative analyses, the numbers of CART- and PNMT-IR axon varicosities on the surface of proTRH neurons were approximately equal in the medial parvocellular subdivision, while in the periventricular subdivision, PNMT-IR varicosities outnumbered CART-IR varicosities by 1.4-fold. Superimposed images of the three fluorochromes revealed that PNMT-immunoreactivity was present in 44.0 ± 3.6% of CART-IR axon varicosities in close apposition to proTRH neurons in the PVN. Conversely, approximately half of the PNMT-IR varicosities in contact with proTRH mRNA-containing neurons also contained CART-immunoreactivity in both the periventricular (51.3 ± 5.6%) and medial (53.2 ± 1.1%) parvocellular subdivisions.

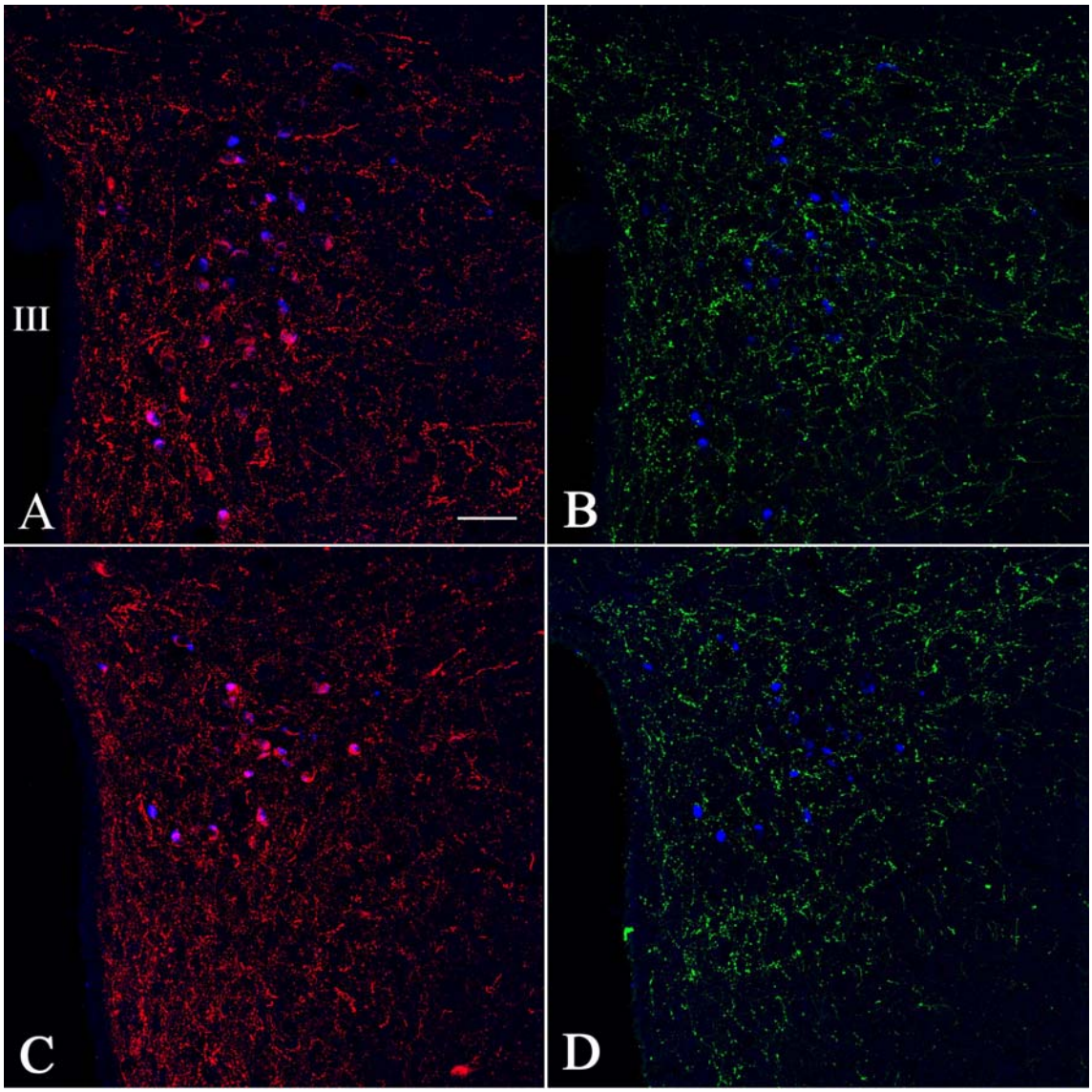

Fig. 11. Relationship between CART- (red) and PNMT-IR (green) axons and proTRH mRNA-containing neurons (blue) in the PVN. Low power magnification images of the same field from the mid (**A**, **B**) and caudal (**C**, **D**) levels of the PVN illustrate that proTRH-synthesizing neurons are embedded in a dense network of CART- (**A**, **C**) and PNMT-IR (**B**, **D**) axons. III: Third ventricle. Scale bar: 50 μm.

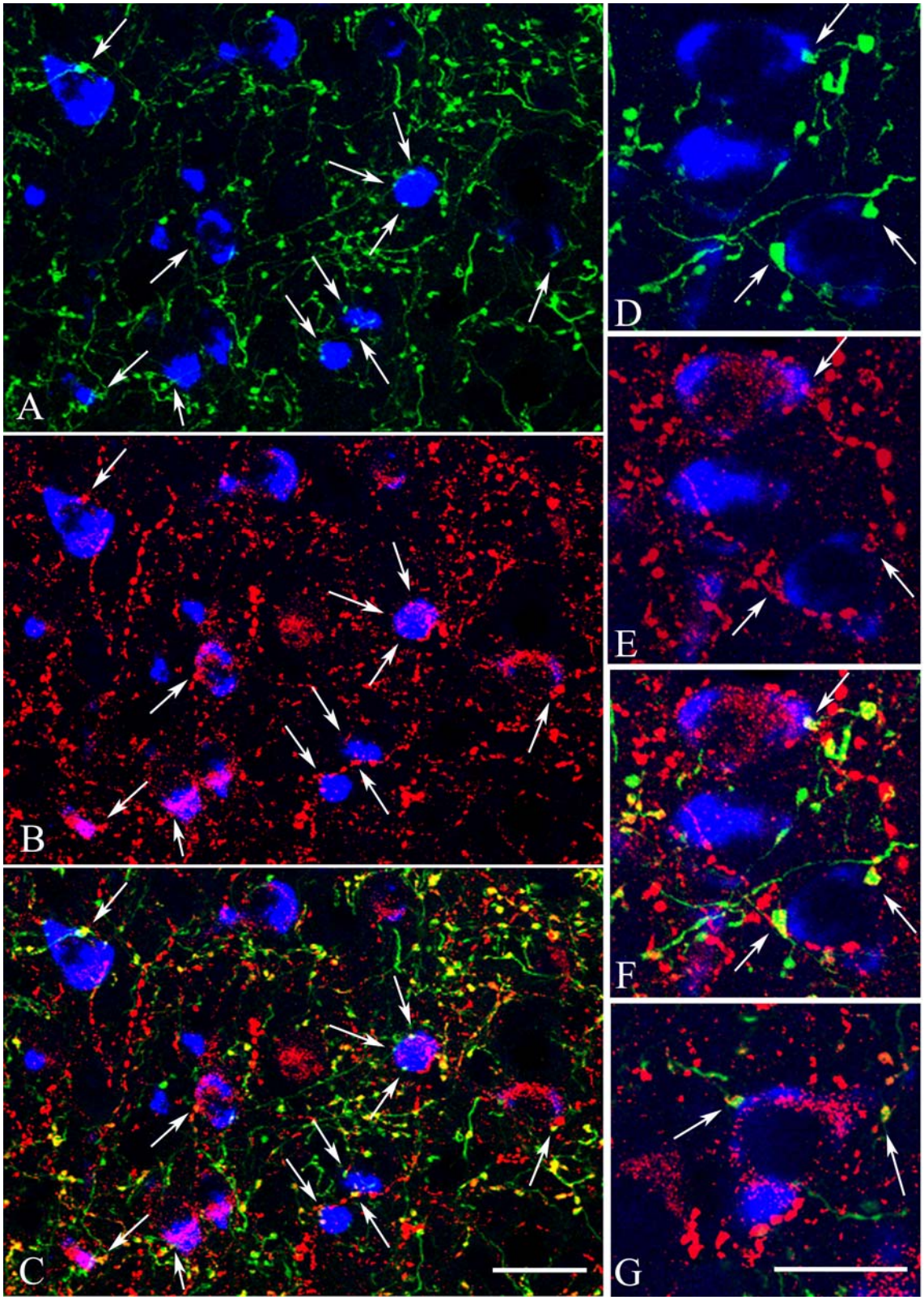
A
B
C
D
E
F
G

4. Ultrastructural examination of CART-IR innervation of CRH-containing neurons in the PVN

At the light microscopic level, varicose CART-IR fibers were in juxtaposition to the majority of CRH-IR neurons in the medial parvocellular subdivision, as described later in detail. By ultrastructural analysis, DAB-labeled CART-IR terminals were seen to establish synapses on CRH neurons, the latter identified by the presence of the highly electron-dense silver particles (**Fig. 13 A–C**). Tracing the juxtaposed CART-IR terminals and CRH-IR neurons through a series of ultrathin sections, both axo-somatic (**Fig. 13 A**) and axo-dendritic (**Fig. 13 B, C**) synaptic specializations were observed.

5. Origin of CART-IR innervation of CRH neurons in the PVN

CART-IR axons densely innervated all parvocellular subdivisions of the PVN. In addition, numerous cell bodies in the parvocellular as well as in the magnocellular division of the PVN were immunofluorescent for CART. For the most part, CART- and CRH-IR neurons formed two distinct neuron populations in the PVN, with only occasional CRH neurons containing CART-immunoreactivity (**Fig. 14**). While only a subpopulation of CART-IR fibers contained α-MSH in the PVN, all α-MSH-containing axons co-contained CART in this nucleus, as we have previously described (65).

Fig. 12. (shown on the previous page) Colocalization of CART- and PNMT-immunoreactivity in axon terminals in contact with proTRH mRNA-containing neurons in the PVN. Medium magnification confocal images of the same field (**A**–**C**) demonstrate (**A**) the PNMT-IR (green) and (**B**) CART-IR (red) innervation of proTRH mRNA-containing neurons (blue) in the medial parvocellular subdivision at the mid level of the PVN. Axons containing both CART and PNMT appear yellow in the composite image (**C**). Arrows denote axon varicosities containing both CART and PNMT juxtaposed to proTRH neurons. High power confocal photomicrographs (**D**–**F**) illustrates (**D**) the PNMT-IR (green) and (**E**) CART-IR (red) innervation of proTRH mRNA-containing neurons (blue) in the medial parvocellular subdivision at the caudal level of the PVN. (**F**) Composite image showing colocalization of PNMT and CART in axons (arrows) juxtaposed to proTRH neurons. (**G**) A high power confocal photomicrograph from the periventricular parvocellular subdivision of the PVN showing two axon varicosities (arrows) containing PNMT and CART in juxtaposition to a proTRH neuron. Note presence of CART immunoreactivity in the majority of proTRH neurons (**B**, **C**, **E**–**G**). The tendency for CART to be primarily located in a perinuclear region of the cytoplasm is obvious in **E**–**G**. Scale bar: 25 μm in **C**, corresponds to **A**– **C**; Scale bar: 15 μm in **G,** corresponds to **D**– **G**.

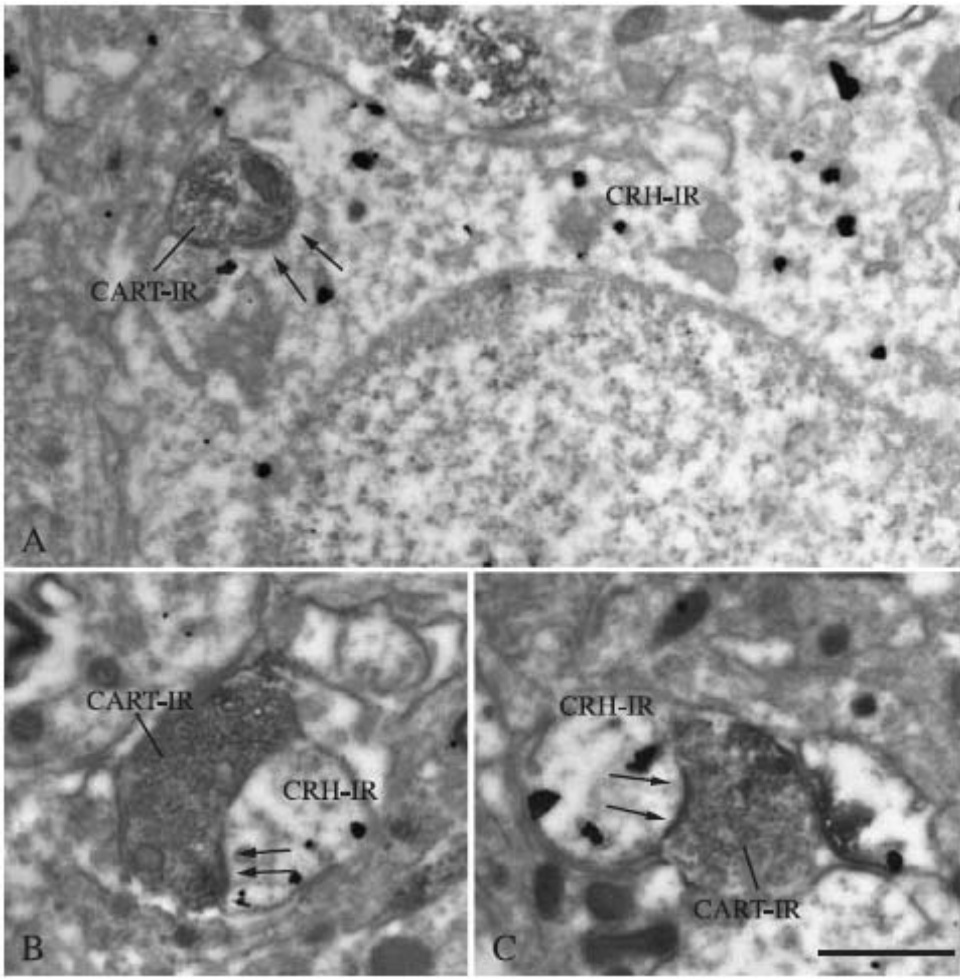

Fig. 13. Electron micrographs demonstrating axo-somatic (**A**) and axo-dendritic (**B** and **C**) synapses (arrows) between CART-IR axon terminals and CRH-containing neurons in the PVN. The CRH-IR elements are labeled with highly electron-dense silver granules, while the CART-IR terminals are detected with electron-dense DAB. Scale bar: 1 μm.

Similarly, the vast majority of PNMT-IR fibers contained CART in the PVN. In the parvocellular subdivisions of the PVN, the distribution of α-MSH- or PNMT-containing CART-IR axons showed major differences. CART/α-MSH-IR axons were mainly concentrated in the periventricular, dorsal, and ventral parvocellular subdivisions, whereas the occurrence of these fibers was less frequent in the medial parvocellular subdivision (**Fig. 14 A1**), except for the ventral part and the most caudal region of this subdivision. In contrast, all parvocellular subdivisions were densely innervated by CART/PNMT-IR axons, and the most abundant network of these fibers was observed in the medial parvocellular subdivision (**Fig. 14 A2**), in which the cluster of CRH neurons is also located.

CART/PNMT-IR axon varicosities were found in juxtaposition to nearly all (95.00 ± 1.53%) CRH neurons (**Figs. 14** and **15**). An average of 5.45 ± 0.14 CART/PNMT

boutons per CRH cell were observed. CART/α-MSH-containing boutons were also found in close proximity to CRH neurons but not as frequently as were CART/PNMT boutons (**Figs. 14** and **15**). CART/α-MSH fibers were in juxtaposition to 58.67 ± 3.71% of CRH neurons, and an average of 2.73 ± 0.13 CART/α-MSH boutons were found on the surface of the innervated cells. CRH neurons were more frequently contacted by CART/α-MSH varicosities in the ventral part of the medial parvocellular subdivision. In this region, more CART/α-MSH boutons were juxtaposed to the CRH neurons than in the dorsal part of the subdivision. Both CART/PNMT-IR and CART/α-MSH-IR varicosities were observed in juxtaposition to the soma as well as to the dendrites of CRH neurons. Of all CART-containing axon varicosities located on the surface of CRH neurons, 59.60 ± 2.10% contained PNMT, whereas only 18.47 ± 1.55% contained α-MSH.

Fig. 14. (shown on the next page) (**A1**, **A2**) Low-magnification confocal images of the same field demonstrate the distribution of CART (red), CRH (blue), and PNMT-IR (green) (**A1**) and CART (red), CRH (blue), and α-MSH-IR (green) (**A2**) elements in the PVN. **A1**, CART immunoreactivity is present in the vast majority of PNMT-IR axons in the PVN, resulting in the yellow color. Note the high density of CART/PNMT-IR fibers surrounding CRH neurons. **A2**, CART immunoreactivity is present in all α-MSH-IR axons in the PVN. CART/α-MSH-IR fibers are sparser in the region in which CRH neurons are located but are more abundant in the dorsal, periventricular, and ventral parvocellular subdivisions and in the ventral part of the medial parvocellular subdivision. (**B1** and **B2**) Medium-power confocal images of the same field illustrate the different CART-IR varicosities in juxtaposition to CRH neurons. **B1**, Color matching: CART, red; PNMT, green; CRH, blue. CRH neurons are embedded in a dense network of CART/PNMT-IR fibers (yellow, due to color mixing). Numerous CART/PNMT-IR varicosities (indicated by arrows) are in tight apposition to CRH neurons. **B2**, Color matching: CART, red; α-MSH, green; CRH, blue. In the same optical section, CART/α-MSH-IR axons (yellow due to color mixing) are much less abundant. Arrows point to CART/α-MSH-IR boutons in contact with CRH neurons. Arrowheads indicate single-labeled CART-IR boutons (containing neither PNMT nor α-MSH) closely apposed to CRH neurons. In both **B1** and **B2**, asterisk labels a CRH neuron contacted by both CART/PNMT-IR and CART/α-MSH-IR boutons; x**,** a CRH neuron contacted by CART/PNMT-IR and single-labeled CART-IR boutons; a, a CART-IR CRH neuron. Scale bars, 100 μm (shown in **A2**) for **A1** and **A2**, and 20 μm (shown in **B2**) for **B1** and **B2**. III, third ventricle.

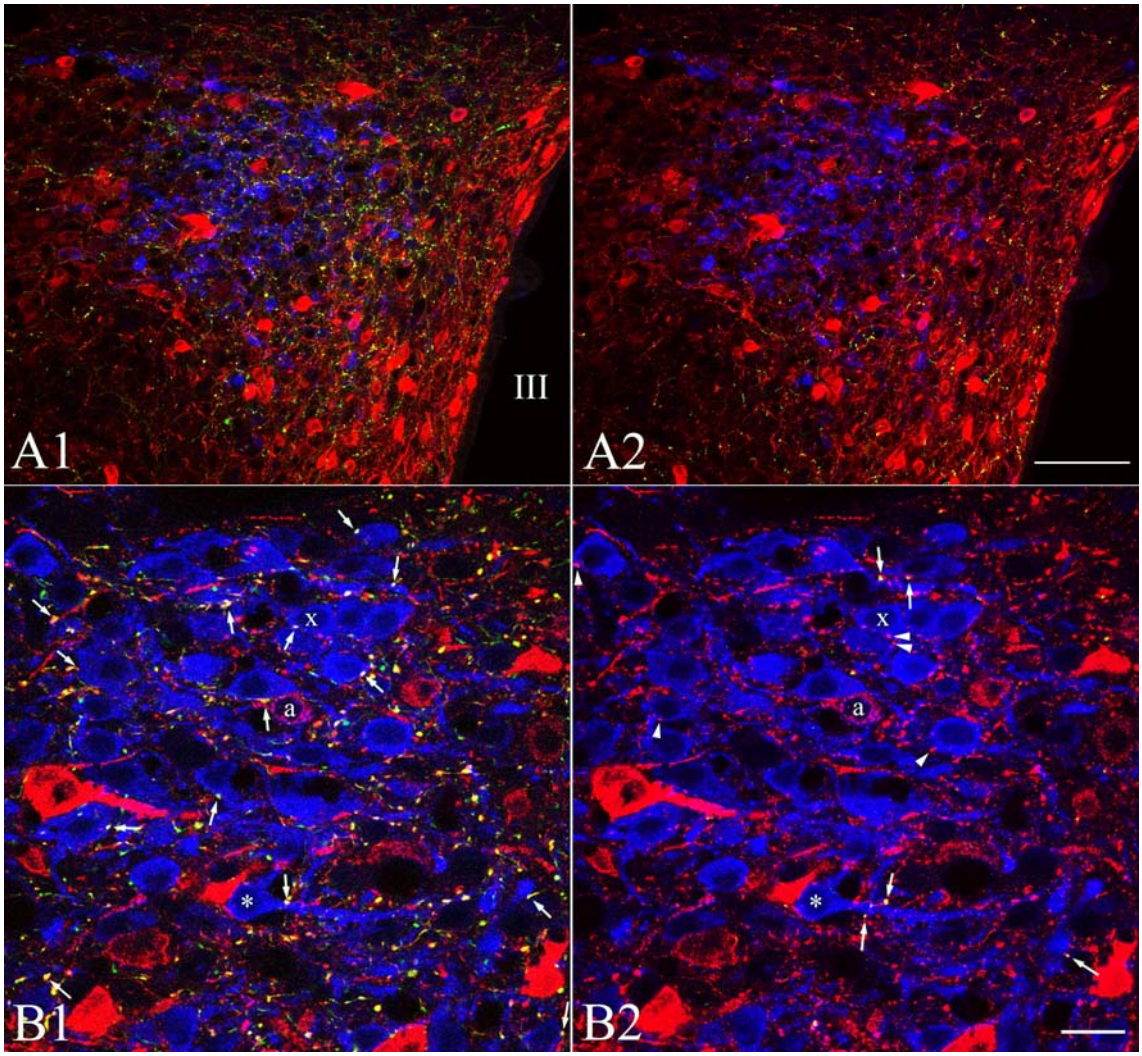

An additional 21.93 ± 1.98% of CART-IR varicosities were single-labeled, suggesting that these axons originate from loci other than the arcuate nucleus and the C1-3 areas. These single-labeled CART-IR varicosities were juxtaposed to 68.33 ± 4.91% of CRH neurons. No regional preference was found in the distribution of neurons innervated by single-labeled CART-IR varicosities. The results of the quantitative analysis are summarized in **Table 4**.

The majority of CRH neurons were contacted by more than one type of CART-IR axons. More than half (56.67 ± 3.71%) of the CRH neurons were contacted by both CART/PNMT and CART/α-MSH-IR varicosities. The ratio of CRH neurons contacted by both single-labeled and CART/PNMT-IR boutons was 64.33 ± 5.84%, whereas 38.67 ± 3.38% of CRH neurons were innervated by the three different types of CART-IR axons. The vast majority (88.26 ± 1.61%) of PNMT-IR boutons and all α-MSH-IR boutons in juxtaposition to CRH neurons contained CART-immunoreactivity.

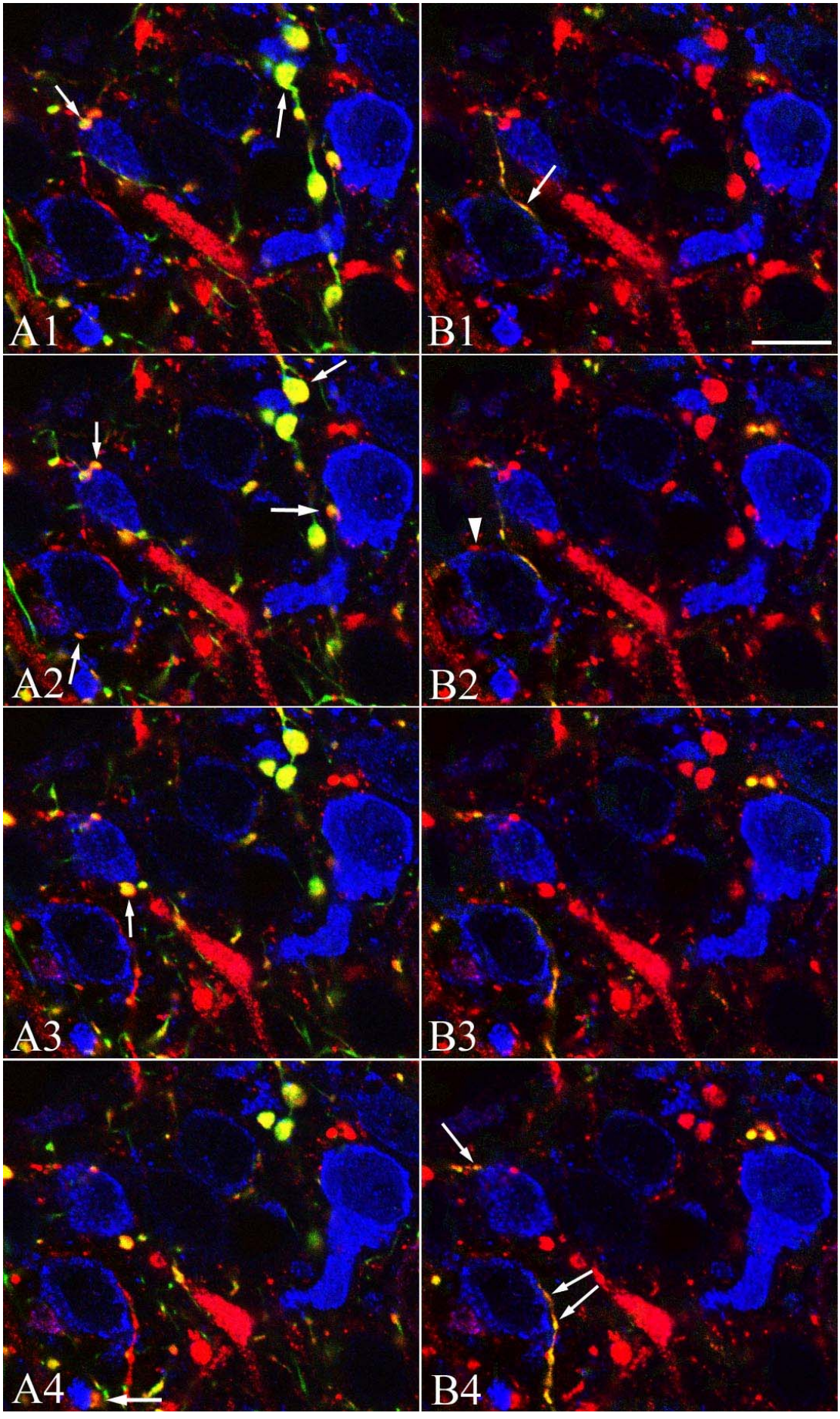
A1
B1
A2
B2
A3
B3
A4
B4

Table 4. Quantitative analysis of subpopulations of CART-IR axon varicosities situated on the surface of CRH-IR neurons in the medial parvocellular subdivision of the PVN

Type of CART-IR bouton	Contacted CRH neurons, %	Average number of CART-IR varicosities per innervated CRH neuron	CART-IR boutons in contact with CRH neurons, %
CART/PNMT	95.00 ± 1.53	5.45 ± 0.14	59.60 ± 2.10
CART/α-MSH	58.67 ± 3.71	2.73 ± 0.13	18.47 ± 1.55
CART single-labeled	68.33 ± 4.91	2.80 ± 0.24	21.93 ± 1.98
All CART types	99.33 ± 0.33	8.77 ± 0.43	100

6. Effect of fasting on NPY and CART mRNA in medullary C1-3 areas

At the beginning of the experiment, fed animals weighed 259.3 ± 4.9 g and gained 22.6 ± 5.8 g weight during 64 hours. Fasted animals initially weighed 257.8 ± 6.6 g and lost 50.4 ± 1.9g (19.5 ± 0.4% of their initial body weight) during the 64 h fasting.

NPY mRNA expressing cells were broadly distributed in the medulla. In the C1-3 regions, NPY mRNA positive cells were found in the characteristic distribution of adrenergic neurons. In all three cell groups, adrenergic neurons are distributed diffusely, thus, we have analyzed the NPY hybridization signal over individual cells. The intensity of NPY mRNA hybridization in the C1-3 areas was similar between fed and fasted animals (**Fig. 16**). Densitometric analysis of the middle portion of the C1 area (approximately between -12.8 and -12.5 mm from the Bregma), and C2 and C3 regions did not reveal significant differences between the fed and fasted groups in either the number of NPY mRNA expressing cells, or in the intensity of hybridization signals of individual neurons in each regions **(Fig. 17)**.

Fig. 15. (on the previous page) High-power confocal images of quadruple immunofluorescence labeling represent four consecutive optical sections with 0.6 μm Z step. CART (red), CRH (blue), and PNMT (green) are shown in **A1-A4**, whereas CART (red), CRH (blue), and α-MSH (green) are shown in **B1-B4**. Arrows in **A1-A4** point to CART/PNMT-IR varicosities in close apposition to CRH-IR cell bodies and dendrites. Arrows in **B1-B4** identify CART/α-MSH-IR boutons juxtaposed to CRH neurons. Arrowhead in **B2** points to a single-labeled CART-IR axon varicosity on the surface of a CRH neuron. Scale bar (shown in **B1**) corresponds to 10 μm and refers to all micrographs.

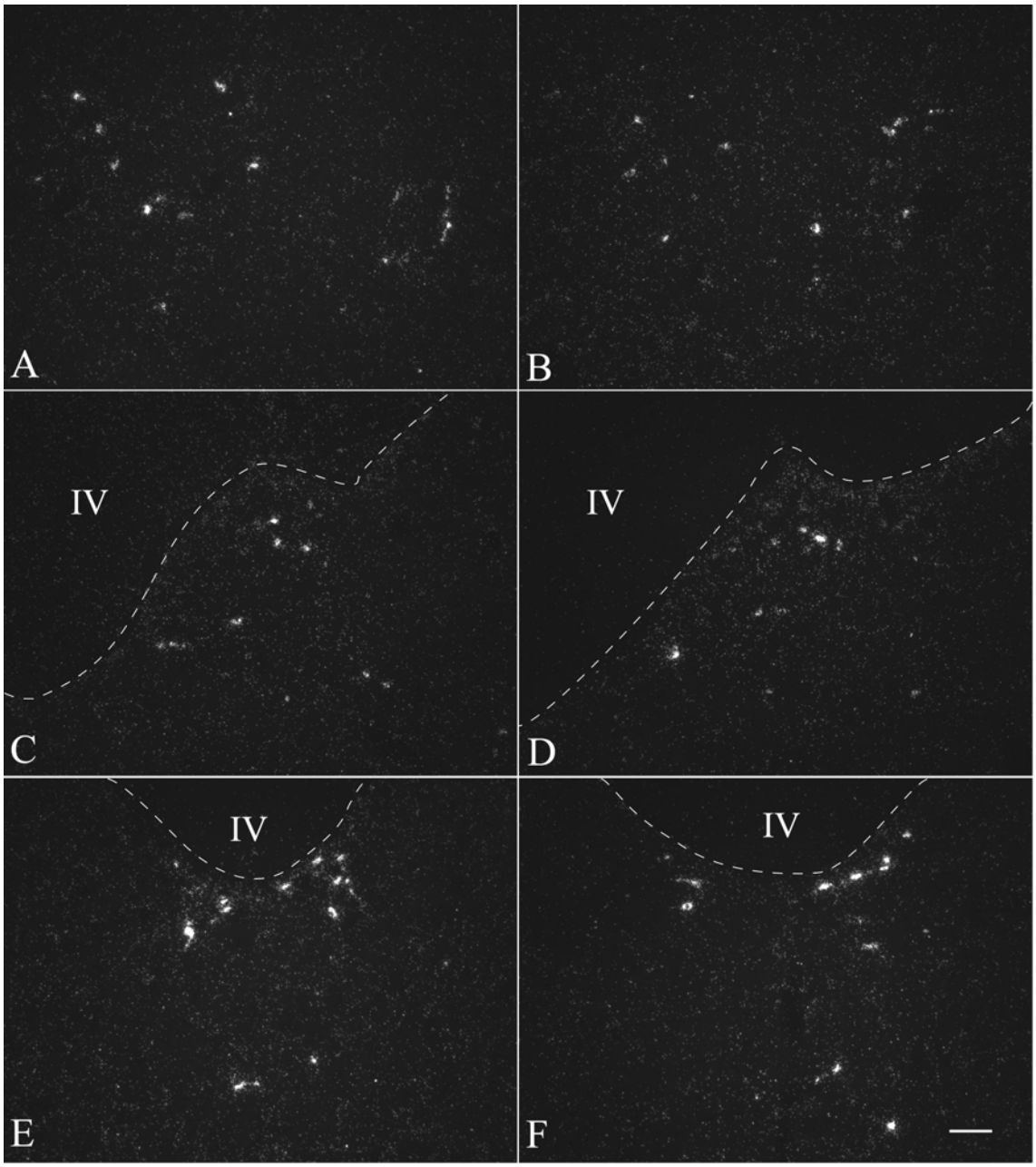

Fig 16. Darkfield photomicrographs of NPY mRNA expressing neurons in the C1 (**A**, **B**), C2 (**C**, **D**) and C3 (**E**, **F**) areas of fed (**A**, **C**, **E**) and fasted (**B**, **D**, **F**) animals. Note that hybridized cells of fed and fasted animals have a comparable intensity of labeling in all three cell groups. Scale bar (shown in **F**) corresponds to 100 μm and refers to all micrographs. IV, fourth ventricle. Broken line indicates the border of the fourth ventricle.

Cells hybridized for CART mRNA were also present in several medullary regions. In the C1 area, CART mRNA-containing cells were located in a distribution typical of adrenergic neurons. Since a small population of CART expressing neurons that are not adrenergic was also described in this area by other investigators (170), we previously studied the distribution of these cells in medullary sections double-immunolabeled for CART and PNMT. We found very few single-labeled CART neurons compared to the

number of adrenergic CART neurons, and these were mainly located medially, closer to the midline than the main group of C1 neurons (data not shown), thus we excluded these medially located CART mRNA positive neurons from our *in situ* hybridization analysis.

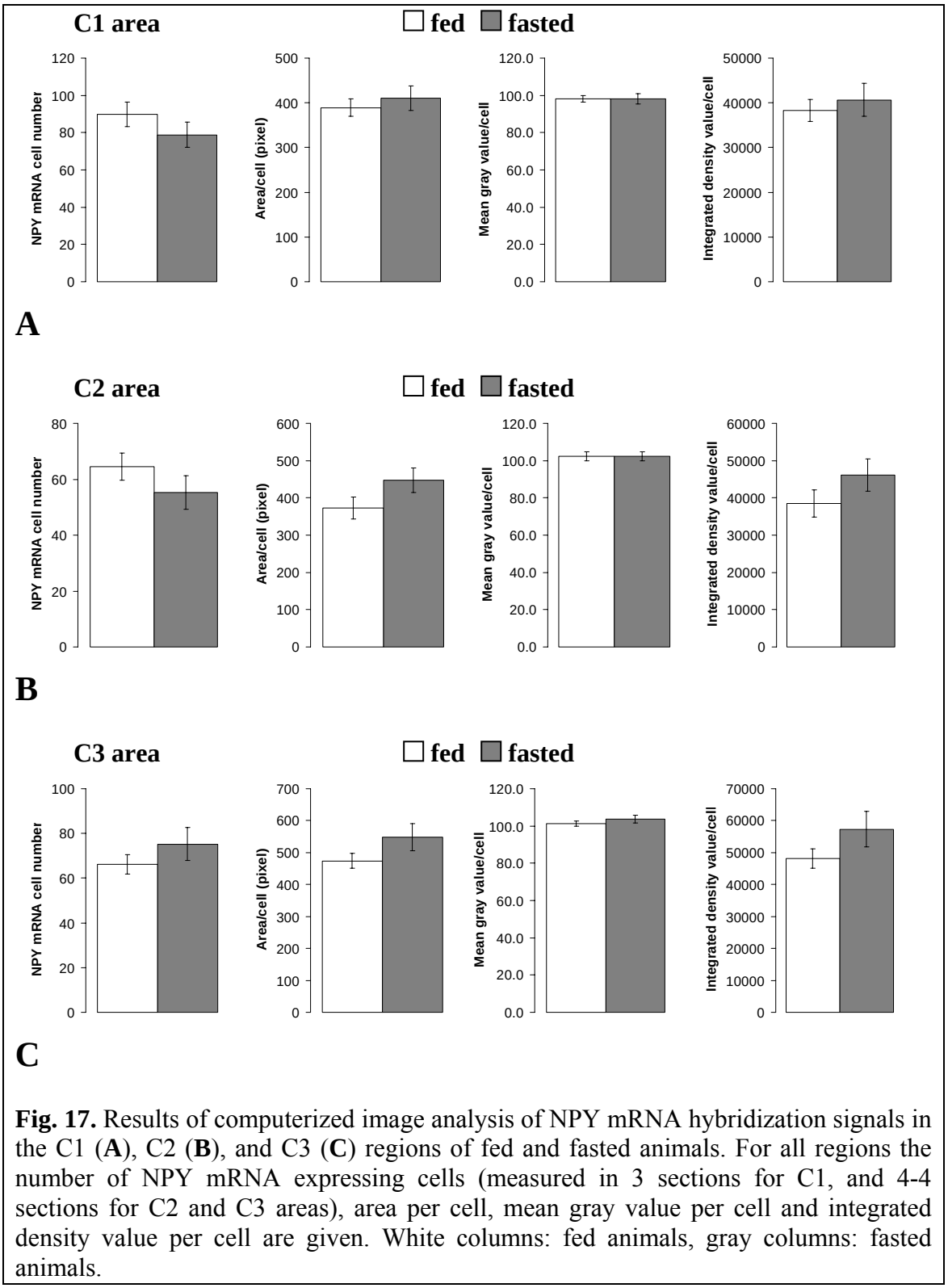

Fig. 17. Results of computerized image analysis of NPY mRNA hybridization signals in the C1 (**A**), C2 (**B**), and C3 (**C**) regions of fed and fasted animals. For all regions the number of NPY mRNA expressing cells (measured in 3 sections for C1, and 4-4 sections for C2 and C3 areas), area per cell, mean gray value per cell and integrated density value per cell are given. White columns: fed animals, gray columns: fasted animals.

C2 adrenergic cells are located mainly at the medial border of the NTS, however, close to these neurons there is also a large group of CART expressing neurons in the medial NTS that are not adrenergic. Because we could not identify unambiguously C2 neurons in our hybridized sections, we did not analyze the CART mRNA expression in this area. In the C3 region CART mRNA positive cells were distributed in the same pattern as adrenergic neurons.

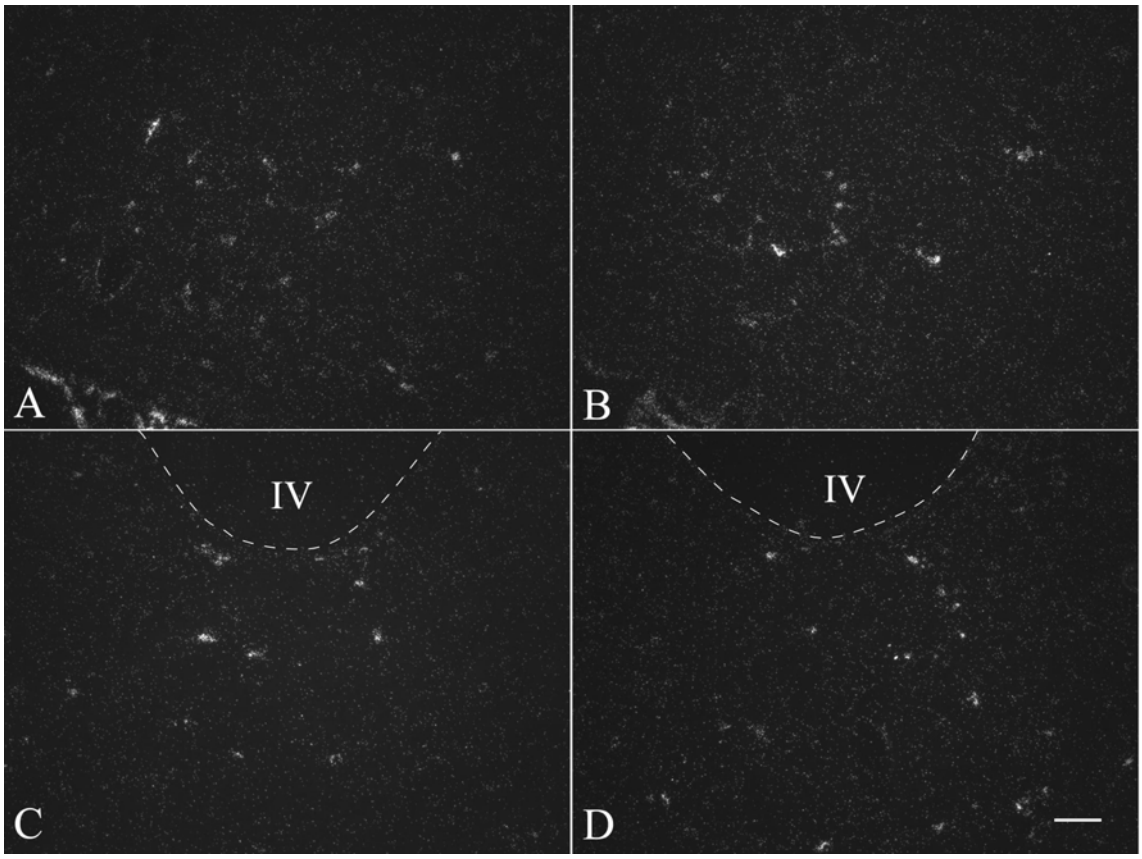

Fig 18. Darkfield photomicrographs of CART mRNA expressing neurons in the C1 (**A**, **B**), and C3 (**C**, **D**) areas of fed (**A**, **C**) and fasted (**B**, **D**) animals. Note the similar intensity of CART mRNA hybridization signals between fed and fasted animals in both regions. Scale bar (shown in **D**) corresponds to 100 μm and refers to all micrographs. IV, fourth ventricle. Broken line indicates the border of the fourth ventricle.

The intensity of CART mRNA hybridization was comparable between fed and fasted animals in both the C1 and C3 regions (**Fig. 18**). Quantitative densitometry of the middle portion of the C1 area revealed no differences in the number of CART mRNA expressing cells, and in the area and integrated density values of CART mRNA positive cells between fed and fasted animals, while the mean gray value of hybridized C1 neurons was slightly but significantly reduced in fasted animals compared to fed controls (fasted vs. fed: 73.07 ± 1.25 vs. 77.01 ± 1.07, p=0.023) (**Fig. 19 A**). We did not

detect significant differences in any of the measured parameters in the C3 region (**Fig. 19 B**).

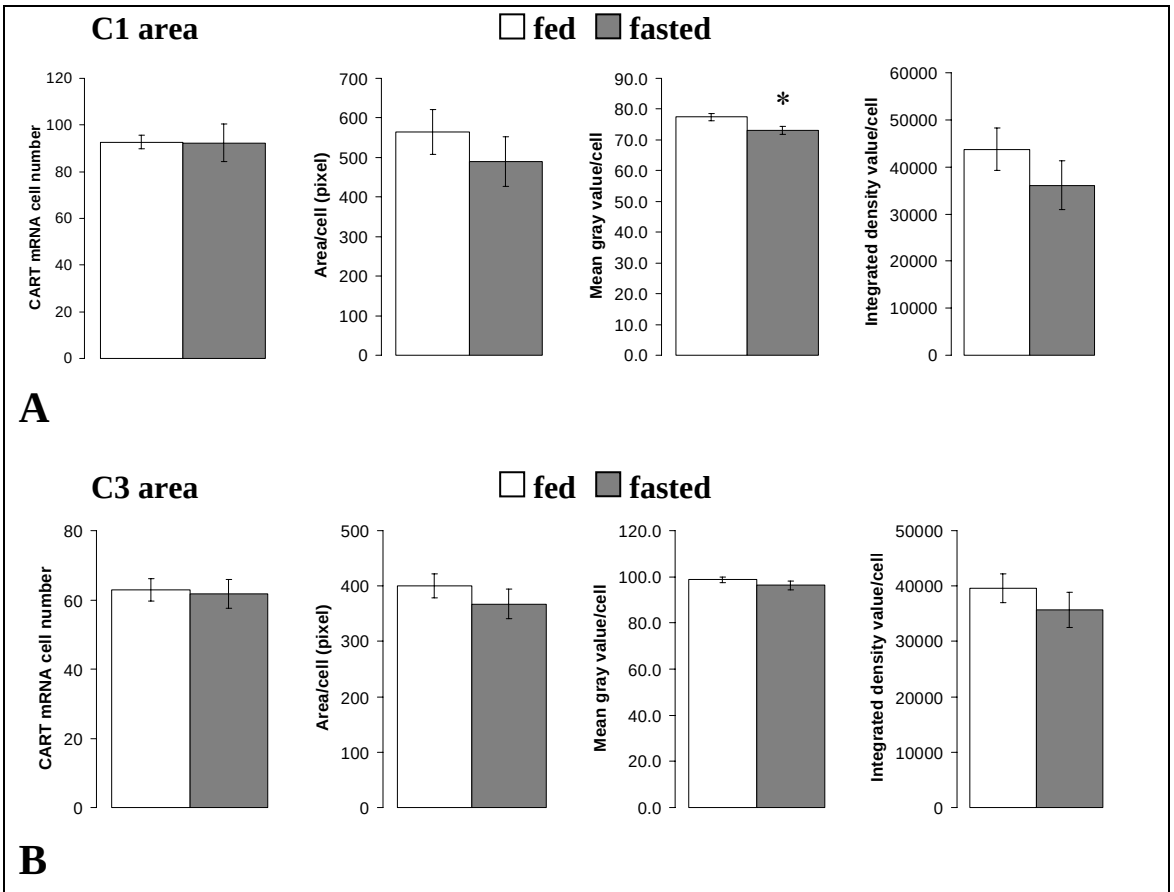

Fig. 19. Results of computerized image analysis of CART mRNA content of the C1 (**A**) and C2 (**B**) regions of fed and fasted animals. For both regions the number of CART mRNA expressing cells (measured in 3 sections for C1, and 4 sections for C2), area per cell, mean gray value per cell and integrated density value per cell are given. White columns: fed animals, gray columns: fasted animals. * $p < 0.05$ compared with fed animals.

7. Galanin- and GALP-IR innervation of proTRH-containing neurons in the PVN

a) Galanin-IR innervation of proTRH neurons in the PVN at light- and electron-microscopic level

Galanin-IR axons densely innervated all of the major parvocellular subdivisions of the PVN where proTRH neurons were identified (**Fig. 20 A–C**). The periventricular and anterior parvocellular subdivisions exhibited the most prominent network of galaninergic nerve fibers, while in the medial subdivision, the innervation was less intense. Galanin-IR cell bodies were observed in both the parvocellular and magnocellular divisions of the PVN (**Fig. 20 A–C**). In all parvocellular subdivisions,

galanin-IR axon varicosities were in juxtaposition to the majority of TRH neurons, with the highest proportion in the anterior and periventricular parvocellular subdivisions (**Fig. 20 D–E**). Semiquantitative analysis revealed that in the periventricular and medial parvocellular subdivisions, 75.8 ± 6.7% and 61.6 ± 3.4% of the proTRH containing neurons, respectively, were in juxtaposition with galanin-IR axon terminals. Additionally, 85.1 ± 2.3% of the proTRH neurons of the anterior parvocellular subdivision, that are not hypophysiotropic, were contacted by galanin-IR boutons.

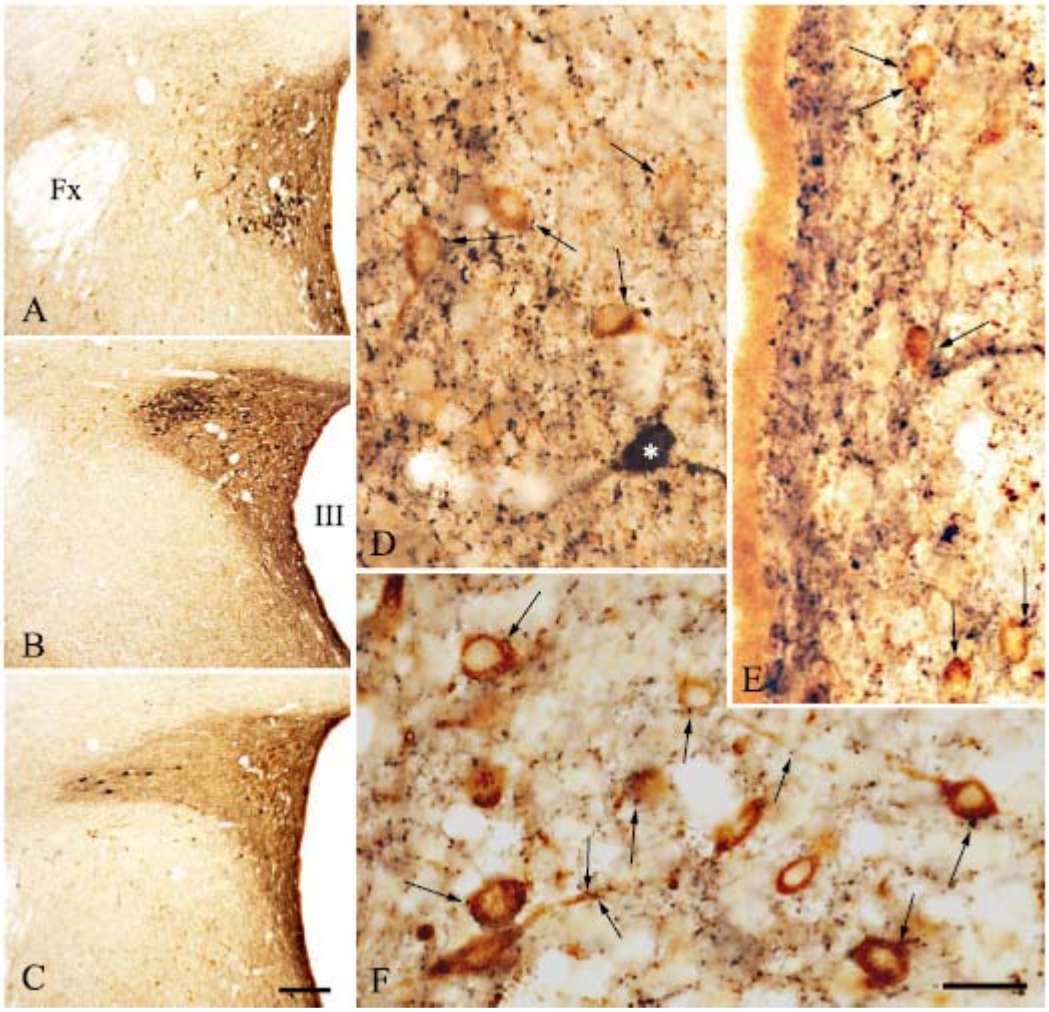

Fig. 20. (**A**–**C**) Low power photomicrographs showing the distribution of galanin- (black) and proTRH-IR (brown) neurons and fibers in different levels of the PVN. (**A**) anterior, (**B**) mid and (**C**) caudal levels of the PVN. While the proTRH-IR neurons are located only in the parvocellular subdivisions, galanin-IR neurons are observed in both the parvo- and magnocellular divisions. Note the dense galanin-IR innervation of the PVN at all levels. (**D**–**F**) High power magnification of galanin-IR axon varicosities (arrows) in association with proTRH neurons in the (**D**) anterior, (**E**) periventricular and (**F**) medial parvocellular subdivisions of the PVN. Asterisk in (**D**) labels a galanin-IR neuron. Fx: Fornix, III: Third ventricle. Scale bar in **C**: 200 µm, corresponds to **A**–**C**; scale bar in **F**: 25 µm, corresponds to **D**– **F**.

By ultrastructural analysis, DAB-labeled galanin-IR terminals were seen to establish synapses on proTRH neurons, the latter recognized by the presence of the highly electron-dense silver particles (**Fig. 21**). In all instances, the synapses were found to be of the symmetric type (**Fig. 21**).

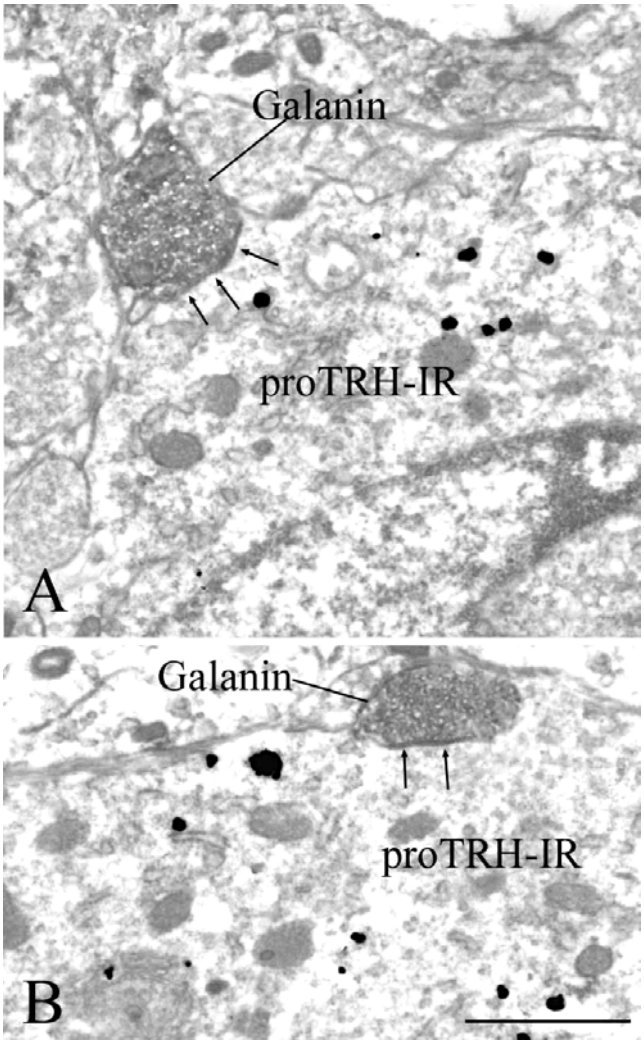

Fig. 21. Electron micrographs showing synaptic associations (arrows) between proTRH-containing neurons in the medial parvocellular subdivision of the PVN and galanin-containing axon terminals. The proTRH-IR perikarya are labeled with highly electron-dense silver granules, while the galanin-IR terminals are recognized by the presence of the electron-dense DAB. Note that the galanin-IR terminals form symmetric type synapses on the surface of the proTRH-IR perikarya (**A**, **B**). Scale bar: 1 μm.

b) GALP-IR innervation of proTRH-containing neurons in the PVN.

Within the PVN, GALP-IR fibers concentrated primarily in the anterior parvocellular subdivision of the PVN and rostral portions of the periventricular parvocellular subdivision, with moderate concentrations in more caudal portions of the periventricular parvocellular subdivision and only low concentrations in the medial parvocellular subdivision (**Fig. 22**). No GALP immunoreactivity was found in the perikarya and dendrites intrinsic to the parvocellular areas of the PVN. By double-labeling light microscopic immunocytochemistry, GALP fibers were found in juxtaposition to only a small number of proTRH-IR neurons in the PVN, primarily in the periventricular and anterior parvocellular subdivisions (**Fig. 23 A–F**). Only rare

associations with proTRH-IR neurons were observed in the medial parvocellular subdivision (**Fig. 23 B, C, E**). Semiquantitative analysis from three animals revealed that, in the periventricular and medial parvocellular subdivisions, only 9.6 ± 1.0% and 2.1 ± 0.2% of the proTRH-IR neurons, respectively, were in juxtaposition with GALP-IR fibers. In contrast, 26.7 ± 0.3% of the proTRH-IR neurons in the anterior parvocellular subdivision showed close appositions with GALP-IR varicosities.

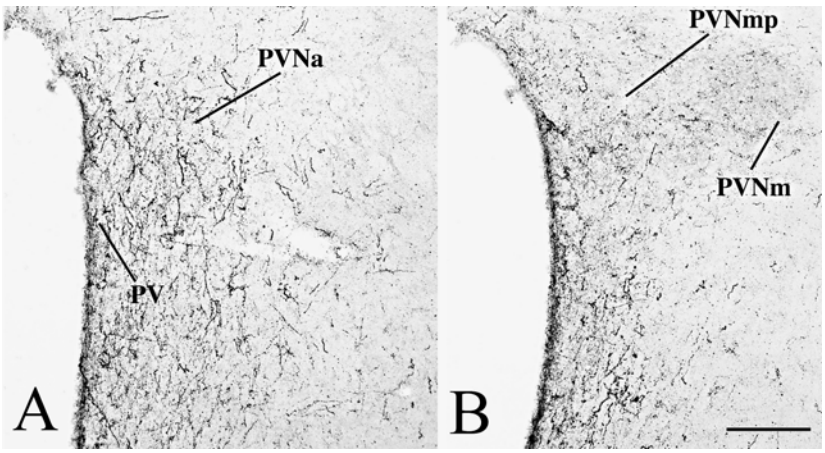

Fig. 22. Distribution of GALP-IR axons in the PVN. Note the density GALP-IR axons in the (**A**) anterior parvocellular subdivision in contrast to the paucity of fibers in the (**B**) medial parvocellular subdivision. Scale bar: 200 μm. Abbreviations: PV: periventricular parvocellular subdivision of the PVN; PVNa: anterior parvocellular subdivision of the PVN; PVNm: magnocellular division of the PVN; PVNmp: medial parvocellular subdivision of the PVN.

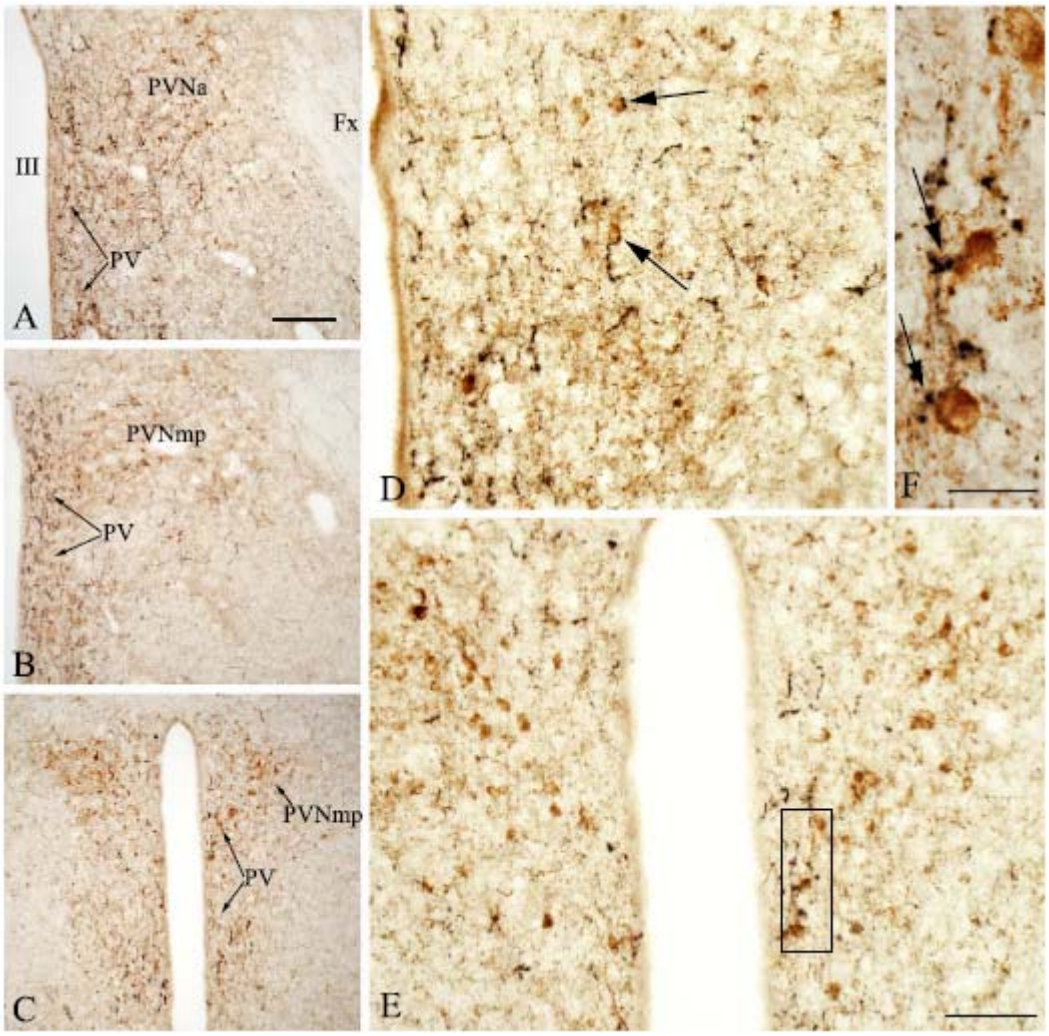

Fig. 23. GALP-IR innervation of proTRH-IR neurons in the PVN. (**A**–**C**) Low power micrographs showing GALP-IR fibers (dark purple) and proTRH-IR neurons (brown) in the (**A**) anterior (**B**) mid and (**C**) caudal levels of the PVN. (**D**) Medium power magnification photomicrograph illustrates association of GALP-IR axon varicosities with two proTRH-IR neurons (arrows) in the anterior parvocellular subdivision of the PVN. (**E**) Medium power magnification at the mid level of the PVN demonstrates that GALP-IR axons are juxtaposed to proTRH-IR neurons only in the periventricular parvocellular subdivision, but not in the medial parvocellular subdivision. (**F**) Oil immersion photomicrograph of boxed area in (**E**) showing GALP-IR axon varicosities in juxtaposition to two proTRH neurons in the periventricular parvocellular subdivision. Abbreviations: PV: periventricular parvocellular subdivision of the PVN; PVNa: anterior parvocellular subdivision of the PVN; PVNmp: medial parvocellular subdivision of the PVN; Fx: Fornix; III: third ventricle. Scale bar: 200 μm in **A** corresponds to **A**– **C**; scale bar in **E**: 250 μm corresponds to **D**, **E**; scale bar in **F**: 50 μm.

Discussion

NPY- and CART-containing afferents to hypophysiotropic TRH and CRH neurons

NPY- and CART-IR innervation of TRH neurons

Previous studies have shown that NPY neurons of the arcuate nucleus densely innervate all hypophysiotropic TRH neurons (91), and the ablation of the arcuate nucleus resulted in the loss of 82% of the NPY-containing boutons on the surface of TRH neurons (123). According to our results, the vast majority of TRH neurons are also innervated by NPY fibers arising from medullary adrenergic neurons, and varicosities of these axons comprise approximately 27% of the NPY boutons closely apposed to the surface of TRH neurons. These data indicate that virtually all TRH neurons receive NPY inputs from both the arcuate nucleus and adrenergic neurons and these two types of fibers represent the vast majority of NPY axons innervating the TRH neurons. Thus, noradrenergic NPY fibers, the third major NPY input to the PVN (124), probably comprise only a small fraction of the total NPY innervation of TRH neurons.

Previous observations from our laboratory indicated that the arcuate nucleus is not the exclusive source of the CART innervation of the TRH neurons (65). After the identification of CART expressing cell groups innervating the PVN demonstrated that the majority of PVN projecting adrenergic neurons contain CART, we observed that adrenergic CART varicosities were closely apposed to the majority of TRH neurons and constituted 44% of all CART boutons on the surface of TRH perikarya. Since approximately 75% and 34% of TRH neurons in the periventricular and medial parvocellular subdivision, respectively, receive contacts from fibers of α-MSH/CART neurons (63) and virtually all TRH neurons receive contacts from the adrenergic CART neurons, a substantial number of TRH neurons are probably innervated by axons from both sources. In accordance with this, we noticed that many proTRH mRNA-containing perikarya that were contacted by PNMT/CART boutons were also in association with single-labeled CART-IR fibers that established several large varicosities, characteristic of α-MSH/CART fibers in this region (65). Further studies are required to clarify whether TRH neurons receive innervation from CART neurons of the zona incerta, lateral hypothalamus and the medial subnucleus of the NTS, regions identified as sources of CART innervation of the PVN. Since a large number of CART neurons

reside in the PVN (129, 131), these cells may also contribute to the innervation of TRH neurons.

NPY- and CART-IR innervation of CRH neurons

Although we did not examine the NPY innervation of CRH neurons in this Ph.D. work, our recent unpublished results indicate that the NPY innervation of CRH neurons is composed of adrenergic NPY fibers (44%), noradrenergic NPY axons (21%) from either one or more of the A1, A2 and A6 noradrenergic cell groups (124), and AGRP/NPY fibers from the arcuate nucleus (35%). Thus, the NPY innervation of CRH neurons arises mostly from catecholaminergic, mainly adrenergic but also noradrenergic, cell groups, while the arcuate nucleus is the source of the remaining one third of the NPY input to CRH neurons. This innervation pattern differs markedly from the NPY innervation of TRH neurons which originates primarily from the arcuate nucleus (75-80%) (123), while the remaining part is composed of adrenergic NPY fibers with only minor or no contribution by noradrenergic NPY axons. These differences in NPY inputs of TRH and CRH neurons raise the possibility that arcuate nucleus NPY neurons functionally are more significant in the regulation of TRH neurons, while the activity of CRH neurons is rather determined by catecholaminergic NPY afferents. The different NPY innervation of hypophysiotropic TRH and CRH neurons also indicates that within a nucleus, closely situated but functionally different cell groups potentially receive different organization of afferent inputs.

Examination of CART innervation of CRH neurons revealed that CART-containing axon varicosities establish synapses with CRH neurons in the PVN. Our detailed confocal microscopic analysis demonstrated that the CART-IR innervation of hypophysiotropic CRH neurons is also heterogeneous and originates from at least three different sources: 1) adrenergic CART neurons in the medullary C1–3 areas, 2) CART/α-MSH neurons in the arcuate nucleus, and 3) an additional population of CART-IR neurons of yet unknown location(s). Approximately 60%, of the CART-IR innervation of hypophysiotropic CRH neurons originates from the adrenergic CART neurons, and CART/PNMT-IR varicosities were found in juxtaposition to nearly all CRH neurons (95%). The second major CART input to hypophysiotropic CRH neurons arises from the arcuate nucleus: CART/α-MSH-IR varicosities comprise 18% of all CART containing boutons in juxtaposition to CRH neurons and contact about 58% of

CRH neurons. The third group of CART-IR axons in contact with the CRH neurons contains neither PNMT nor α-MSH. They were found in juxtaposition to approximately 68% of CRH neurons in the PVN and comprise approximately 22% of the CART-IR varicosities on the surface of CRH neurons. These results suggest that similarly to TRH neurons, a substantial population (more than half) of CRH neurons receive innervation from both the arcuate nucleus and adrenergic CART neurons, while the remaining CART innervation of CRH neurons may arise from CART neurons in the zona incerta/lateral hypothalamus, medial subnucleus of the NTS and the PVN, itself.

We should note that immunocytochemical labelings of TRH and CRH even after colchicine treatment do not allow us to visualize the whole dendritic tree of these cells including the most distal dendritic segments and spines. Therefore, we could not assess the association of NPY and CART varicosities with the distal dendritic regions of TRH and CRH neurons. The innervation of these regions may differ from that seen on the cell body and proximal dendrites. As a further technical comment, in our quantitative estimates of NPY and CART innervation of TRH and CRH neurons we considered the close contacts between axon-varicosities and TRH or CRH cell bodies and dendrites. Although it is obvious that these close contacts do not necessarily represent synaptic associations, NPY, PNMT, α-MSH and CART-containing fibers were all shown to establish synaptic contacts with both TRH and CRH neurons (63, 65, 108, 126, 127, 171).

Possible signaling mechanisms of adrenergic NPY- and CART-containing axons in the PVN

Based on several observations including selective lesioning experiments described below in detail, adrenergic neurons are suggested to exert a net stimulatory effect on both TRH and CRH neurons in various physiological conditions. The characteristic transmitter of adrenergic neurons, adrenaline, was also proposed to activate TRH and CRH neurons. Depletion of the classical neurotransmitter content of the central noradrenergic/adrenergic systems leads to a decrease in serum TSH levels (133), while stimulation of adrenergic receptors by noradrenaline injection into the PVN markedly and rapidly increases CRH heteronuclear RNA in the medial parvocellular subdivision (172, 173), and causes CRH release into the hypophyseal portal circulation, suggested by a rapid increase in ACTH levels and pituitary proopiomelanocortin mRNA (174).

The transcriptional activation of CRH neurons might be a result of the activation of postsynaptic α1-adrenergic receptors, which is expressed in virtually all CRH neurons (175). Activation of this receptor can induce CREB phosphorylation (176) and thus the stimulation of the CRH promoter (111). However, the effects of adrenaline on hypophysiotropic neurons might involve multiple pathways. Electrophysiologic studies demonstrate that the activity of various PVN neurons are strongly influenced through activation of adrenergic receptors located postsynaptically (177-179), presynaptically (177-183) and on glial cells (184). Unfortunately, only few of these studies examined parvocellular neurons that probably included hypophysiotropic TRH and/or CRH neurons. In these experiments, adrenergic stimulation did not have direct electrophysiological effects in about 85% of the examined parvocellular neurons (178), while in the majority of parvocellular neurons the frequency of spontaneous GABA-ergic inhibitory postsynaptic currents was decreased by the activation of presynaptic α2-adrenoreceptors (182).

Presently we can only speculate about the possible roles of CART and NPY as co-transmitters of adrenaline. Our results indicate that both NPY and CART are present in more than half of the adrenergic varicosities innervating TRH and CRH neurons. Based on several observations described in the Introduction, CART and NPY are suggested to oppositely regulate TRH and CRH neurons, therefore it seems paradoxical that these antagonistic peptides are present in the same nerve terminals on these hypophysiotropic neurons. However, the endogenous effects of these peptides in the PVN are probably complex and similarly to adrenaline, might involve both postsynaptic and presynaptic actions. In support of this hypothesis, the activation of postsynaptic and presynaptic NPY receptors, both present in the PVN (185), are suggested to oppositely affect CRH gene expression. Since NPY receptors are coupled to G proteins that inhibit adenylate cyclase (95), NPY is assumed to be inhibitory on CRH gene transcription when acts directly on the cell (111). However, NPY also has presynaptic effects to decrease GABA-ergic inhibitory transmission on medial parvocellular PVN neurons (116), which effect was shown to increase CRH gene transcription (186). The suppressive and stimulatory effects of chronic (Fekete et al., unpublished) and acute NPY administration (114), respectively, on CRH mRNA might be due to preferential postsynaptic or presynaptic effects of exogenous NPY. Therefore, the precise spatial localisation of NPY and CART receptors in relation to adrenergic nerve terminals would be an

important step to understand the mechanisms by which adrenergic NPY and CART affect CRH and TRH neurons.

Regulation of hypophysiotropic TRH and CRH neurons by adrenergic neurons

The observation that NPY- and CART-containing adrenergic fibers heavily innervate TRH and CRH neurons suggests that this ascending neuronal input has profound regulatory effects on these neurons. However, relatively little is known about the functional significance of this pathway. Investigators have focused mostly on the catecholaminergic regulation of CRH neurons while much less data are available on the regulation of TRH neurons.

Role of adrenergic neurons in the regulation of energy homeostasis

Since the brain utilizes only glucose as energy source, the regulation of glucose availability by central glucose sensing neuronal groups is critical for the normal functioning of the brain. Central adrenergic neurons have been proposed to be able to sense the changes of glucose level (187) and play critical role in the activation of CRH neurons as well as to elicit feeding in response to glucoprivation (136, 138). Well-established models of glucoprivation, the reduced cellular availability of glucose, are the administration of either insulin (hypoglycemia) or 2-deoxy-glucose (2DG), an inhibitor of intracellular glucose metabolism (cytoglucopenia) (188, 189). Glucoprivation evokes adaptive physiological responses crucial for survival, like feeding behaviour (190), activation of the sympathoadrenal system (191, 192) and the HPA axis, the latter indicated by an increase in corticosterone level and the increase of CRH heteronuclear RNA level in the PVN (138). Catecholaminergic neurons with projections to the PVN are strongly implicated in establishing these physiological responses, particularly adrenergic neurons in the C1-3 areas, but also medullary noradrenergic neurons in A1-A2 regions. In response to subcutaneous 2DG administration, the expression of c-fos, an immediate-early gene considered as a marker for functionally activated neurons (193), is induced in a substantial portion (21-46%) of adrenergic neurons in the C1-3 areas, while a less robust appearance of c-fos is observed in the A1 area (137). The fact that PVN projecting adrenergic and noradrenergic neurons are essential in HPA axis activation to glucoprivation was

demonstrated by the selective ablation of these catecholaminergic neurons (the immunolesioning technique is described in the **boxed text**). The intra-PVN injection of the toxin-antibody complex, anti-dopamine-β-hydroxylase (DBH)-saporin, results in a marked inhibition of the glucoprivation-induced rise in corticosterone levels and CRH gene expression (138).

Selective ablation of catecholaminergic neurons by anti-DBH-saporin

In the anti-dopamine-β-hydroxylase-saporin complex, saporin, a ribosome-inactivating protein (194), is coupled to a monoclonal antibody against dopamine-β-hydroxylase (DBH), the enzyme synthesizing noradrenaline. DBH is expressed in both noradrenergic and adrenergic neurons and is present in both membrane-bound and soluble forms in secretory vesicles (195). DBH is exposed to the exterior milieu upon release of noradrenaline/adrenaline and thus the anti-DBH-saporin complex can be selectively taken up by catecholaminergic nerve terminals, and transported retrogradely to the cell body. Then the toxic effect of saporin destroys the catecholaminergic perikarya and processes (196, 197). The injection of anti-DBH-saporin into the PVN causes a severe loss in noradrenergic and adrenergic cell populations known to innervate the PVN, resulting in a nearly total loss of DBH-containing axons in the PVN but without any visible aspecific damage (136, 138).

The selective destruction of PVN-projecting catecholaminergic cell groups also abolishes the feeding response to glucoprivation (136). This suggests that catecholaminergic neurons signaling in the PVN, and/or in other regions where they send axon-collaterals, evoke feeding in states of glucose deficit. Both catecholamines and NPY produced by these neurons are proposed to contribute to glucoprivic feeding. In C1-3 and A1 regions, NPY mRNA content is dramatically increased after 2DG treatment (142), while DBH mRNA levels are increased in C1, A1 and A2 (141). Studies in knockout animals demonstrated a more critical role for NPY, since NPY knockout mice have a markedly attenuated feeding response even to a moderate glucoprivation (139). In contrast, DBH knockout mice show impaired feeding response only to severe hypoglycemia or cytoglucopenia, but eat normally in response to a moderate glucoprivation (140). It is worth of note that arcuate nucleus NPY/AGRP neurons, although being activated by glucoprivation through this catecholaminergic pathway (198), are not essential for glucoprivic feeding, because mice with selective

neonatal ablation of NPY/AGRP neurons have normal feeding response to glucoprivation (199).

As shown by these data, adrenergic neurons not only express feeding-related peptides, but are also able to regulate both feeding and the activity of hypophysiotropic neurons. Therefore, we have raised the possibility that adrenergic neurons might also contribute to the generation of increased appetite and to the suppression of TRH and CRH synthesis in hypophysiotropic neurons of the PVN during fasting. We hypothesized that NPY and CART could be possible mediators of these putative roles of adenergic neurons, therefore we examined whether NPY and CART mRNA contents of the C1-3 areas are altered during fasting. However, we failed to detect any changes in the level of NPY mRNA in any of the C1-3 areas between fed and fasted animals by quantitative *in situ* hybridization. CART mRNA levels remained unchanged in the C3 area, while in the C1 region a slight but significant reduction was detected only in the mean gray value of hybridized CART neurons from fasted animals. However, this was a very modest decrease, especially compared to the robust reduction in CART mRNA levels in the arcuate nucleus during fasting (54, 59). Thus, we propose that this reduction in CART mRNA content of the C1 cell group may have only minor importance in the physiology of fasting.

Based on our *in situ* hybridization data that NPY and CART mRNA levels are practically unchanged in adrenergic neurons during fasting, it seems unlikely that during starvation NPY and CART secreted from adrenergic axons contribute to the changes in appetite and activity of TRH and CRH neurons. This is further supported by the recent data from our laboratories demonstrating that transection of the ascending brainstem input to the hypothalamus has no effect on the fasting-induced inhibition of TRH and CRH gene expression in the PVN (Fekete et al., unpublished).

It is important to note that the intra-PVN injection of anti-DBH-saporin causes a long-term weight gain which is significantly higher compared to the normal growth of control animals (136, 138), indicating that PVN projecting catecholaminergic neurons contribute to the long-term maintenance of body weight and energy homeostasis. Further investigations are needed to reveal the net weight-reducing effect of catecholaminergic neurons. This may be caused by the release of anorexigenic CART into the PVN, or, by tonic stimulatory effects of CART and adrenaline on the hypophysiotropic TRH neurons.

Regulatory roles of adrenergic neurons in other physiological states

The adrenergic neurons are also described to play important role in the mediation of the central effects of infection. The experimental models of bacterial infection and inflammation include the administration of bacterial lipopolysaccharide (LPS), a bacterial cell wall component, or interleukin-1 β (IL-1), a proinflammatory cytokine secreted by immune cells. Intravenous administration of IL-1 induces the expression of c-fos in PVN-projecting adrenergic neurons of the C1 and C2 areas (134), and also in CRH neurons in the PVN (132, 134). The same treatment induces a marked increase in CRH gene expression of the PVN (132, 134). The contribution of adrenergic fibers to the activation of CRH neurons to IL-1 or LPS was suggested by experiments showing that unilateral transection of the ascending fiber tracts rostral to the medulla prevents the LPS and IL-1 induced c-fos expression in CRH neurons and the increase in CRH mRNA on the side of the knifecut (132, 134, 135, 200). More recently, Schiltz et al. have demonstrated that the specific ablation of catecholaminergic input to the PVN by immunotoxin also prevents the rise in CRH mRNA level and the appearance of c-fos expression in CRH neurons in response to IL-1 (132). In contrast to the regulation of CRH neurons, brainstem pathways do not contribute to the LPS-induced decrease in TRH mRNA in the PVN, as it was reported in a previous work from our laboratory (135).

Glucoprivation and infection are considered as two different types of stress, and some studies addressed the question whether adrenergic and noradrenergic neurons are generally involved in the activation of CRH neurons to categorically different type of stressors. C-fos activation is, indeed, also present in the C1 region after restraint or forced swim stress, although not as robustly as after IL-1 adminstration or glucoprivation (201). However, the increase in CRH mRNA levels to restraint, and the increase in corticosterone levels to forced swim are both maintained after the immunotoxin ablation of PVN-projecting adrenergic/noradrenergic neurons (132, 138). Furthermore, c-fos expression in the CRH neurons and the increase in CRH mRNA to footshock stress remain intact after transection of ascending fibers rostral to the medulla (200). These experiments indicate that adrenergic neurons are involved in the activation of CRH neurons by only certain kind of physical stressors.

The only physiological state in which adrenergic neurons have been proposed to regulate hypophysiotropic TRH neurons so far is cold exposure. When animals are

transferred to a cold (4°C) environment, the activation of TRH neurons, and increase in TSH and thyroid hormone levels are observed (202, 203). The cold-induced activation of the HPT axis serves to increase thermogenesis and maintain body temperature. The pharmacological depletion of the central catecholaminergic system prevents the cold-stimulated TSH response (133). Furthermore, central administration of the β-adrenoreceptor antagonist propranolol blocks the cold-induced TRH synthesis in the PVN (204). Adrenergic afferents to TRH and CRH neurons together with the formerly known NPY and CART inputs from the arcuate nucleus are summarized in **Fig 24**.

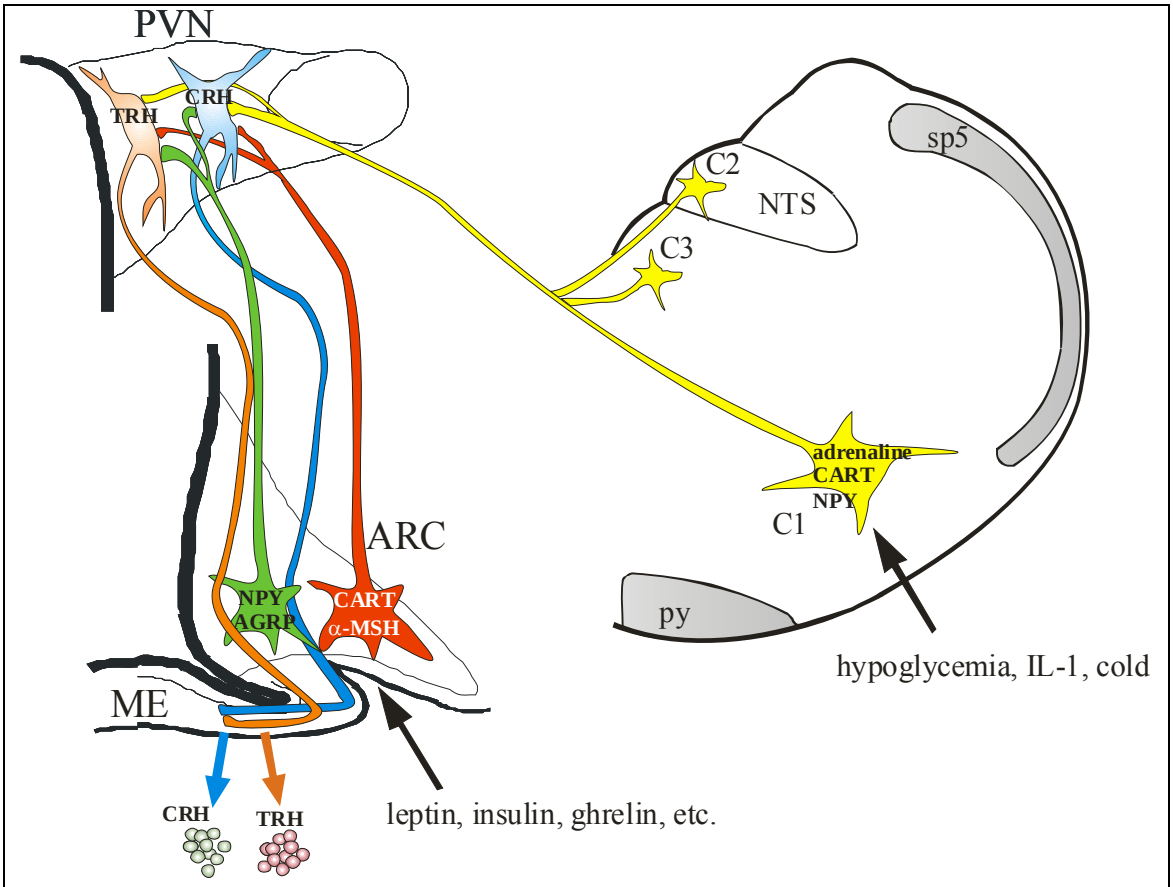

Fig. 24. Schematic figure illustrates the known NPY- and CART-containing neural afferents to hypophysiotropic TRH and CRH neurons. NPY and CART are produced in separate cell groups of the arcuate nucleus: both AGRP/NPY and α-MSH/CART neurons innervate hypophysiotropic TRH and CRH neurons. Other major sources of NPY and CART innervation of these hypophysiotropic cells are medullary adrenergic neurons that constitute three cell groups: C1, C2 and C3. The majority of adrenergic neurons co-synthesize CART and NPY. ARC, arcuate nucleus; ME, median eminence; py, pyramidal tract; sp5, spinal trigeminal tract.

In the foregoing we summarized the relatively well-delineated regulatory functions of adrenergic neurons, however, much of this area is yet unknown. Further investigations are needed to clarify the putative roles of adrenergic neurons in the regulation of TRH neurons in glucoprivation. The contribution of adrenergic afferents

also seems likely in the activation of the HPA axis to cold exposure (205). In addition, adrenergic neurons might mediate changes in blood pressure on hypophysotropic neurons, as hypothalamically projecting adrenergic C1 neurons are reported to be barosensitive (206, 207). Future studies are required to elucidate the role of CART and NPY signaling from adrenergic axons in the regulation of hypophysiotropic TRH and CRH neurons under these physiological circumstances.

CART-IR innervation of TRH and CRH neurons from other sources

Our quantitative data showed that CART/α-MSH fibers innervate about 58% of hypophysiotropic CRH neurons. As it is described in the Introduction, CART/α-MSH neurons are principal mediators of leptin signaling and are suggested to participate in the fasting-induced reduction in CRH mRNA in the PVN (58, 99). In contrast, the leptin-induced increase of CART and α-MSH synthesis in arcuate nucleus neurons may contribute to the recovery of CRH synthesis after refeeding (99). Additionally, since CART mRNA is increased by endotoxin in neurons of the arcuate nucleus (208), this neuron population may also contribute to the LPS-induced activation of the hypophysiotropic CRH neurons described above.

We revealed that a group of CART-IR axons that does not belong to either adrenergic or arcuate nucleus CART neurons also contributes to the innervation of CRH neurons, innervating approximately 68% of them. Although we do not have similar indications of TRH neurons, these neurons might be also innervated by CART neurons outside the arcuate nucleus and adrenergic neurons. In our retrograde tracing experiment we found two other CART-producing cell groups that project to the PVN and thus may innervate TRH and CRH neurons: CART neurons in the zona incerta / lateral hypothalamus and in the medial subnucleus of the NTS.

CART neurons of the zona incerta and lateral hypothalamus that project to the PVN co-express MCH. The essential role of MCH in energy homeostasis, shown by the lean phenotype of MCH knockout animals (209) and the obesity of MCH-overexpressing mice (210), suggests that the putative innervation of TRH and CRH neurons by MCH/CART fibers would be a neural input that conveys important metabolic signals to these hypophysiotropic neurons. The co-expression of CART and MCH seems similarly paradoxical to the colocalisation of CART and NPY in adrenergic neurons, because CART and MCH also have opposite effects on energy homeostasis. In contrast to the

food intake-reducing effect of CART (54), MCH increases food intake (211), and whereas CART synthesis is stimulated by leptin in the lateral hypothalamus and zona incerta similarly as in the arcuate nucleus (54), leptin inhibits MCH expression (212). Furthermore, contrary to the stimulatory role of CART on TRH neurons, central MCH injection decreases plasma TSH levels, and MCH reduces TRH release from hypothalamic explants (213). If endogenous MCH indeed inhibits the HPT axis, then the loss of this inhibition may underlie the observation that ablation of MCH in ob/ob animals leads to dramatic reduction in body fat due to marked increase in resting energy expenditure and locomotor activity (214). These data together enlarge the significance of whether CART/MCH neurons innervate, and therefore, are able to directly regulate hypophysiotropic TRH neurons.

CART neurons in the medial subnucleus of the NTS may also give rise to neural afferents to TRH and CRH neurons. The NTS is a major viscero-sensory relay center that receives a wide variety of inputs from gustatory, cardiovascular, respiratory, pulmonary, and gastrointestinal afferents and from several brain nuclei, targeted to specific subdivisions within this complex structure which are then carried to the forebrain by ascending projections (215). This viscerotopic pattern of innervation suggests that the different subnuclei of the NTS may have distinct roles in the mediation of different physiological functions, although extensive interconnections within the NTS also exist (215). The location of CART in medial subnucleus neurons of the NTS is particularly interesting since, collectively, these neurons receive afferent fibers from multiple organs and, together with the commissural nucleus, give rise to the majority of ascending fibers of NTS origin (215). Thus, CART produced by medial subnucleus neurons may serve as an important signal peptide responsible for carrying visceral information from multiple organs to the hypophysiotropic TRH and CRH neurons.

It is well known that CART-producing neurons are also present in the PVN (129, 131) and, therefore, the potential contribution of these neurons to the innervation of hypophysiotropic TRH and CRH neurons should also be considered. Local neural circuits within the PVN have been, indeed, suggested by morphological and electrophysiological data (177, 216). For insurmountable technical reasons, however, we were unable to address this possibility in our tracing experiment due to tracer deposition in the PVN which obscured any potential retrogradely labeled neurons. In the PVN, CART is expressed in a subpopulation of magnocellular oxytocinergic and vasopressinergic neurons (49, 217), while in the parvocellular division, CART is

synthesized in more than 80% of hypophysiotropic TRH neurons (65, 167, 169), in a subpopulation of the somatostatin neurons (49, 217), but also expressed in yet uncharacterized cell groups. Further investigations are required to determine whether any of these CART-producing cell groups signal on TRH and/or CRH neurons through local axonal projections.

Regulation of TRH neurons by galanin-containing fibers

Our studies demonstrate that galanin-containing axons innervate the majority of hypophysiotropic TRH neurons in the PVN. The synapses of galanin-containing axon terminals on TRH neurons were found to be of the symmetric type, indicating an inhibitory nature of this input (218). The inhibitory role of galanin on the activity of TRH neurons was also suggested by the fact that central galanin administration decreases circulating levels of TSH, and *in vitro*, galanin inhibits TRH release from hypothalamic slices (152). The presumed direct inhibitory action of galanin on TRH neurons may be mediated by type 1 galanin receptor that is coupled to Gi protein (219, 220) and is expressed in the medial parvocellular subdivision (221).

The origin of the galaninergic innervation of TRH neurons may arise from several sources. Within the hypothalamus, the dorsomedial nucleus (DMN), arcuate nucleus and medial preoptic area contain populations of galanin-producing neurons that project to the PVN (153). The DMN contains the largest population of galanin cells retrogradely labeled from the PVN and, therefore, it is believed to be the principal source for the galanin-IR fibers in the PVN (153). Since practically all TRH neurons in the PVN receive innervation from neurons residing in the DMN (158), the DMN may also be the principal source for galanin-IR fibers in contact with TRH neurons.

The PVN also contains galanin-producing neurons (143), located both in the parvocellular and magnocellular divisions. Since galanin mRNA expression is increased in the anterior parvocellular subdivision of the PVN during food deprivation (222), if this cell population is involved in the innervation of hypophysiotropic TRH neurons, galanin may contribute to the inhibition of the HPT axis during fasting.

The galanin innervation to the PVN may also derive from neuronal populations outside of the hypothalamus. Galanin is expressed in noradrenergic neurons of the A1 and A6 regions of the brainstem that project to the PVN (153). Since DBH-IR axons densely innervate the TRH neurons in the PVN (126), it is conceivable that at least a

portion of the galaninergic innervation to TRH neurons in the PVN arises from the brainstem. Galaninergic neurons also project to the PVN from serotonergic B7 and B8 cell groups in the raphe (153), where galanin colocalizes with serotonin (223, 224). Further investigations are required to determine the relative involvement of these galaninergic cell groups in the innervation of TRH neurons, and their possible role in the regulation of TRH synthesis.

We have found that in contrast to galanin, GALP-containing axons very rarely innervate hypophysiotropic TRH neurons. GALP is another member of the galanin peptide family with orexigenic properties (148, 150), and is expressed exclusively in neurons of the arcuate nucleus (149, 151, 225). The vast majority of these neurons express leptin receptor (151), indicating the potential importance of GALP as a central mediator of leptin. However, contrary to the other arcuate-derived orexigenic peptides, NPY and AGRP, GALP mRNA is increased rather than reduced by the systemic administration of leptin (151). Since GALP-containing nerve terminals are associated with only very few TRH neurons in the hypophysiotropic regions of the PVN, GALP may have only indirect regulatory effects, if any, over hypophysiotropic TRH neurons. Nevertheless, Seth et al. have recently reported that GALP can inhibit the release of TRH from hypothalamic explants and administration of GALP into the PVN decreases TSH levels (152). However, as GALP is an agonist of galanin receptors (148), it is conceivable that the exogenous administration of GALP into the PVN may bind to galanin receptors and mimic the effect of endogenous galanin input. Alternatively, exogenous GALP administration may influence the HPT axis through an indirect pathway.

Conclusions

We conclude that in addition to neurons of the arcuate nucleus, adrenergic neurons in the C1-3 regions represent another major source of both NPY and CART innervation of hypophysiotropic TRH and CRH neurons. In contrast to the arcuate nucleus, NPY and CART mRNA levels in the C1-3 regions are unchanged in starvation; thus, NPY and CART expressed by adrenergic neurons probably do not contribute to the suppression of TRH and CRH synthesis in the PVN during fasting. CART expressing neurons located in the zona incerta and lateral hypothalamus, the NTS and the PVN may also be involved in the innervation of hypophysiotropic TRH and CRH neurons. Galanin is another orexigenic peptide that is in anatomic position to regulate TRH neurons.

Therefore, our data suggest that TRH and CRH neurons are innervated by axons containing feeding-related peptides that arise from multiple sources and differentially regulate these hypophysiotropic neurons.

Summary

Hypophysiotropic thyrotropin-releasing hormone (TRH)- and corticotropin-releasing hormone (CRH)-synthesizing neurons in the hypothalamic paraventricular nucleus (PVN) play important roles in the regulation of energy homeostasis through the regulation of the hypothalamic-pituitary-thyroid and hypothalamic-pituitary-adrenocortical axes, respectively. During the period of fasting, both TRH and CRH syntheses are inhibited, mainly through neural inputs arising from orexigenic neuropeptide Y (NPY)- and agouti-related protein (AGRP)-synthesizing neurons and anorexigenic α-melanocyte-stimulating hormone (α-MSH)- and cocaine-and-amphetamine-regulated transcript (CART)-producing neurons of the arcuate nucleus. Previous morphological observations suggested that the arcuate nucleus is not the exclusive source of the dense NPY and CART innervation of the TRH and CRH neurons. We conducted a series of experiments to reveal the sources of NPY and CART innervation of TRH and CRH neurons, using retrograde tract-tracing, multiple-labeling immunocytochemistry and combined fluorescent *in situ* hybridization and immunofluorescence. We revealed that about 27% of the NPY innervation of TRH neurons arises from medullary adrenergic neurons. We identified the CART-producing cell groups that innervate the PVN: these included CART neurons of the arcuate nucleus, the zona incerta and the lateral hypothalamus, medullary adrenergic neurons in the C1-3 regions, and the nucleus of the solitary tract. TRH neurons were found to receive 44% of their CART-immunoreactive (IR) innervation from adrenergic neurons. The CART innervation of CRH neurons consisted of adrenergic CART fibers (60%), α-MSH/CART fibers (18%) and CART-IR axons from other sources (22%). To reveal whether NPY or CART expression in adrenergic neurons is altered in fasting and may contribute to the suppression of TRH and CRH synthesis, we performed quantitative *in situ* hybridization for NPY and CART in the medulla. Except for a small reduction in CART mRNA level in the C1 cell group, we did not detect any changes in NPY and CART mRNA in the C1-3 regions, suggesting that these peptides mediate other stimuli on TRH and CRH neurons. We also revealed that axons containing the orexigenic peptide galanin densely innervate TRH neurons, while only a very small fraction of TRH neurons receives innervation from galanin-like peptide (GALP)-containing axons. Our data indicate that TRH and CRH neurons are innervated by axons containing feeding-related peptides that arise from multiple sources and diferentially regulate these hypophysiotropic neurons.

Összefoglaló

A hipotalamusz paraventrikuláris magjában (PVN) elhelyezkedő hipofizeotróf thyrotropin-releasing hormon (TRH)- és corticotropin-releasing hormon (CRH)-termelő idegsejtek fontos szerepet játszanak az energia homeosztázis szabályozásában a hipotalamusz-hipofízis-pajzsmirigy, illetve a hipotalamusz-hipofízis-mellékvesekéreg tengely irányításán keresztül. Éhezésben a TRH és CRH neuronok működése gátlódik, elsősorban a nucleus arcuatusban található orexigén hatású neuropeptid Y-t (NPY) és agouti-related protein-t termelő neuronok megnövekedett gátló hatása, és az anorexigén α-melanocita-stimuláló hormont (α-MSH) és cocaine- and amphetamine-regulated transcript (CART)-et termelő neuronok csökkent serkentő hatása következtében. Korábbi morfológiai adatok valószínűsítették, hogy a nucleus arcuatus nem kizárólagos forrása a TRH és CRH idegsejteket sűrűn beidegző NPY és a CART idegrostoknak. A TRH és CRH neuronok CART és NPY beidegzésének feltárásához kísérleteinkben retrográd idegpálya-jelölési, többesjelöléses immuncitokémiai és kombinált *in situ* hibridizációs és immunfluoreszcens módszereket alkalmaztunk. Feltártuk, hogy a TRH neuronok NPY innervációjának 27%-át agytörzsi eredetű adrenerg idegrostok képezik. Azonosítottuk a PVN-be vetülő CART-termelő idegsejtcsoportokat, melyek az arcuatus idegmagban, a zona incertában és a laterális hipotalamuszban, a nyúltvelői C1-3 adrenerg régiókban és a nucleus tractus solitarius-ban helyezkedtek el. A TRH neuronok CART-immunreaktív (IR) beidegzésének 44%-a a nyúltvelői adrenerg idegsejtektől származott. A CRH neuronok CART-IR beidegzését adrenerg CART idegrostok (60%), α-MSH/CART axonok (18%) és egyéb agyterületekről eredő CART-IR axonok (22%) alkották. Feltételezve, hogy az adrenerg eredetű NPY és CART éhezésben hozzájárulhat a TRH és CRH szintézis csökkenéséhez, kvantitatív izotópos *in situ* hibridizációval vizsgáltuk az NPY és CART mRNS szinteket a nyúltvelőben. A CART mRNS szint C1 régióban detektált kismértékű csökkenésén kívül sem az NPY, sem a CART mRNS mennyisége nem változott meg a C1-3 regiókban éhezésben, valószínűsítve, hogy ezek a peptidek más hatásokat közvetítenek a TRH és CRH neuronok felé. Feltártuk továbbá, hogy az orexigén galanint tartalmazó idegrostok sűrűn beidegzik a TRH neuronokat. Ezzel szemben a TRH neuronoknak csak igen kis hányadát innerválják galanin-like peptid-et tartalmazó idegrostok. Eredményeinkből arra következtetünk, hogy a TRH és CRH neuronokat beidegző orexigén illetve anorexigén peptideket tartalmazó idegrostok számos agyterületről érkeznek, és eltérően szabályozzák a hipofizeotróf TRH és CRH neuronokat.

References

1 Kawano H, Tsuruo Y, Bando H, Daikoku S (1991) Hypophysiotrophic TRH-producing neurons identified by combining immunohistochemistry for pro-TRH and retrograde tracing. J Comp Neurol, 307:531-538

2 Lennard DE, Eckert WA, Merchenthaler I (1993) Corticotropin-releasing hormone neurons in the paraventricular nucleus project to the external zone of the median eminence: a study combining retrograde labeling with immunocytochemistry. J Neuroendocrinol, 5:175-181

3 Niimi M, Takahara J, Hashimoto K, Kawanishi K (1988) Immunohistochemical identification of corticotropin releasing factor-containing neurons projecting to the stalk-median eminence of the rat. Peptides, 9:589-593

4 Legradi G, Emerson CH, Ahima RS, Flier JS, Lechan RM (1997) Leptin prevents fasting-induced suppression of prothyrotropin-releasing hormone messenger ribonucleic acid in neurons of the hypothalamic paraventricular nucleus. Endocrinology, 138:2569-2576

5 Rondeel JM, Heide R, de Greef WJ, van Toor H, van Haasteren GA, Klootwijk W, Visser TJ (1992) Effect of starvation and subsequent refeeding on thyroid function and release of hypothalamic thyrotropin-releasing hormone. Neuroendocrinology, 56:348-353

6 Sapolsky RM, Romero LM, Munck AU (2000) How do glucocorticoids influence stress responses? Integrating permissive, suppressive, stimulatory, and preparative actions. Endocr Rev, 21:55-89

7 Cone RD, Low MJ, Elmquist JK, Cameron JL. Neuroendocrinology. In: Kronenberg HM, Melmed S, Larsen PR, Polonsky KS (eds.), Williams Textbook of Endocrinology. 10th ed. W.B. Saunders Co., Philadelphia, 2003: 81-177

8 Larsen PR, Davies TF, Schlumberger M-J, Hay ID. Thyroid Physiology and Diagnostic Evaluation of Patients with Thyroid Disorders. In: Larsen PR, Kronenberg HM, Melmed S, Polonsky KS (eds.), Williams Textbook of Endocrinology. 10th. ed. W.B. Saunders Co., Philadelphia, 2003: 331-373

9 Stewart PM. The Adrenal Cortex. In: Larsen PR, Kronenberg HM, Melmed S, Polonsky KS (eds.), Williams Textbook of Endocrinology. W.B. Saunders Co., Philadelphia, 2003: 475-543

10 Nussey SS, Whitehead SA. The thyroid gland. In: Endocrinology: An Integrated Approach. BIOS Scientific Publishers Limited, Oxford, 2001: 71-115

11 Silva JE (2003) The thermogenic effect of thyroid hormone and its clinical implications. Ann Intern Med, 139:205-213

12 Cannon B, Nedergaard J (2004) Brown adipose tissue: function and physiological significance. Physiol Rev, 84:277-359

13 Brooks SL, Rothwell NJ, Stock MJ, Goodbody AE, Trayhurn P (1980) Increased proton conductance pathway in brown adipose tissue mitochondria of rats exhibiting diet-induced thermogenesis. Nature, 286:274-276

14 Rothwell NJ, Stock MJ (1979) A role for brown adipose tissue in diet-induced thermogenesis. Nature, 281:31-35

15 de Jesus LA, Carvalho SD, Ribeiro MO, Schneider M, Kim SW, Harney JW, Larsen PR, Bianco AC (2001) The type 2 iodothyronine deiodinase is essential for adaptive thermogenesis in brown adipose tissue. J Clin Invest, 108:1379-1385

16 Ribeiro MO, Carvalho SD, Schultz JJ, Chiellini G, Scanlan TS, Bianco AC, Brent GA (2001) Thyroid hormone--sympathetic interaction and adaptive thermogenesis are thyroid hormone receptor isoform--specific. J Clin Invest, 108:97-105

17 Boss O, Samec S, Paoloni-Giacobino A, Rossier C, Dulloo A, Seydoux J, Muzzin P, Giacobino JP (1997) Uncoupling protein-3: a new member of the mitochondrial carrier family with tissue-specific expression. FEBS Lett, 408:39-42

18 de Lange P, Lanni A, Beneduce L, Moreno M, Lombardi A, Silvestri E, Goglia F (2001) Uncoupling protein-3 is a molecular determinant for the regulation of resting metabolic rate by thyroid hormone. Endocrinology, 142:3414-3420

19 Gong DW, He Y, Karas M, Reitman M (1997) Uncoupling protein-3 is a mediator of thermogenesis regulated by thyroid hormone, beta3-adrenergic agonists, and leptin. J Biol Chem, 272:24129-24132

20 Lebon V, Dufour S, Petersen KF, Ren J, Jucker BM, Slezak LA, Cline GW, Rothman DL, Shulman GI (2001) Effect of triiodothyronine on mitochondrial energy coupling in human skeletal muscle. J Clin Invest, 108:733-737

21 Queiroz MS, Shao Y, Ismail-Beigi F (2004) Effect of thyroid hormone on uncoupling protein-3 mRNA expression in rat heart and skeletal muscle. Thyroid, 14:177-185

22 Ukropec J, Anunciado RV, Ravussin Y, Kozak LP (2006) Leptin is required for uncoupling protein-1-independent thermogenesis during cold stress. Endocrinology, 147:2468-2480

23 Lowell BB, Bachman ES (2003) Beta-Adrenergic receptors, diet-induced thermogenesis, and obesity. J Biol Chem, 278:29385-29388

24 Bianco AC, Carvalho SD, Carvalho CR, Rabelo R, Moriscot AS (1998) Thyroxine 5'-deiodination mediates norepinephrine-induced lipogenesis in dispersed brown adipocytes. Endocrinology, 139:571-578

25 Bianco AC, Silva JE (1987) Optimal response of key enzymes and uncoupling protein to cold in BAT depends on local T3 generation. Am J Physiol, 253:E255-263

26 Carvalho SD, Negrao N, Bianco AC (1993) Hormonal regulation of malic enzyme and glucose-6-phosphate dehydrogenase in brown adipose tissue. Am J Physiol, 264:E874-881

27 Goodridge AG (1978) Regulation of malic enzyme synthesis by thyroid hormone and glucagon: inhibitor and kinetic experiments. Mol Cell Endocrinol, 11:19-29

28 Miksicek RJ, Towle HC (1982) Changes in the rates of synthesis and messenger RNA levels of hepatic glucose-6-phosphate and 6-phosphogluconate dehydrogenases following induction by diet or thyroid hormone. J Biol Chem, 257:11829-11835

29 Oppenheimer JH, Schwartz HL, Lane JT, Thompson MP (1991) Functional relationship of thyroid hormone-induced lipogenesis, lipolysis, and thermogenesis in the rat. J Clin Invest, 87:125-132

30 Luo L, MacLean DB (2003) Effects of thyroid hormone on food intake, hypothalamic Na/K ATPase activity and ATP content. Brain Res, 973:233-239

31 Kong WM, Martin NM, Smith KL, Gardiner JV, Connoley IP, Stephens DA, Dhillo WS, Ghatei MA, Small CJ, Bloom SR (2004) Triiodothyronine stimulates food intake via the hypothalamic ventromedial nucleus independent of changes in energy expenditure. Endocrinology, 145:5252-5258

32 Jamieson PM, Nyirenda MJ, Walker BR, Chapman KE, Seckl JR (1999) Interactions between oestradiol and glucocorticoid regulatory effects on liver-specific glucocorticoid-inducible genes: possible evidence for a role of hepatic 11beta-hydroxysteroid dehydrogenase type 1. J Endocrinol, 160:103-109

33 Sasaki K, Cripe TP, Koch SR, Andreone TL, Petersen DD, Beale EG, Granner DK (1984) Multihormonal regulation of phosphoenolpyruvate carboxykinase gene transcription. The dominant role of insulin. J Biol Chem, 259:15242-15251

34 Watts LM, Manchem VP, Leedom TA, Rivard AL, McKay RA, Bao D, Neroladakis T, Monia BP, Bodenmiller DM, Cao JX, Zhang HY, Cox AL, Jacobs SJ, Michael MD, Sloop KW, Bhanot S (2005) Reduction of hepatic and adipose tissue glucocorticoid receptor expression with antisense oligonucleotides improves hyperglycemia and hyperlipidemia in diabetic rodents without causing systemic glucocorticoid antagonism. Diabetes, 54:1846-1853

35 Rooney DP, Neely RD, Cullen C, Ennis CN, Sheridan B, Atkinson AB, Trimble ER, Bell PM (1993) The effect of cortisol on glucose/glucose-6-phosphate cycle activity and insulin action. J Clin Endocrinol Metab, 77:1180-1183

36 Delaunay F, Khan A, Cintra A, Davani B, Ling ZC, Andersson A, Ostenson CG, Gustafsson J, Efendic S, Okret S (1997) Pancreatic beta cells are important targets for the diabetogenic effects of glucocorticoids. J Clin Invest, 100:2094-2098

37 Masuzaki H, Paterson J, Shinyama H, Morton NM, Mullins JJ, Seckl JR, Flier JS (2001) A transgenic model of visceral obesity and the metabolic syndrome. Science, 294:2166-2170

38 De Vos P, Saladin R, Auwerx J, Staels B (1995) Induction of ob gene expression by corticosteroids is accompanied by body weight loss and reduced food intake. J Biol Chem, 270:15958-15961

39 Slieker LJ, Sloop KW, Surface PL, Kriauciunas A, LaQuier F, Manetta J, Bue-Valleskey J, Stephens TW (1996) Regulation of expression of ob mRNA and protein by glucocorticoids and cAMP. J Biol Chem, 271:5301-5304

40 Wiper-Bergeron N, Salem HA, Tomlinson JJ, Wu D, Hache RJ (2007) Glucocorticoid-stimulated preadipocyte differentiation is mediated through acetylation of C/EBPbeta by GCN5. Proc Natl Acad Sci U S A, 104:2703-2708

41 Kershaw EE, Morton NM, Dhillon H, Ramage L, Seckl JR, Flier JS (2005) Adipocyte-specific glucocorticoid inactivation protects against diet-induced obesity. Diabetes, 54:1023-1031

42 Densmore VS, Morton NM, Mullins JJ, Seckl JR (2006) 11 beta-hydroxysteroid dehydrogenase type 1 induction in the arcuate nucleus by high-fat feeding: A novel constraint to hyperphagia? Endocrinology, 147:4486-4495

43 Schwartz MW, Woods SC, Porte D, Jr., Seeley RJ, Baskin DG (2000) Central nervous system control of food intake. Nature, 404:661-671

44 van Haasteren GA, Linkels E, Klootwijk W, van Toor H, Rondeel JM, Themmen AP, de Jong FH, Valentijn K, Vaudry H, Bauer K, et al. (1995) Starvation-induced changes in the hypothalamic content of prothyrotrophin-releasing hormone (proTRH) mRNA and the hypothalamic release of proTRH-derived peptides: role of the adrenal gland. J Endocrinol, 145:143-153

45 Ahima RS, Prabakaran D, Mantzoros C, Qu D, Lowell B, Maratos-Flier E, Flier JS (1996) Role of leptin in the neuroendocrine response to fasting. Nature, 382:250-252

46 Legradi G, Emerson CH, Ahima RS, Rand WM, Flier JS, Lechan RM (1998) Arcuate nucleus ablation prevents fasting-induced suppression of ProTRH mRNA in the hypothalamic paraventricular nucleus. Neuroendocrinology, 68:89-97

47 Elmquist JK, Bjorbaek C, Ahima RS, Flier JS, Saper CB (1998) Distributions of leptin receptor mRNA isoforms in the rat brain. J Comp Neurol, 395:535-547

48 Elias CF, Lee C, Kelly J, Aschkenasi C, Ahima RS, Couceyro PR, Kuhar MJ, Saper CB, Elmquist JK (1998) Leptin activates hypothalamic CART neurons projecting to the spinal cord. Neuron, 21:1375-1385

49 Vrang N, Larsen PJ, Clausen JT, Kristensen P (1999) Neurochemical characterization of hypothalamic cocaine- amphetamine-regulated transcript neurons. J Neurosci, 19:RC5

50 Broberger C, Johansen J, Johansson C, Schalling M, Hokfelt T (1998) The neuropeptide Y/agouti gene-related protein (AGRP) brain circuitry in normal, anorectic, and monosodium glutamate-treated mice. Proc Natl Acad Sci U S A, 95:15043-15048

51 Hahn TM, Breininger JF, Baskin DG, Schwartz MW (1998) Coexpression of Agrp and NPY in fasting-activated hypothalamic neurons. Nat Neurosci, 1:271-272

52 Cheung CC, Clifton DK, Steiner RA (1997) Proopiomelanocortin neurons are direct targets for leptin in the hypothalamus. Endocrinology, 138:4489-4492

53 Mercer JG, Hoggard N, Williams LM, Lawrence CB, Hannah LT, Morgan PJ, Trayhurn P (1996) Coexpression of leptin receptor and preproneuropeptide Y mRNA in arcuate nucleus of mouse hypothalamus. J Neuroendocrinol, 8:733-735

54 Kristensen P, Judge ME, Thim L, Ribel U, Christjansen KN, Wulff BS, Clausen JT, Jensen PB, Madsen OD, Vrang N, Larsen PJ, Hastrup S (1998) Hypothalamic CART is a new anorectic peptide regulated by leptin. Nature, 393:72-76

55 Mizuno TM, Kleopoulos SP, Bergen HT, Roberts JL, Priest CA, Mobbs CV (1998) Hypothalamic pro-opiomelanocortin mRNA is reduced by fasting and

[corrected] in ob/ob and db/db mice, but is stimulated by leptin. Diabetes, 47:294-297

56 Mizuno TM, Mobbs CV (1999) Hypothalamic agouti-related protein messenger ribonucleic acid is inhibited by leptin and stimulated by fasting. Endocrinology, 140:814-817

57 Stephens TW, Basinski M, Bristow PK, Bue-Valleskey JM, Burgett SG, Craft L, Hale J, Hoffmann J, Hsiung HM, Kriauciunas A, et al. (1995) The role of neuropeptide Y in the antiobesity action of the obese gene product. Nature, 377:530-532

58 Brady LS, Smith MA, Gold PW, Herkenham M (1990) Altered expression of hypothalamic neuropeptide mRNAs in food-restricted and food-deprived rats. Neuroendocrinology, 52:441-447

59 Fekete C, Singru PS, Sanchez E, Sarkar S, Christoffolete MA, Riberio RS, Rand WM, Emerson CH, Bianco AC, Lechan RM (2006) Differential effects of central leptin, insulin, or glucose administration during fasting on the hypothalamic-pituitary-thyroid axis and feeding-related neurons in the arcuate nucleus. Endocrinology, 147:520-529

60 Guo F, Bakal K, Minokoshi Y, Hollenberg AN (2004) Leptin signaling targets the thyrotropin-releasing hormone gene promoter in vivo. Endocrinology, 145:2221-2227

61 Harris M, Aschkenasi C, Elias CF, Chandrankunnel A, Nillni EA, Bjoorbaek C, Elmquist JK, Flier JS, Hollenberg AN (2001) Transcriptional regulation of the thyrotropin-releasing hormone gene by leptin and melanocortin signaling. J Clin Invest, 107:111-120

62 Perello M, Stuart RC, Nillni EA (2006) The role of intracerebroventricular administration of leptin in the stimulation of prothyrotropin releasing hormone neurons in the hypothalamic paraventricular nucleus. Endocrinology, 147:3296-3306

63 Fekete C, Legradi G, Mihaly E, Huang QH, Tatro JB, Rand WM, Emerson CH, Lechan RM (2000) alpha-Melanocyte-stimulating hormone is contained in nerve terminals innervating thyrotropin-releasing hormone-synthesizing neurons in the hypothalamic paraventricular nucleus and prevents fasting-induced suppression of prothyrotropin-releasing hormone gene expression. J Neurosci, 20:1550-1558

64 Kim MS, Small CJ, Stanley SA, Morgan DG, Seal LJ, Kong WM, Edwards CM, Abusnana S, Sunter D, Ghatei MA, Bloom SR (2000) The central melanocortin system affects the hypothalamo-pituitary thyroid axis and may mediate the effect of leptin. J Clin Invest, 105:1005-1011

65 Fekete C, Mihaly E, Luo LG, Kelly J, Clausen JT, Mao Q, Rand WM, Moss LG, Kuhar M, Emerson CH, Jackson IM, Lechan RM (2000) Association of cocaine- and amphetamine-regulated transcript-immunoreactive elements with thyrotropin-releasing hormone-synthesizing neurons in the hypothalamic paraventricular nucleus and its role in the regulation of the hypothalamic-pituitary-thyroid axis during fasting. J Neurosci, 20:9224-9234

66 Stanley SA, Small CJ, Murphy KG, Rayes E, Abbott CR, Seal LJ, Morgan DG, Sunter D, Dakin CL, Kim MS, Hunter R, Kuhar M, Ghatei MA, Bloom SR (2001) Actions of cocaine- and amphetamine-regulated transcript (CART)

peptide on regulation of appetite and hypothalamo-pituitary axes in vitro and in vivo in male rats. Brain Res, 893:186-194

67 Cowley MA, Smart JL, Rubinstein M, Cerdan MG, Diano S, Horvath TL, Cone RD, Low MJ (2001) Leptin activates anorexigenic POMC neurons through a neural network in the arcuate nucleus. Nature, 411:480-484

68 Takahashi KA, Cone RD (2005) Fasting induces a large, leptin-dependent increase in the intrinsic action potential frequency of orexigenic arcuate nucleus neuropeptide Y/Agouti-related protein neurons. Endocrinology, 146:1043-1047

69 Bouret SG, Draper SJ, Simerly RB (2004) Trophic action of leptin on hypothalamic neurons that regulate feeding. Science, 304:108-110

70 Bagnol D, Lu XY, Kaelin CB, Day HE, Ollmann M, Gantz I, Akil H, Barsh GS, Watson SJ (1999) Anatomy of an endogenous antagonist: relationship between Agouti-related protein and proopiomelanocortin in brain. J Neurosci, 19:RC26

71 Pritchard LE, Armstrong D, Davies N, Oliver RL, Schmitz CA, Brennand JC, Wilkinson GF, White A (2004) Agouti-related protein (83-132) is a competitive antagonist at the human melanocortin-4 receptor: no evidence for differential interactions with pro-opiomelanocortin-derived ligands. J Endocrinol, 180:183-191

72 Yang YK, Thompson DA, Dickinson CJ, Wilken J, Barsh GS, Kent SB, Gantz I (1999) Characterization of Agouti-related protein binding to melanocortin receptors. Mol Endocrinol, 13:148-155

73 Cone RD, Lu D, Koppula S, Vage DI, Klungland H, Boston B, Chen W, Orth DN, Pouton C, Kesterson RA (1996) The melanocortin receptors: agonists, antagonists, and the hormonal control of pigmentation. Recent Prog Horm Res, 51:287-317; discussion 318

74 Graham M, Shutter JR, Sarmiento U, Sarosi I, Stark KL (1997) Overexpression of Agrt leads to obesity in transgenic mice. Nat Genet, 17:273-274

75 Levine AS, Morley JE (1984) Neuropeptide Y: a potent inducer of consummatory behavior in rats. Peptides, 5:1025-1029

76 Ollmann MM, Wilson BD, Yang YK, Kerns JA, Chen Y, Gantz I, Barsh GS (1997) Antagonism of central melanocortin receptors in vitro and in vivo by agouti-related protein. Science, 278:135-138

77 Stanley BG, Leibowitz SF (1985) Neuropeptide Y injected in the paraventricular hypothalamus: a powerful stimulant of feeding behavior. Proc Natl Acad Sci U S A, 82:3940-3943

78 Fekete C, Kelly J, Mihaly E, Sarkar S, Rand WM, Legradi G, Emerson CH, Lechan RM (2001) Neuropeptide Y has a central inhibitory action on the hypothalamic-pituitary-thyroid axis. Endocrinology, 142:2606-2613

79 Fekete C, Sarkar S, Rand WM, Harney JW, Emerson CH, Bianco AC, Lechan RM (2002) Agouti-related protein (AGRP) has a central inhibitory action on the hypothalamic-pituitary-thyroid (HPT) axis; comparisons between the effect of AGRP and neuropeptide Y on energy homeostasis and the HPT axis. Endocrinology, 143:3846-3853

80 Voss-Andreae A, Murphy JG, Ellacott KL, Stuart RC, Nillni EA, Cone RD, Fan W (2007) Role of the central melanocortin circuitry in adaptive thermogenesis of brown adipose tissue. Endocrinology, 148:1550-1560

81 Huszar D, Lynch CA, Fairchild-Huntress V, Dunmore JH, Fang Q, Berkemeier LR, Gu W, Kesterson RA, Boston BA, Cone RD, Smith FJ, Campfield LA, Burn P, Lee F (1997) Targeted disruption of the melanocortin-4 receptor results in obesity in mice. Cell, 88:131-141

82 Chen AS, Marsh DJ, Trumbauer ME, Frazier EG, Guan XM, Yu H, Rosenblum CI, Vongs A, Feng Y, Cao L, Metzger JM, Strack AM, Camacho RE, Mellin TN, Nunes CN, Min W, Fisher J, Gopal-Truter S, MacIntyre DE, Chen HY, Van der Ploeg LH (2000) Inactivation of the mouse melanocortin-3 receptor results in increased fat mass and reduced lean body mass. Nat Genet, 26:97-102

83 Erickson JC, Hollopeter G, Palmiter RD (1996) Attenuation of the obesity syndrome of ob/ob mice by the loss of neuropeptide Y. Science, 274:1704-1707

84 Gropp E, Shanabrough M, Borok E, Xu AW, Janoschek R, Buch T, Plum L, Balthasar N, Hampel B, Waisman A, Barsh GS, Horvath TL, Bruning JC (2005) Agouti-related peptide-expressing neurons are mandatory for feeding. Nat Neurosci, 8:1289-1291

85 Luquet S, Perez FA, Hnasko TS, Palmiter RD (2005) NPY/AgRP neurons are essential for feeding in adult mice but can be ablated in neonates. Science, 310:683-685

86 Erickson JC, Clegg KE, Palmiter RD (1996) Sensitivity to leptin and susceptibility to seizures of mice lacking neuropeptide Y. Nature, 381:415-421

87 Qian S, Chen H, Weingarth D, Trumbauer ME, Novi DE, Guan X, Yu H, Shen Z, Feng Y, Frazier E, Chen A, Camacho RE, Shearman LP, Gopal-Truter S, MacNeil DJ, Van der Ploeg LH, Marsh DJ (2002) Neither agouti-related protein nor neuropeptide Y is critically required for the regulation of energy homeostasis in mice. Mol Cell Biol, 22:5027-5035

88 Satoh T, Yamada M, Iwasaki T, Mori M (1996) Negative regulation of the gene for the preprothyrotropin-releasing hormone from the mouse by thyroid hormone requires additional factors in conjunction with thyroid hormone receptors. J Biol Chem, 271:27919-27926

89 Sarkar S, Legradi G, Lechan RM (2002) Intracerebroventricular administration of alpha-melanocyte stimulating hormone increases phosphorylation of CREB in TRH- and CRH-producing neurons of the hypothalamic paraventricular nucleus. Brain Res, 945:50-59

90 Sarkar S, Wittmann G, Fekete C, Lechan RM (2004) Central administration of cocaine- and amphetamine-regulated transcript increases phosphorylation of cAMP response element binding protein in corticotropin-releasing hormone-producing neurons but not in prothyrotropin-releasing hormone-producing neurons in the hypothalamic paraventricular nucleus. Brain Res, 999:181-192

91 Legradi G, Lechan RM (1999) Agouti-related protein containing nerve terminals innervate thyrotropin-releasing hormone neurons in the hypothalamic paraventricular nucleus. Endocrinology, 140:3643-3652

92 Fekete C, Sarkar S, Rand WM, Harney JW, Emerson CH, Bianco AC, Beck-Sickinger A, Lechan RM (2002) Neuropeptide Y1 and Y5 receptors mediate the

effects of neuropeptide Y on the hypothalamic-pituitary-thyroid axis. Endocrinology, 143:4513-4519

93 Broberger C, Visser TJ, Kuhar MJ, Hokfelt T (1999) Neuropeptide Y innervation and neuropeptide-Y-Y1-receptor-expressing neurons in the paraventricular hypothalamic nucleus of the mouse. Neuroendocrinology, 70:295-305

94 Kishi T, Aschkenasi CJ, Choi BJ, Lopez ME, Lee CE, Liu H, Hollenberg AN, Friedman JM, Elmquist JK (2005) Neuropeptide Y Y1 receptor mRNA in rodent brain: distribution and colocalization with melanocortin-4 receptor. J Comp Neurol, 482:217-243

95 Michel MC, Beck-Sickinger A, Cox H, Doods HN, Herzog H, Larhammar D, Quirion R, Schwartz T, Westfall T (1998) XVI. International Union of Pharmacology recommendations for the nomenclature of neuropeptide Y, peptide YY, and pancreatic polypeptide receptors. Pharmacol Rev, 50:143-150

96 Sarkar S, Lechan RM (2003) Central administration of neuropeptide Y reduces alpha-melanocyte-stimulating hormone-induced cyclic adenosine 5'-monophosphate response element binding protein (CREB) phosphorylation in pro-thyrotropin-releasing hormone neurons and increases CREB phosphorylation in corticotropin-releasing hormone neurons in the hypothalamic paraventricular nucleus. Endocrinology, 144:281-291

97 Haskell-Luevano C, Monck EK (2001) Agouti-related protein functions as an inverse agonist at a constitutively active brain melanocortin-4 receptor. Regul Pept, 99:1-7

98 Nijenhuis WA, Oosterom J, Adan RA (2001) AgRP(83-132) acts as an inverse agonist on the human-melanocortin-4 receptor. Mol Endocrinol, 15:164-171

99 Fekete C, Legradi G, Mihaly E, Tatro JB, Rand WM, Lechan RM (2000) alpha-Melanocyte stimulating hormone prevents fasting-induced suppression of corticotropin-releasing hormone gene expression in the rat hypothalamic paraventricular nucleus. Neurosci Lett, 289:152-156

100 Isse T, Ueta Y, Serino R, Noguchi J, Yamamoto Y, Nomura M, Shibuya I, Lightman SL, Yamashita H (1999) Effects of leptin on fasting-induced inhibition of neuronal nitric oxide synthase mRNA in the paraventricular and supraoptic nuclei of rats. Brain Res, 846:229-235

101 Dallman MF, Akana SF, Bhatnagar S, Bell ME, Choi S, Chu A, Horsley C, Levin N, Meijer O, Soriano LR, Strack AM, Viau V (1999) Starvation: early signals, sensors, and sequelae. Endocrinology, 140:4015-4023

102 Habold C, Foltzer-Jourdainne C, Le Maho Y, Lignot JH, Oudart H (2005) Intestinal gluconeogenesis and glucose transport according to body fuel availability in rats. J Physiol, 566:575-586

103 Hanson ES, Levin N, Dallman MF (1997) Elevated corticosterone is not required for the rapid induction of neuropeptide Y gene expression by an overnight fast. Endocrinology, 138:1041-1047

104 Darlington DN, Chew G, Ha T, Keil LC, Dallman MF (1990) Corticosterone, but not glucose, treatment enables fasted adrenalectomized rats to survive moderate hemorrhage. Endocrinology, 127:766-772

105 Darlington DN, Neves RB, Ha T, Chew G, Dallman MF (1990) Fed, but not fasted, adrenalectomized rats survive the stress of hemorrhage and hypovolemia. Endocrinology, 127:759-765

106 Schwartz MW, Seeley RJ, Campfield LA, Burn P, Baskin DG (1996) Identification of targets of leptin action in rat hypothalamus. J Clin Invest, 98:1101-1106

107 Li C, Chen P, Smith MS (2000) Corticotropin releasing hormone neurons in the paraventricular nucleus are direct targets for neuropeptide Y neurons in the arcuate nucleus: an anterograde tracing study. Brain Res, 854:122-129

108 Liposits Z, Sievers L, Paull WK (1988) Neuropeptide-Y and ACTH-immunoreactive innervation of corticotropin releasing factor (CRF)-synthesizing neurons in the hypothalamus of the rat. An immunocytochemical analysis at the light and electron microscopic levels. Histochemistry, 88:227-234

109 Dhillo WS, Small CJ, Seal LJ, Kim MS, Stanley SA, Murphy KG, Ghatei MA, Bloom SR (2002) The hypothalamic melanocortin system stimulates the hypothalamo-pituitary-adrenal axis in vitro and in vivo in male rats. Neuroendocrinology, 75:209-216

110 Lu XY, Barsh GS, Akil H, Watson SJ (2003) Interaction between alpha-melanocyte-stimulating hormone and corticotropin-releasing hormone in the regulation of feeding and hypothalamo-pituitary-adrenal responses. J Neurosci, 23:7863-7872

111 Seasholtz AF, Thompson RC, Douglass JO (1988) Identification of a cyclic adenosine monophosphate-responsive element in the rat corticotropin-releasing hormone gene. Mol Endocrinol, 2:1311-1319

112 Smith SM, Vaughan JM, Donaldson CJ, Rivier J, Li C, Chen A, Vale WW (2004) Cocaine- and amphetamine-regulated transcript activates the hypothalamic-pituitary-adrenal axis through a corticotropin-releasing factor receptor-dependent mechanism. Endocrinology, 145:5202-5209

113 Suda T, Tozawa F, Iwai I, Sato Y, Sumitomo T, Nakano Y, Yamada M, Demura H (1993) Neuropeptide Y increases the corticotropin-releasing factor messenger ribonucleic acid level in the rat hypothalamus. Brain Res Mol Brain Res, 18:311-315

114 Brunton PJ, Bales J, Russell JA (2006) Neuroendocrine stress but not feeding responses to centrally administered neuropeptide Y are suppressed in pregnant rats. Endocrinology, 147:3737-3745

115 Garcia MC, Lopez M, Gualillo O, Seoane LM, Dieguez C, Senaris RM (2003) Hypothalamic levels of NPY, MCH, and prepro-orexin mRNA during pregnancy and lactation in the rat: role of prolactin. FASEB J, 17:1392-1400

116 Pronchuk N, Beck-Sickinger AG, Colmers WF (2002) Multiple NPY receptors Inhibit GABA(A) synaptic responses of rat medial parvocellular effector neurons in the hypothalamic paraventricular nucleus. Endocrinology, 143:535-543

117 Hakansson ML, Brown H, Ghilardi N, Skoda RC, Meister B (1998) Leptin receptor immunoreactivity in chemically defined target neurons of the hypothalamus. J Neurosci, 18:559-572

118 Monnikes H, Heymann-Monnikes I, Tache Y (1992) CRF in the paraventricular nucleus of the hypothalamus induces dose-related behavioral profile in rats. Brain Res, 574:70-76

119 Morley JE, Levine AS (1982) Corticotrophin releasing factor, grooming and ingestive behavior. Life Sci, 31:1459-1464

120 Dallman MF, Strack AM, Akana SF, Bradbury MJ, Hanson ES, Scribner KA, Smith M (1993) Feast and famine: critical role of glucocorticoids with insulin in daily energy flow. Front Neuroendocrinol, 14:303-347

121 Kwak SP, Young EA, Morano I, Watson SJ, Akil H (1992) Diurnal corticotropin-releasing hormone mRNA variation in the hypothalamus exhibits a rhythm distinct from that of plasma corticosterone. Neuroendocrinology, 55:74-83

122 Kiss JZ, Cassell MD, Palkovits M (1984) Analysis of the ACTH/beta-End/alpha-MSH-immunoreactive afferent input to the hypothalamic paraventricular nucleus of rat. Brain Res, 324:91-99

123 Legradi G, Lechan RM (1998) The arcuate nucleus is the major source for neuropeptide Y-innervation of thyrotropin-releasing hormone neurons in the hypothalamic paraventricular nucleus. Endocrinology, 139:3262-3270

124 Sawchenko PE, Swanson LW, Grzanna R, Howe PR, Bloom SR, Polak JM (1985) Colocalization of neuropeptide Y immunoreactivity in brainstem catecholaminergic neurons that project to the paraventricular nucleus of the hypothalamus. J Comp Neurol, 241:138-153

125 Sahu A, Kalra SP, Crowley WR, Kalra PS (1988) Evidence that NPY-containing neurons in the brainstem project into selected hypothalamic nuclei: implication in feeding behavior. Brain Res, 457:376-378

126 Liposits Z, Paull WK, Wu P, Jackson IM, Lechan RM (1987) Hypophysiotrophic thyrotropin releasing hormone (TRH) synthesizing neurons. Ultrastructure, adrenergic innervation and putative transmitter action. Histochemistry, 88:1-10

127 Liposits Z, Phelix C, Paull WK (1986) Adrenergic innervation of corticotropin releasing factor (CRF)-synthesizing neurons in the hypothalamic paraventricular nucleus of the rat. A combined light and electron microscopic immunocytochemical study. Histochemistry, 84:201-205

128 Diano S, Naftolin F, Goglia F, Horvath TL (1998) Segregation of the intra- and extrahypothalamic neuropeptide Y and catecholaminergic inputs on paraventricular neurons, including those producing thyrotropin-releasing hormone. Regul Pept, 75-76:117-126

129 Douglass J, McKinzie AA, Couceyro P (1995) PCR differential display identifies a rat brain mRNA that is transcriptionally regulated by cocaine and amphetamine. J Neurosci, 15:2471-2481

130 Koylu EO, Couceyro PR, Lambert PD, Kuhar MJ (1998) Cocaine- and amphetamine-regulated transcript peptide immunohistochemical localization in the rat brain. J Comp Neurol, 391:115-132

131 Koylu EO, Couceyro PR, Lambert PD, Ling NC, DeSouza EB, Kuhar MJ (1997) Immunohistochemical localization of novel CART peptides in rat hypothalamus, pituitary and adrenal gland. J Neuroendocrinol, 9:823-833

132 Schiltz JC, Sawchenko PE (2007) Specificity and generality of the involvement of catecholaminergic afferents in hypothalamic responses to immune insults. J Comp Neurol, 502:455-467

133 Tuomisto J, Ranta T, Mannisto P, Saarinen A, Leppalioto J (1975) Neurotransmitter control of thyrotropin secretion in the rat. Eur J Pharmacol, 30:221-229

134 Ericsson A, Kovacs KJ, Sawchenko PE (1994) A functional anatomical analysis of central pathways subserving the effects of interleukin-1 on stress-related neuroendocrine neurons. J Neurosci, 14:897-913

135 Fekete C, Singru PS, Sarkar S, Rand WM, Lechan RM (2005) Ascending brainstem pathways are not involved in lipopolysaccharide-induced suppression of thyrotropin-releasing hormone gene expression in the hypothalamic paraventricular nucleus. Endocrinology, 146:1357-1363

136 Ritter S, Bugarith K, Dinh TT (2001) Immunotoxic destruction of distinct catecholamine subgroups produces selective impairment of glucoregulatory responses and neuronal activation. J Comp Neurol, 432:197-216

137 Ritter S, Llewellyn-Smith I, Dinh TT (1998) Subgroups of hindbrain catecholamine neurons are selectively activated by 2-deoxy-D-glucose induced metabolic challenge. Brain Res, 805:41-54

138 Ritter S, Watts AG, Dinh TT, Sanchez-Watts G, Pedrow C (2003) Immunotoxin lesion of hypothalamically projecting norepinephrine and epinephrine neurons differentially affects circadian and stressor-stimulated corticosterone secretion. Endocrinology, 144:1357-1367

139 Sindelar DK, Ste Marie L, Miura GI, Palmiter RD, McMinn JE, Morton GJ, Schwartz MW (2004) Neuropeptide Y is required for hyperphagic feeding in response to neuroglucopenia. Endocrinology, 145:3363-3368

140 Ste Marie L, Palmiter RD (2003) Norepinephrine and epinephrine-deficient mice are hyperinsulinemic and have lower blood glucose. Endocrinology, 144:4427-4432

141 Li AJ, Wang Q, Ritter S (2006) Differential responsiveness of dopamine-beta-hydroxylase gene expression to glucoprivation in different catecholamine cell groups. Endocrinology, 147:3428-3434

142 Li AJ, Ritter S (2004) Glucoprivation increases expression of neuropeptide Y mRNA in hindbrain neurons that innervate the hypothalamus. Eur J Neurosci, 19:2147-2154

143 Melander T, Hokfelt T, Rokaeus A (1986) Distribution of galaninlike immunoreactivity in the rat central nervous system. J Comp Neurol, 248:475-517

144 Merchenthaler I, Lopez FJ, Negro-Vilar A (1993) Anatomy and physiology of central galanin-containing pathways. Prog Neurobiol, 40:711-769

145 Bartfai T, Hokfelt T, Langel U (1993) Galanin--a neuroendocrine peptide. Crit Rev Neurobiol, 7:229-274

146 Kyrkouli SE, Stanley BG, Leibowitz SF (1986) Galanin: stimulation of feeding induced by medial hypothalamic injection of this novel peptide. Eur J Pharmacol, 122:159-160

147 Sahu A (1998) Evidence suggesting that galanin (GAL), melanin-concentrating hormone (MCH), neurotensin (NT), proopiomelanocortin (POMC) and neuropeptide Y (NPY) are targets of leptin signaling in the hypothalamus. Endocrinology, 139:795-798

148 Ohtaki T, Kumano S, Ishibashi Y, Ogi K, Matsui H, Harada M, Kitada C, Kurokawa T, Onda H, Fujino M (1999) Isolation and cDNA cloning of a novel galanin-like peptide (GALP) from porcine hypothalamus. J Biol Chem, 274:37041-37045

149 Takatsu Y, Matsumoto H, Ohtaki T, Kumano S, Kitada C, Onda H, Nishimura O, Fujino M (2001) Distribution of galanin-like peptide in the rat brain. Endocrinology, 142:1626-1634

150 Matsumoto Y, Watanabe T, Adachi Y, Itoh T, Ohtaki T, Onda H, Kurokawa T, Nishimura O, Fujino M (2002) Galanin-like peptide stimulates food intake in the rat. Neurosci Lett, 322:67-69

151 Jureus A, Cunningham MJ, McClain ME, Clifton DK, Steiner RA (2000) Galanin-like peptide (GALP) is a target for regulation by leptin in the hypothalamus of the rat. Endocrinology, 141:2703-2706

152 Seth A, Stanley S, Dhillo W, Murphy K, Ghatei M, Bloom S (2003) Effects of galanin-like peptide on food intake and the hypothalamo-pituitary-thyroid axis. Neuroendocrinology, 77:125-131

153 Levin MC, Sawchenko PE, Howe PR, Bloom SR, Polak JM (1987) Organization of galanin-immunoreactive inputs to the paraventricular nucleus with special reference to their relationship to catecholaminergic afferents. J Comp Neurol, 261:562-582

154 Paxinos G, Watson C. The Rat Brain in Stereotaxic Coordinates. 4th ed. Academic Press, San Diego, CA, 1998

155 Adams JC (1992) Biotin amplification of biotin and horseradish peroxidase signals in histochemical stains. J Histochem Cytochem, 40:1457-1463

156 Lechan RM, Wu P, Jackson IM, Wolf H, Cooperman S, Mandel G, Goodman RH (1986) Thyrotropin-releasing hormone precursor: characterization in rat brain. Science, 231:159-161

157 Liposits Z, Setalo G, Flerko B (1984) Application of the silver-gold intensified 3,3'-diaminobenzidine chromogen to the light and electron microscopic detection of the luteinizing hormone-releasing hormone system of the rat brain. Neuroscience, 13:513-525

158 Mihaly E, Fekete C, Legradi G, Lechan RM (2001) Hypothalamic dorsomedial nucleus neurons innervate thyrotropin-releasing hormone-synthesizing neurons in the paraventricular nucleus. Brain Res, 891:20-31

159 Elias CF, Saper CB, Maratos-Flier E, Tritos NA, Lee C, Kelly J, Tatro JB, Hoffman GE, Ollmann MM, Barsh GS, Sakurai T, Yanagisawa M, Elmquist JK (1998) Chemically defined projections linking the mediobasal hypothalamus and the lateral hypothalamic area. J Comp Neurol, 402:442-459

160 Thim L, Kristensen P, Nielsen PF, Wulff BS, Clausen JT (1999) Tissue-specific processing of cocaine- and amphetamine-regulated transcript peptides in the rat. Proc Natl Acad Sci U S A, 96:2722-2727

161 Mihaly E, Fekete C, Lechan RM, Liposits Z (2002) Corticotropin-releasing hormone-synthesizing neurons of the human hypothalamus receive neuropeptide Y-immunoreactive innervation from neurons residing primarily outside the infundibular nucleus. J Comp Neurol, 446:235-243

162 Sawchenko PE, Swanson LW, Vale WW (1984) Co-expression of corticotropin-releasing factor and vasopressin immunoreactivity in parvocellular neurosecretory neurons of the adrenalectomized rat. Proc Natl Acad Sci U S A, 81:1883-1887

163 Lazar GY, Liposits ZS, Toth P, Trasti SL, Maderdrut JL, Merchenthaler I (1991) Distribution of galanin-like immunoreactivity in the brain of Rana esculenta and Xenopus laevis. J Comp Neurol, 310:45-67

164 Bohn MC, Dreyfus CF, Friedman WJ, Markey KA (1987) Glucocorticoid effects on phenylethanolamine N-methyltransferase (PNMT) in explants of embryonic rat medulla oblongata. Brain Res, 465:257-266

165 Segerson TP, Hoefler H, Childers H, Wolfe HJ, Wu P, Jackson IM, Lechan RM (1987) Localization of thyrotropin-releasing hormone prohormone messenger ribonucleic acid in rat brain in situ hybridization. Endocrinology, 121:98-107

166 Morris BJ (1989) Neuronal localisation of neuropeptide Y gene expression in rat brain. J Comp Neurol, 290:358-368

167 Broberger C (1999) Hypothalamic cocaine- and amphetamine-regulated transcript (CART) neurons: histochemical relationship to thyrotropin-releasing hormone, melanin-concentrating hormone, orexin/hypocretin and neuropeptide Y. Brain Res, 848:101-113

168 Goldstein M, Fuxe K, Hokfelt T (1972) Characterization and tissue localization of catecholamine synthesizing enzymes. Pharmacol Rev, 24:293-309

169 Elias CF, Lee CE, Kelly JF, Ahima RS, Kuhar M, Saper CB, Elmquist JK (2001) Characterization of CART neurons in the rat and human hypothalamus. J Comp Neurol, 432:1-19

170 Burman KJ, Sartor DM, Verberne AJ, Llewellyn-Smith IJ (2004) Cocaine- and amphetamine-regulated transcript in catecholamine and noncatecholamine presympathetic vasomotor neurons of rat rostral ventrolateral medulla. J Comp Neurol, 476:19-31

171 Toni R, Jackson IM, Lechan RM (1990) Neuropeptide-Y-immunoreactive innervation of thyrotropin-releasing hormone-synthesizing neurons in the rat hypothalamic paraventricular nucleus. Endocrinology, 126:2444-2453

172 Itoi K, Helmreich DL, Lopez-Figueroa MO, Watson SJ (1999) Differential regulation of corticotropin-releasing hormone and vasopressin gene transcription in the hypothalamus by norepinephrine. J Neurosci, 19:5464-5472

173 Cole RL, Sawchenko PE (2002) Neurotransmitter regulation of cellular activation and neuropeptide gene expression in the paraventricular nucleus of the hypothalamus. J Neurosci, 22:959-969

174 Itoi K, Suda T, Tozawa F, Dobashi I, Ohmori N, Sakai Y, Abe K, Demura H (1994) Microinjection of norepinephrine into the paraventricular nucleus of the hypothalamus stimulates corticotropin-releasing factor gene expression in conscious rats. Endocrinology, 135:2177-2182

175 Day HE, Campeau S, Watson SJ, Jr., Akil H (1999) Expression of alpha(1b) adrenoceptor mRNA in corticotropin-releasing hormone-containing cells of the rat hypothalamus and its regulation by corticosterone. J Neurosci, 19:10098-10106

176 Thonberg H, Fredriksson JM, Nedergaard J, Cannon B (2002) A novel pathway for adrenergic stimulation of cAMP-response-element-binding protein (CREB) phosphorylation: mediation via alpha1-adrenoceptors and protein kinase C activation. Biochem J, 364:73-79

177 Daftary SS, Boudaba C, Szabo K, Tasker JG (1998) Noradrenergic excitation of magnocellular neurons in the rat hypothalamic paraventricular nucleus via intranuclear glutamatergic circuits. J Neurosci, 18:10619-10628

178 Daftary SS, Boudaba C, Tasker JG (2000) Noradrenergic regulation of parvocellular neurons in the rat hypothalamic paraventricular nucleus. Neuroscience, 96:743-751

179 Gordon GR, Bains JS (2003) Priming of excitatory synapses by alpha1 adrenoceptor-mediated inhibition of group III metabotropic glutamate receptors. J Neurosci, 23:6223-6231

180 Boudaba C, Di S, Tasker JG (2003) Presynaptic noradrenergic regulation of glutamate inputs to hypothalamic magnocellular neurones. J Neuroendocrinol, 15:803-810

181 Chen Q, Li DP, Pan HL (2006) Presynaptic alpha1 adrenergic receptors differentially regulate synaptic glutamate and GABA release to hypothalamic presympathetic neurons. J Pharmacol Exp Ther, 316:733-742

182 Han SK, Chong W, Li LH, Lee IS, Murase K, Ryu PD (2002) Noradrenaline excites and inhibits GABAergic transmission in parvocellular neurons of rat hypothalamic paraventricular nucleus. J Neurophysiol, 87:2287-2296

183 Li DP, Atnip LM, Chen SR, Pan HL (2005) Regulation of synaptic inputs to paraventricular-spinal output neurons by alpha2 adrenergic receptors. J Neurophysiol, 93:393-402

184 Gordon GR, Baimoukhametova DV, Hewitt SA, Rajapaksha WR, Fisher TE, Bains JS (2005) Norepinephrine triggers release of glial ATP to increase postsynaptic efficacy. Nat Neurosci, 8:1078-1086

185 Kopp J, Xu ZQ, Zhang X, Pedrazzini T, Herzog H, Kresse A, Wong H, Walsh JH, Hokfelt T (2002) Expression of the neuropeptide Y Y1 receptor in the CNS of rat and of wild-type and Y1 receptor knock-out mice. Focus on immunohistochemical localization. Neuroscience, 111:443-532

186 Bali B, Kovacs KJ (2003) GABAergic control of neuropeptide gene expression in parvocellular neurons of the hypothalamic paraventricular nucleus. Eur J Neurosci, 18:1518-1526

187 Ritter S, Dinh TT, Zhang Y (2000) Localization of hindbrain glucoreceptive sites controlling food intake and blood glucose. Brain Res, 856:37-47

188 Brown J (1962) Effects of 2-deoxyglucose on carbohydrate metablism: review of the literature and studies in the rat. Metabolism, 11:1098-1112

189 Wick AN, Drury DR, Nakada HI, Wolfe JB (1957) Localization of the primary metabolic block produced by 2-deoxyglucose. J Biol Chem, 224:963-969

190 Smith GP, Epstein AN (1969) Increased feeding in response to decreased glucose utilization in the rat and monkey. Am J Physiol, 217:1083-1087

191 Hokfelt B, Bydgeman S (1961) Increased adrenaline production following administration of 2-deoxy-D-glucose in the rat. Proc Soc Exp Biol Med, 106:537-539

192 Scheurink A, Ritter S (1993) Sympathoadrenal responses to glucoprivation and lipoprivation in rats. Physiol Behav, 53:995-1000

193 Morgan JI, Curran T (1991) Stimulus-transcription coupling in the nervous system: involvement of the inducible proto-oncogenes fos and jun. Annu Rev Neurosci, 14:421-451

194 Barthelemy I, Martineau D, Ong M, Matsunami R, Ling N, Benatti L, Cavallaro U, Soria M, Lappi DA (1993) The expression of saporin, a ribosome-inactivating protein from the plant Saponaria officinalis, in Escherichia coli. J Biol Chem, 268:6541-6548

195 Feng Z, Angeletti RH, Levin BE, Sabban EL (1992) Glycosylation and membrane insertion of newly synthesized rat dopamine beta-hydroxylase in a cell-free system without signal cleavage. J Biol Chem, 267:21808-21815

196 Studelska DR, Brimijoin S (1989) Partial isolation of two classes of dopamine beta-hydroxylase-containing particles undergoing rapid axonal transport in rat sciatic nerve. J Neurochem, 53:622-631

197 Wrenn CC, Picklo MJ, Lappi DA, Robertson D, Wiley RG (1996) Central noradrenergic lesioning using anti-DBH-saporin: anatomical findings. Brain Res, 740:175-184

198 Fraley GS, Ritter S (2003) Immunolesion of norepinephrine and epinephrine afferents to medial hypothalamus alters basal and 2-deoxy-D-glucose-induced neuropeptide Y and agouti gene-related protein messenger ribonucleic acid expression in the arcuate nucleus. Endocrinology, 144:75-83

199 Luquet S, Phillips CT, Palmiter RD (2007) NPY/AgRP neurons are not essential for feeding responses to glucoprivation. Peptides, 28:214-225

200 Li HY, Ericsson A, Sawchenko PE (1996) Distinct mechanisms underlie activation of hypothalamic neurosecretory neurons and their medullary catecholaminergic afferents in categorically different stress paradigms. Proc Natl Acad Sci U S A, 93:2359-2364

201 Dayas CV, Buller KM, Crane JW, Xu Y, Day TA (2001) Stressor categorization: acute physical and psychological stressors elicit distinctive recruitment patterns in the amygdala and in medullary noradrenergic cell groups. Eur J Neurosci, 14:1143-1152

202 Uribe RM, Redondo JL, Charli JL, Joseph-Bravo P (1993) Suckling and cold stress rapidly and transiently increase TRH mRNA in the paraventricular nucleus. Neuroendocrinology, 58:140-145

203 Zoeller RT, Kabeer N, Albers HE (1990) Cold exposure elevates cellular levels of messenger ribonucleic acid encoding thyrotropin-releasing hormone in paraventricular nucleus despite elevated levels of thyroid hormones. Endocrinology, 127:2955-2962

204 Perello M, Stuart RC, Varslet CA, Nillni EA (2007) Cold Exposure Increases the Biosynthesis and Proteolytic Processing of Prothyrotropin Releasing Hormone in the Hypothalamic Paraventricular Nucleus via Beta-adrenoreceptors. Endocrinology,

205 Djordjevic J, Cvijic G, Davidovic V (2003) Different activation of ACTH and corticosterone release in response to various stressors in rats. Physiol Res, 52:67-72

206 Stornetta RL, Akey PJ, Guyenet PG (1999) Location and electrophysiological characterization of rostral medullary adrenergic neurons that contain neuropeptide Y mRNA in rat medulla. J Comp Neurol, 415:482-500

207 Verberne AJ, Stornetta RL, Guyenet PG (1999) Properties of C1 and other ventrolateral medullary neurones with hypothalamic projections in the rat. J Physiol, 517 (Pt 2):477-494

208 Sergeyev V, Broberger C, Hokfelt T (2001) Effect of LPS administration on the expression of POMC, NPY, galanin, CART and MCH mRNAs in the rat hypothalamus. Brain Res Mol Brain Res, 90:93-100

209 Shimada M, Tritos NA, Lowell BB, Flier JS, Maratos-Flier E (1998) Mice lacking melanin-concentrating hormone are hypophagic and lean. Nature, 396:670-674

210 Ludwig DS, Tritos NA, Mastaitis JW, Kulkarni R, Kokkotou E, Elmquist J, Lowell B, Flier JS, Maratos-Flier E (2001) Melanin-concentrating hormone overexpression in transgenic mice leads to obesity and insulin resistance. J Clin Invest, 107:379-386

211 Qu D, Ludwig DS, Gammeltoft S, Piper M, Pelleymounter MA, Cullen MJ, Mathes WF, Przypek R, Kanarek R, Maratos-Flier E (1996) A role for melanin-concentrating hormone in the central regulation of feeding behaviour. Nature, 380:243-247

212 Tritos NA, Mastaitis JW, Kokkotou E, Maratos-Flier E (2001) Characterization of melanin concentrating hormone and preproorexin expression in the murine hypothalamus. Brain Res, 895:160-166

213 Kennedy AR, Todd JF, Stanley SA, Abbott CR, Small CJ, Ghatei MA, Bloom SR (2001) Melanin-concentrating hormone (MCH) suppresses thyroid stimulating hormone (TSH) release, in vivo and in vitro, via the hypothalamus and the pituitary. Endocrinology, 142:3265-3268

214 Segal-Lieberman G, Bradley RL, Kokkotou E, Carlson M, Trombly DJ, Wang X, Bates S, Myers MG, Jr., Flier JS, Maratos-Flier E (2003) Melanin-concentrating hormone is a critical mediator of the leptin-deficient phenotype. Proc Natl Acad Sci U S A, 100:10085-10090

215 Loewy AD. Central autonomic pathways. In: Loewy AD, Spyer KM (eds.), Central regulation of autonomic functions. Oxford University Press, New York, 1990: 88-103

216 van den Pol AN (1982) The magnocellular and parvocellular paraventricular nucleus of rat: intrinsic organization. J Comp Neurol, 206:317-345

217 Larsen PJ, Seier V, Fink-Jensen A, Holst JJ, Warberg J, Vrang N (2003) Cocaine- and amphetamine-regulated transcript is present in hypothalamic neuroendocrine neurones and is released to the hypothalamic-pituitary portal circuit. J Neuroendocrinol, 15:219-226

218 Peters A, Palay SL, deF Webster H. The fine structure of the nervous system. Neurons and their supporting cells. 3rd ed. Oxford University Press, Oxford, 1991

219 Parker EM, Izzarelli DG, Nowak HP, Mahle CD, Iben LG, Wang J, Goldstein ME (1995) Cloning and characterization of the rat GALR1 galanin receptor from Rin14B insulinoma cells. Brain Res Mol Brain Res, 34:179-189

220 Wang S, Hashemi T, Fried S, Clemmons AL, Hawes BE (1998) Differential intracellular signaling of the GalR1 and GalR2 galanin receptor subtypes. Biochemistry, 37:6711-6717

221 Mitchell V, Habert-Ortoli E, Epelbaum J, Aubert JP, Beauvillain JC (1997) Semiquantitative distribution of galanin-receptor (GAL-R1) mRNA-containing cells in the male rat hypothalamus. Neuroendocrinology, 66:160-172

222 Wang J, Akabayashi A, Yu HJ, Dourmashkin J, Alexander JT, Silva I, Lighter J, Leibowitz SF (1998) Hypothalamic galanin: control by signals of fat metabolism. Brain Res, 804:7-20

223 Xu ZQ, Hokfelt T (1997) Expression of galanin and nitric oxide synthase in subpopulations of serotonin neurons of the rat dorsal raphe nucleus. J Chem Neuroanat, 13:169-187

224 Xu ZQ, Zhang X, Pieribone VA, Grillner S, Hokfelt T (1998) Galanin-5-hydroxytryptamine interactions: electrophysiological, immunohistochemical and in situ hybridization studies on rat dorsal raphe neurons with a note on galanin R1 and R2 receptors. Neuroscience, 87:79-94

225 Larm JA, Gundlach AL (2000) Galanin-like peptide (GALP) mRNA expression is restricted to arcuate nucleus of hypothalamus in adult male rat brain. Neuroendocrinology, 72:67-71

List of publications underlying the thesis

1. Wittmann G., Liposits Z., Lechan R.M., Fekete C.
   Medullary adrenergic neurons contribute to the neuropeptide Y-ergic innervation of hypophysiotropic thyrotropin-releasing hormone-synthesizing neurons in the rat
   Neurosci Lett, 324 (2002) 69-73

2. Fekete C., Wittmann G., Liposits Z., Lechan R.M.
   Origin of cocaine- and amphetamine-regulated transcript (CART)-immunoreactive innervation of the hypothalamic paraventricular nucleus
   J Comp Neurol, 469 (2004) 340-350

3. Sarkar S., Wittmann G., Fekete C., Lechan R.M.
   Central administration of cocaine- and amphetamine-regulated transcript increases phosphorylation of cAMP response element binding protein in corticotropin-releasing hormone-producing neurons but not in prothyrotropin-releasing hormone-producing neurons i n the hypothalamic paraventricular nucleus
   Brain Res, 999 (2004) 181-192

4. Wittmann G., Sarkar S., Hrabovszky E., Liposits Z., Lechan R.M., Fekete C.
   Galanin- but not galanin-like peptide-containing axon terminals innervate hypophysiotropic TRH-synthesizing neurons in the hypothalamic paraventricular nucleus
   Brain Res, 1002 (2004) 43-50

5. Wittmann G., Liposits Z., Lechan R.M., Fekete C.
   Medullary adrenergic neurons contribute to the cocaine- and amphetamine-regulated transcript-immunoreactive innervation of thyrotropin-releasing hormone synthesizing neurons in the hypothalamic paraventricular nucleus
   Brain Res, 1006 (2004) 1-7

6. Wittmann G., Liposits Z., Lechan R.M., Fekete C.
   Origin of cocaine- and amphetamine-regulated transcript-containing axons innervating hypophysiotropic corticotropin-releasing hormone-synthesizing neurons in the rat
   Endocrinology, 146 (2005) 2985-2991

List of publications related to the subject of the thesis

7. Fekete C., Wittmann G., Liposits Z., Lechan R.M.
   GABA-ergic innervation of thyrotropin-releasing hormone-synthesizing neurons in the hypothalamic paraventricular nucleus of the rat
   Brain Res, 957 (2002) 251-258

8. Hrabovszky E., Wittmann G., Túri G.F., Liposits Z., Fekete C.
   Hypophysiotropic thyrotropin-releasing hormone and corticotropin-releasing hormone neurons of the rat contain vesicular glutamate transporter-2
   Endocrinology, 146 (2005) 341-347

9. Wittmann G., Lechan R.M., Liposits Z., Fekete C.
   Glutamatergic innervation of corticotropin-releasing hormone- and thyrotropin-releasing hormone-synthesizing neurons in the hypothalamic paraventricular nucleus of the rat
   Brain Res, 1039 (2005) 53-62

10. Menyhért J., Wittmann G., Hrabovszky E., Keller É., Liposits Z., Fekete C.
    Interconnection between orexigenic neuropeptide Y- and anorexigenic alpha-melanocyte stimulating hormone-synthesizing neuronal systems of the human hypothalamus
    Brain Res, 1076 (2006) 101-105

11. Hrabovszky E., Kalló I., Túri G.F., May K., Wittmann G., Fekete C., Liposits Z.
    Expression of vesicular glutamate transporter-2 in gonadotrope and thyrotrope cells of the rat pituitary. Regulation by estrogen and thyroid hormone status
    Endocrinology, 147 (2006) 3818-3825

12. Menyhért J., Wittmann G., Hrabovszky E., Szlávik N., Keller É., Tschöp M., Liposits Z., Fekete C.
    Distribution of ghrelin-immunoreactive neuronal networks in the human hypothalamus
    Brain Res, 1125 (2006) 31-36

13. Wittmann G., Deli L., Kalló I., Hrabovszky E., Watanabe M., Liposits Z., Fekete C.
    Distribution of type 1 cannabinoid receptor (CB1)-immunoreactive axons in the mouse hypothalamus
    J Comp Neurol, 503 (2007) 270-9.

14. Menyhért J., Wittmann G., Lechan R.M., Keller É., Liposits Z., Fekete C.
    Cocaine- and amphetamine regulated transcript (CART) is colocalized with the orexigenic NPY and AGRP and absent from the anorexigenic α-MSH neurons in the infundibular nucleus of the human hypothalamus
    Endocrinology, 2007 May 24 [Epub ahead of print]

Acknowledgements

I express my deep gratitude to Dr. Csaba Fekete, my tutor. He devoted so much time and attention to teach me scientific research from the years I was a graduate student at university. I thank him that he has fully promoted my professional development.

I am very grateful to Professor Zsolt Liposits, my co-tutor and Head of the Laboratory of Endocrine Neurobiology, who has provided me absolute support to progress in scientific research.

My sincere thanks to Professor Ronald M. Lechan at Tufts University in Boston, for his important contribution to writing the papers of this Ph.D. thesis.

Thanks to Dr. Summit Sarkar who performed the GALP-TRH immunocytochemistry at Tufts University.

I wish to express my thanks to our assistants whom I worked together with: Zsuzsanna Fodor, Éva Laki, Andrea Kádár and Ágnes Simon. I appreciate their careful and precise work that was a great help of me.

Special thanks to my closest colleagues Tamás Füzesi and Judit Menyhért for successful cooperation and the joyful hours spent together, and to Gergely Túri and Barbara Vida for their fellowship.

I would like to thank all of my colleagues in the Laboratory of Endocrine Neurobiology for many pieces of advice and technical helps, and for their great companionship: Bekó Norbertné, Levente Deli, Dr. Orsolya Dohán, Dr. Márton Doleschall, Dr. Imre Farkas, Dr. Balázs Gereben, Vivien Hársfalvi, Dr. Erik Hrabovszky, Csilla Jekkel, Edit Juhász, Dr. Imre Kalló, Dr. Miklós Sárvári, Dr. Patrícia Varjú, Dr. Anikó Zeöld.

I would also like to express my thanks to the members of the Medical Gene Technological Unit, especially to Dr. Balázs Bényei, Head of the Unit, and to Mária Szűcs and Rozália Szafner for having always been helpful when I worked in the animal facility.